

Drivers of plant nutrient acquisition and allocation strategies and their influence
on plant responses to environmental change

by

Evan A. Perkowski, B.S.

A Dissertation

In

Biological Sciences

Submitted to the Graduate Faculty
of Texas Tech University in
Partial Fulfillment of
the Requirements for
the Degree of

Doctor of Philosophy

Approved

Nicholas G. Smith, Ph.D.
Chair of Committee

Aimée T. Classen, Ph.D.

Natasja van Gestel, Ph.D.

Lindsey C. Slaughter, Ph.D.

Dylan W. Schwilk, Ph.D.

Mark Sheridan, Ph.D.
Dean of the Graduate School

May 2023

Copyright 2023, Evan A. Perkowski

Acknowledgements

Placeholder for text

Table of Contents

Acknowledgements	ii
Abstract	vii
List of Tables	viii
List of Figures	x
1. Introduction	1
2. Structural carbon costs to acquire nitrogen are determined by nitrogen and light availability in two species with different nitrogen acquisition strategies	8
2.1 Introduction	8
2.2 Methods	12
2.2.1 <i>Experiment setup</i>	12
2.2.2 <i>Plant measurements and calculations</i>	13
2.2.3 <i>Statistical analyses</i>	14
2.3 Results	16
2.3.1 <i>Carbon costs to acquire nitrogen</i>	16
2.3.2 <i>Whole plant nitrogen biomass</i>	19
2.3.3 <i>Root carbon biomass</i>	21
2.3.4 <i>Root nodule biomass</i>	23
2.4 Discussion	27
3. Soil nitrogen availability modifies leaf nitrogen economies in mature temperate deciduous forests: a direct test of photosynthetic least-cost theory	35
3.1 Introduction	35
3.2 Methods	39
3.2.1 <i>Study site description</i>	39
3.2.2 <i>Experimental design</i>	40
3.2.3 <i>Leaf gas exchange and trait measurements</i>	40
3.2.4 <i>A_{net}/C_i curve-fitting and parameter estimation</i>	43

3.2.5 <i>Proportion of leaf nitrogen allocated to photosynthesis and structure</i>	45
3.2.6 <i>Tradeoffs between nitrogen and water use</i>	46
3.2.7 <i>Soil nitrogen availability and pH</i>	47
3.2.8 <i>Statistical analyses</i>	49
3.3 Results	51
3.3.1 <i>Leaf N content</i>	51
3.3.2 <i>Net photosynthesis and leaf biochemistry</i>	54
3.3.3 <i>Leaf N allocation</i>	57
3.3.4 <i>Tradeoffs between nitrogen and water use</i>	60
3.4 Discussion	63
3.4.1 <i>Soil nitrogen availability modifies tradeoffs between nitrogen and water use</i>	64
3.4.2 <i>Soil pH did not modify tradeoffs between nitrogen and water usage</i>	66
3.4.3 <i>Species identity explains a large amount of variation in leaf and whole plant traits</i>	67
3.4.4 <i>Implications for photosynthetic least-cost theory model development</i>	68
3.4.5 <i>Conclusions</i>	70
4. The relative cost of resource use for photosynthesis drives variance in leaf nitrogen content across climate and soil resource availability gradients	71
4.1 Introduction	71
4.2 Methods	77
4.2.1 <i>Site descriptions and sampling methodology</i>	77
4.2.2 <i>Leaf trait measurements</i>	77
4.2.3 <i>Site climate data</i>	83
4.2.4 <i>Site edaphic characteristics</i>	83
4.2.5 <i>Plant functional group assignments</i>	85
4.2.6 <i>Data analysis</i>	86

4.3 Results	88
4.3.1 <i>Cost to acquire nitrogen relative to water</i>	88
4.3.2 <i>Leaf C_i:C_a</i>	92
4.3.3 <i>Leaf nitrogen content</i>	95
4.3.4 <i>Structural equation model</i>	99
4.4 Discussion	102
5. Optimal resource investment to photosynthetic capacity maximizes nutrient allocation to whole plant growth under elevated CO₂	103
5.1 Introduction	103
5.2 Methods	108
5.2.1 <i>Seed treatments and experimental design</i>	108
5.2.2 <i>Growth chamber conditions</i>	109
5.2.3 <i>Leaf gas exchange measurements</i>	111
5.2.4 <i>Leaf trait measurements</i>	112
5.2.5 <i>A/C_i curve fitting and parameter estimation</i>	114
5.2.6 Stomatal limitation	114
5.2.7 <i>Proportion of leaf nitrogen allocated to photosynthesis and structure</i>	115
5.2.8 <i>Whole plant traits</i>	117
5.2.9 <i>Statistical analyses</i>	119
5.3 Results	121
5.3.1 <i>Leaf nitrogen content, chlorophyll content, and mass per area</i>	121
5.3.2 <i>Leaf biochemistry and stomatal conductance</i>	125
5.3.3 <i>Leaf nitrogen allocation</i>	129
5.3.4 <i>Whole plant growth and total leaf area</i>	133
5.3.5 <i>Carbon costs to acquire nitrogen</i>	133
5.3.6 <i>Nitrogen fixation</i>	137
5.4 Discussion	141

5.4.1	<i>Soil nitrogen fertilization has divergent effects on leaf and whole plant acclimation responses to CO₂</i>	142
5.4.2	<i>Implications for future model development</i>	146
5.4.3	<i>Study limitations and future directions</i>	147
5.4.4	<i>Conclusions</i>	149
6.	Conclusions	151
	References	153

Abstract

List of Tables

2.1 Analysis of variance results exploring species-specific effects of light availability, nitrogen fertilization, and their interactions on carbon costs to acquire nitrogen (N_{cost}), whole-plant nitrogen biomass (N_{wp}), and root carbon biomass (C_{bg})	17
2.2 Analysis of variance results exploring effects of light availability, nitrogen fertilization, and their interactions on <i>G. max</i> root nodule biomass and the ratio of root nodule biomass to root biomass*	24
2.3 Slopes of the regression line describing the relationship between each dependent variable and nitrogen fertilization at each light level*	25
3.1 Effects of soil N availability, soil pH, and species on leaf N content per unit leaf area (N_{area}), leaf N content per unit leaf mass (N_{mass}), and leaf mass per unit leaf area (M_{area})	52
3.2 Effects of soil N availability, soil pH, species, and N_{area} on leaf biochemistry	55
3.3 Effects of soil N availability, soil pH, and species on the proportion of leaf nitrogen content allocated to photosynthesis, Rubisco, bioenergetics, and structure	58
3.4 Effects of soil N availability, soil pH, species, and N_{area} on tradeoffs between nitrogen and water use	61

4.1	Site locality information, sampling year(s), 2006-2020 mean annual precipitation (MAP; mm), mean annual temperature (MAT; °C), and water holding capacity (WHC; mm)*	81
4.2	Effects of soil moisture, soil nitrogen availability, and plant functional group on β	90
4.3	Effects of soil moisture, soil nitrogen availability, and plant functional group on χ^*	93
4.4	Effects of soil nitrogen fertilization, inoculation, and CO ₂ treatments on N_{area} , N_{mass} , and M_{area}	97
4.5	Structural equation model results investigating direct effects of climatic and soil resource availability on N_{area} , N_{mass} , M_{area} , χ , and β	100
5.1	Effects of soil nitrogen fertilization, inoculation, and CO ₂ treatments on N_{area} , N_{mass} , M_{area} , and Chl_{area}	123
5.2	Effects of soil nitrogen fertilization, inoculation, and CO ₂ on leaf biochemistry	127
5.3	Effects of soil N availability, soil pH, species, and N_{area} on leaf nitrogen allocation	131
5.4	Effects of soil N availability, soil pH, species, and N_{area} on total leaf area, whole plant biomass, and costs of nitrogen acquisition	135
5.5	Effects of soil N availability, soil pH, species, and N_{area} on root nodule biomass and plant investments in symbiotic nitrogen fixation	139

List of Figures

2.1 Relationships between soil nitrogen fertilization and light availability on carbon costs to acquire nitrogen in <i>G. hirsutum</i> and <i>G. max</i>	18
2.2 Relationships between soil nitrogen fertilization and light availability on whole-plant nitrogen biomass in <i>G. hirsutum</i> and <i>G. max</i>	20
2.3 Relationships between soil nitrogen fertilization and light availability on root carbon biomass in <i>G. hirsutum</i> and <i>G. max</i>	22
2.4 Effects of shade cover and nitrogen fertilization on root nodule biomass and the ratio of root nodule biomass to root biomass in <i>G. max</i>	26
3.1 Effects of soil N availability and species on leaf N content per unit leaf area, leaf nitrogen content per unit leaf biomass, and leaf mass per leaf area	53
3.2 Effects of soil N availability, species, and leaf N content leaf biochemistry	56
3.3 Effects of soil N availability, species, and leaf N content on the fraction of leaf nitrogen allocated to photosynthesis and structure	59
3.4 Effects of soil N availability, species, and leaf N content on tradeoffs between nitrogen and water use	62
4.1 Maps that detail site locations along 2006-2020 mean annual precipitation and mean annual temperature gradients in Texas, USA.	82

4.2 Effects of soil nitrogen availability and soil moisture on the unit cost ratio β	91
4.3 Effects of 4-day mean vapor pressure deficit, 2-day soil moisture (per water holding capacity), and soil nitrogen availability on χ	94
4.4 Effects of χ , soil nitrogen availability, and soil moisture on leaf nitrogen content per unit leaf area, leaf nitrogen content per unit leaf biomass, and leaf mass per area.	98
4.5 Structural equation model results exploring direct and indirect drivers of N_{area}	101
5.1 Effects of CO_2 , fertilization, and inoculation on leaf nitrogen per unit leaf area, leaf nitrogen content, leaf mass per unit leaf area, and chlorophyll content per unit leaf area.	124
5.2 Effects of CO_2 , fertilization, and inoculation on maximum rate of Rubisco carboxylation, the maximum rate of RuBP regeneration, and the ratio of the maximum rate of RuBP regeneration to the maximum rate of Rubisco carboxylation leaf mass per unit leaf area, dark respiration, stomatal conductance, and stomatal limitation.	128
5.3 Effects of CO_2 , fertilization, and inoculation on the relative fraction of leaf nitrogen allocated to photosynthesis and the fraction of leaf nitrogen allocated to structure.	132
5.4 Effects of CO_2 , fertilization, and inoculation on total leaf area, total biomass, and structural carbon costs to acquire nitrogen.	136

5.5 Effects of CO ₂ , fertilization, and inoculation on nodule biomass, nodule: root biomass, and percent nitrogen fixed from the atmo- sphere.	140
--	-----

1 Chapter 1

2 Introduction

3 Photosynthesis represents the largest carbon flux between the atmosphere
4 and biosphere, and is regulated by complex ecosystem carbon and nutrient cy-
5 cles (Hungate et al. 2003; IPCC 2021). As a result, the inclusion of robust,
6 empirically tested representations of photosynthetic processes is critical in order
7 for terrestrial biosphere models to accurately and reliably simulate carbon and
8 nutrient fluxes between the atmosphere and terrestrial biosphere (Wieder et al.
9 2015; Smith and Dukes 2013; Prentice et al. 2015; Oreskes et al. 1994). Despite
10 evidence that the inclusion of coupled carbon and nutrient cycles can improve
11 model uncertainty, widespread divergence in predicted carbon and nutrient fluxes
12 is still apparent across model products (Arora et al. 2020; Friedlingstein et al.
13 2014; Davies-Barnard et al. 2020). Divergence in predicted carbon and nutrient
14 fluxes across terrestrial biosphere models may be due to an incomplete under-
15 standing of how plants acclimate to changing environments (Smith and Dukes
16 2013; Davies-Barnard et al. 2020), as terrestrial biosphere models are sensitive to
17 the formulation of photosynthetic processes (Ziehn et al. 2011; Bonan et al. 2011;
18 Booth et al. 2012; Smith et al. 2016; Smith et al. 2017; Rogers et al. 2017).

Many terrestrial biosphere models predict leaf-level photosynthesis through linear relationships between area-based leaf nitrogen content and the maximum rate of Ribulose-1,5-bisphosphate carboxylase/oxygenase ("Rubisco"), following from the idea that large fractions of leaf nitrogen content are allocated to the construction and maintenance of Rubisco and other photosynthetic enzymes (Evans

24 1989). The inclusion of coupled carbon and nutrient cycles in terrestrial biosphere
25 models (Shi et al. 2016; Braghieri et al. 2022) allows for the prediction of leaf ni-
26 trogen content through soil nitrogen availability, which causes models to indirectly
27 predict photosynthetic processes through shifts in soil nitrogen availability (Smith
28 et al. 2014; Lawrence et al. 2019). While these patterns are commonly observed
29 in ecosystems globally (Brix 1971; Evans 1989; Liang et al. 2020; Firn et al. 2019),
30 this formulation of photosynthetic processes does not allow for the prediction of
31 leaf and whole plant acclimation responses to changing environments (Smith and
32 Dukes 2013; Rogers et al. 2017; Harrison et al. 2021), and suggests that con-
33 stant leaf nitrogen-photosynthesis relationships are ubiquitous across ecosystems.
34 Incorporating leaf and whole plant acclimation schemes in terrestrial biosphere
35 models is important (Smith and Dukes 2013), particularly because recent work
36 indicates that variance in leaf nitrogen content and leaf photosynthesis across en-
37 vironmental gradients may be better explained as an integrated product of leaf
38 acclimation responses to changing climates and soil nitrogen availability than soil
39 nitrogen availability alone (Dong et al. 2017; Dong et al. 2020; Smith et al. 2019;
40 Querejeta et al. 2022; Dong et al. 2022; Westerband et al. 2023).

41 Photosynthetic least-cost theory (Prentice et al. 2014; Wang et al. 2017;
42 Smith et al. 2019; Scott and Smith 2022; Harrison et al. 2021) provides a con-
43 temporary framework for predicting leaf and whole plant acclimation responses
44 to environmental change. The theory, which unifies photosynthetic optimal coor-
45 dination (Chen et al. 1993; Maire et al. 2012) and least-cost (Wright et al. 2003)
46 theories, posits that plants optimize photosynthetic processes by minimizing the
47 summed cost of nitrogen and water use (referred to here and in the rest of this dis-

48 sertation as β). The minimized summed cost of nitrogen and water use is dictated
49 by the ratio of intercellular CO₂ to atmospheric CO₂ (referred to here and in the
50 rest of this dissertation as leaf C_a:C_a, or χ), which is determined by factors that
51 influence leaf nitrogen demand, such as CO₂, temperature, vapor pressure deficit,
52 and light availability (Prentice et al. 2014; Smith et al. 2019; Stocker et al. 2020;
53 Wang et al. 2017). Photosynthetic processes are optimized such that nitrogen
54 is allocated to photosynthetic enzymes in to allow net photosynthesis rates to be
55 equally co-limited by the maximum rate of Rubisco carboxylation and the max-
56 imum rate of Ribulose-1,5-bisphosphate (RuBP) regeneration (Chen et al. 1993;
57 Maire et al. 2012). The theory indicates that costs of nitrogen and water use
58 are substitutable such that, in a given environment, optimal photosynthesis rates
59 can be achieved by sacrificing inefficient use of a relatively more abundant (and
60 less costly to acquire) resource for more efficient use of a relatively less abundant
61 (and more costly to acquire) resource. These predictions imply that acclimation
62 responses to changing environments may be partially driven by trade-offs between
63 nitrogen and water use, though empirical tests of the theory are sparse.

64 Optimality models leveraging patterns expected from photosynthetic least-
65 cost theory have been developed for both C₃ (Wang et al. 2017; Smith et al. 2019;
66 Stocker et al. 2020) and more recently for C₄ species (Scott and Smith 2022). Such
67 models show broad agreement with patterns observed across environmental gradi-
68 ents (Paillassa et al. 2020; Querejeta et al. 2022; Smith et al. 2019; Westerband
69 et al. 2023), and are capable of reconciling dynamic leaf nitrogen-photosynthesis
70 relationships and acclimation responses to elevated CO₂, temperature, light avail-
71 ability, and vapor pressure deficit (Dong et al. 2017; Dong et al. 2020; Dong et al.

72 2022; Dong et al. 2022; Smith and Keenan 2020; Luo et al. 2021; Peng et al. 2021;
73 Querejeta et al. 2022; Westerband et al. 2023). Current versions of optimality
74 models that invoke patterns expected from photosynthetic least-cost theory hold
75 β constant across growing environments. As growing evidence suggests that costs
76 of nitrogen use change across resource availability and climatic gradients in species
77 with different nutrient acquisition strategies (Fisher et al. 2010; Brzostek et al.
78 2014; Allen et al. 2020; Terrer et al. 2018), one might expect that β should
79 dynamically change across environments and in species with different acquisition
80 strategies. However, manipulative experiments that test mechanisms underlying
81 nitrogen-water use trade-offs and leaf nitrogen-photosynthesis relationships pre-
82 dicted from theory across soil resource availability and climatic gradients are rare.
83 Furthermore, no study has related shifts in β to nitrogen-water use trade-offs or
84 leaf nitrogen-photosynthesis relationships. Understanding the dynamic nature of
85 β across different environmental contexts and impacts of β on patterns expected
86 from theory are critical for further optimality model development, and is the cen-
87 tral motivation for the experiments presented in this dissertation.

88 In this dissertation, I use four experiments to quantify nutrient acquisition
89 and allocation responses under different environmental conditions and in species
90 with different nutrient acquisition strategies. These experiments provide impor-
91 tant empirical data needed to evaluate patterns expected from photosynthetic
92 least-cost theory and test mechanisms that drive such patterns. In the first ex-
93 perimental chapter, I re-analyze data from a greenhouse experiment that grew
94 *Glycine max* L. (Merr) and *Gossypium hirsutum* seedlings under full-factorial
95 combinations of four light treatments and four fertilization treatments. This re-

96 analysis examined the effect of soil nitrogen availability and light availability on
97 structural carbon costs to acquire nitrogen in a species capable of forming associa-
98 tions with symbiotic nitrogen-fixing bacteria (*G. max*) and a species not capable
99 of forming such associations (*G. hirsutum*). I find strong evidence suggesting that
100 increasing light availability increases structural carbon costs to acquire nitrogen
101 and that increasing soil nitrogen fertilization decreases structural carbon costs to
102 acquire nitrogen.

103 In the second experimental chapter, I measure leaf physiological traits in
104 the upper canopy of mature trees growing in a 9-year nitrogen-by-pH field manip-
105 ulation experiment to assess whether changes in soil nitrogen availability or soil
106 pH modify nitrogen-water use trade-offs expected from photosynthetic least-cost
107 theory. I find strong nitrogen-water use trade-offs in response to increasing soil ni-
108 trogen availability, indicated by a strong negative relationship between leaf $C_i:C_a$
109 (referred to here and in the rest of this dissertation as χ) and leaf nitrogen content,
110 as well as a strong increase in leaf nitrogen content per unit leaf χ with increas-
111 ing soil nitrogen availability. Interestingly, I also find a null effect of soil pH on
112 nitrogen-water use trade-offs. These patterns provide strong support for patterns
113 expected from photosynthetic least-cost theory across soil nitrogen availability
114 gradients, and indicate that previous studies which note strong nitrogen-water
115 use trade-offs in response to soil pH may be driven by covariation between soil
116 nitrogen availability and soil pH (Paillassa et al. 2020; Westerband et al. 2023).

117 In the third experimental chapter, I leverage a broad precipitation and soil
118 nutrient availability gradient in Texan grasslands to investigate primary drivers of
119 leaf nitrogen content. In this chapter, I directly quantify β and χ using leaf $\delta^{13}\text{C}$ to

120 examine primary drivers of leaf nitrogen content and find that leaf nitrogen content
121 is driven through a negative relationship with χ . I also show that soil nitrogen
122 availability is negatively associated with β , and that β is positively associated
123 with χ . I show strong support for patterns expected from theory, showing for
124 the first time that positive effects of increasing soil nitrogen availability on leaf
125 nitrogen content are mediated by changes in β .

126 In the fourth experimental chapter, I use reach-in growth chambers to
127 quantify leaf and whole plant acclimation responses to CO₂ across a soil nitro-
128 gen fertilization gradient, while also manipulating nutrient acquisition strategy
129 by controlling whether seedlings were able to form associations with symbiotic
130 nitrogen-fixing bacteria. Specifically, I measure leaf physiological and whole plant
131 growth responses of 7-week *G. max* seedlings grown under one of two CO₂ treat-
132 ments, one of nine fertilization treatments, and one of two inoculation treatments
133 in a full factorial design. I find a down-regulation in leaf nitrogen content and
134 leaf photosynthesis under elevated CO₂, a pattern that is not modified across
135 the fertilization gradient or between inoculation treatments. However, I also find
136 strong stimulation in total leaf area and whole plant growth under elevated CO₂
137 that are enhanced with increasing fertilization. There was no observable effect of
138 inoculation in modifying whole plant growth responses to CO₂, which I speculate
139 is the result of a down-regulation in plant investments to nitrogen fixation with
140 increasing fertilization. Results from this experiment provide strong evidence sug-
141 gesting that leaf acclimation responses to CO₂ were controlled by optimal resource
142 investment to photosynthetic capacity, following patterns expected from photo-
143 synthetic least-cost theory, and suggest divergent roles of soil nitrogen fertilization

144 in modifying leaf and whole plant acclimation responses to CO₂.

145 Throughout the four experimental chapters, I find strong and consistent
146 patterns supportive of patterns expected from photosynthetic least-cost theory.
147 Specifically, I find strong nitrogen-water use trade-offs in response to changing
148 climates and soil resources, that shifts in soil nitrogen availability have strong
149 negative impacts on costs of nitrogen acquisition, and therefore tend to increase
150 β , and that constant leaf nitrogen-photosynthesis relationships only occur in sys-
151 tems where nitrogen is limiting. In a final conclusion chapter, I summarize ma-
152 jor findings from each of the four experimental chapters and synthesize common
153 mechanisms that drive leaf and whole plant responses to changing environmen-
154 tal conditions. I conclude this dissertation with brief dialogue on lessons learned
155 throughout experimental chapters, and propose future experiments that will tar-
156 get additional uncertainties in photosynthetic least-cost theory responses across
157 environmental gradients.

158

Chapter 2

159

Structural carbon costs to acquire nitrogen are determined by
160 nitrogen and light availability in two species with different nitrogen
161 acquisition strategies

162 2.1 Introduction

163

Carbon and nitrogen cycles are tightly coupled in terrestrial ecosystems.

164

This tight coupling influences photosynthesis (Walker et al. 2014; Rogers et al.

165

2017), net primary productivity (LeBauer and Treseder 2008; Thomas et al. 2013),

166

decomposition (Cornwell et al. 2008; Bonan et al. 2013; Sulman et al. 2019), and

167

plant resource competition (Gill and Finzi 2016; Xu-Ri and Prentice 2017). Ter-

168

restrial biosphere models are beginning to include connected carbon and nitrogen

169

cycles to improve the realism of their simulations (Fisher et al. 2010; Brzostek

170

et al. 2014; Wieder et al. 2015; Shi et al. 2016; Zhu et al. 2019). Simula-

171

tions from these models indicate that coupling carbon and nitrogen cycles can

172

drastically influence future biosphere-atmosphere feedbacks under global change,

173

such as elevated carbon dioxide or nitrogen deposition (Thornton et al. 2007;

174

Goll et al. 2012; Wieder et al. 2015; Wieder et al. 2019). Nonetheless, there

175

are still limitations in our quantitative understanding of connected carbon and

176

nitrogen dynamics (Thomas et al. 2015; Meyerholt et al. 2016; Rogers et al.

177

2017; Exbrayat et al. 2018; Shi et al. 2019), forcing models to make potentially

178

unreliable assumptions.

179

Plant nitrogen acquisition is a process in terrestrial ecosystems by which

180

carbon and nitrogen are tightly coupled (Vitousek and Howarth 1991; Delaire

181

et al. 2005; Brzostek et al. 2014). Plants must allocate photosynthetically de-

182 rived carbon belowground to produce and maintain root systems or exchange with
183 symbiotic soil microbes in order to acquire nitrogen (Högberg et al. 2008; Hög-
184 berg et al. 2010). Thus, plants have an inherent carbon cost associated with
185 acquiring nitrogen, which can include both direct energetic costs associated with
186 nitrogen acquisition and indirect costs associated with building structures that
187 support nitrogen acquisition (Gutschick 1981; Rastetter et al. 2001; Vitousek
188 et al. 2002; Menge et al. 2008). Model simulations (Fisher et al. 2010; Brzostek
189 et al. 2014; Shi et al. 2016; Allen et al. 2020) and meta-analyses (Terrer et al.
190 2018) suggest that these carbon costs vary between species, particularly those
191 with different nitrogen acquisition strategies. For example, simulations using iter-
192 ations of the Fixation and Uptake of Nitrogen (FUN) model indicate that species
193 that acquire nitrogen from non-symbiotic active uptake pathways (e.g. mass flow)
194 generally have larger carbon costs to acquire nitrogen than species that acquire
195 nitrogen through symbiotic associations with nitrogen-fixing bacteria (Brzostek
196 et al. 2014; Allen et al. 2020).

197 Carbon costs to acquire nitrogen likely vary in response to changes in soil
198 nitrogen availability. For example, if the primary mode of nitrogen acquisition
199 is through non-symbiotic active uptake, then nitrogen availability could decrease
200 carbon costs to acquire nitrogen as a result of increased per-root nitrogen up-
201 take (Franklin et al. 2009; Wang et al. 2018). However, if the primary mode of
202 nitrogen acquisition is through symbiotic active uptake, then nitrogen availabil-
203 ity may incur additional carbon costs to acquire nitrogen if it causes microbial
204 symbionts to shift toward parasitism along the parasitism–mutualism continuum
205 (Johnson et al. 1997; Hoek et al. 2016; Friel and Friesen 2019) or if it reduces

206 the nitrogen acquisition capacity of a microbial symbiont (van Diepen et al. 2007;
207 Soudzilovskaia et al. 2015; Muñoz et al. 2016). Species may respond to shifts in
208 soil nitrogen availability by switching their primary mode of nitrogen acquisition
209 to a strategy with lower carbon costs to acquire nitrogen in order to maximize
210 the magnitude of nitrogen acquired from a belowground carbon investment and
211 outcompete other individuals for soil resources (Rastetter et al. 2001; Menge et al.
212 2008).

213 Environmental conditions that affect demand to acquire nitrogen to sup-
214 port new and existing tissues could also be a source of variance in plant carbon
215 costs to acquire nitrogen. For example, an increase in plant nitrogen demand could
216 increase carbon costs to acquire nitrogen if this increases the carbon that must be
217 allocated belowground to acquire a proportional amount of nitrogen (Kulmatiski
218 et al. 2017; Noyce et al. 2019). This could be driven by a temporary state of
219 diminishing return associated with investing carbon toward building and main-
220 taining structures that are necessary to support enhanced nitrogen uptake, such
221 as fine roots (Matamala and Schlesinger 2000; Norby et al. 2004; Arndal et al.
222 2018), mycorrhizal hyphae (Saleh et al. 2020), or root nodules (Parvin et al. 2020).
223 Alternatively, if the environmental factor that increases plant nitrogen demand
224 causes nitrogen to become more limiting in the system (e.g. atmospheric CO₂;
225 Luo et al. (2004), LeBauer and Treseder (2008), Vitousek et al. (2010), Liang
226 et al. (2016)), species might switch their primary mode of nitrogen acquisition to
227 a strategy with lower relative carbon costs to acquire nitrogen in order to gain a
228 competitive advantage over species with either different or more limited modes of
229 nitrogen acquisition (Ainsworth and Long 2005; Taylor and Menge 2018).

230 Using a plant economics approach, I examined the influence of plant ni-
231 trogen demand and soil nitrogen availability on plant carbon costs to acquire
232 nitrogen. This was done by growing a species capable of forming associations
233 with nitrogen-fixing bacteria (*Glycine max* L. (Merr)) and a species not capable
234 of forming these associations (*Gossypium hirsutum* L.) under four levels of light
235 availability (plant nitrogen demand proxy) and four levels of soil nitrogen fertil-
236 ization (soil nitrogen availability proxy) in a full-factorial, controlled greenhouse
237 experiment. I used this experimental set-up to test the following hypotheses:

- 238 1. An increase in plant nitrogen demand due to increasing light availability will
239 increase carbon costs to acquire nitrogen through a proportionally larger
240 increase in belowground carbon than whole-plant nitrogen acquisition. This
241 will be the result of an increased investment of carbon toward belowground
242 structures that support enhanced nitrogen uptake, but at a lower nitrogen
243 return.
- 244 2. An increase in soil nitrogen availability will decrease carbon costs to acquire
245 nitrogen as a result of increased per root nitrogen uptake in *G. hirsutum*.
246 However, soil nitrogen availability will not affect carbon costs to acquire
247 nitrogen in *G. max* because of the already high return of nitrogen supplied
248 through nitrogen fixation.

249 2.2 Methods

250 2.2.1 *Experiment setup*

251 *Gossypium hirsutum* and *G. max* were planted in individual 3 liter pots
252 (NS-300; Nursery Supplies, Orange, CA, USA) containing a 3:1 mix of unfertil-
253 ized potting mix (Sungro Sunshine Mix #2, Agawam, MA, USA) to native soil
254 extracted from an agricultural field most recently planted with *G. max* at the
255 USDA-ARS Laboratory in Lubbock, TX, USA (33.59°N, -101.90°W). The field
256 soil was classified as Amarillo fine sandy loam (75% sand, 10% silt, 15% clay).
257 Upon planting, all *G. max* pots were inoculated with *Bradyrhizobium japonicum*
258 (Verdesian N-Dure™ Soybean, Cary, NC, USA) to stimulate root nodulation. In-
259 dividuals of both species were grown under similar, unshaded, ambient greenhouse
260 conditions for 2 weeks to germinate and begin vegetative growth. Three blocks
261 were set up in the greenhouse, each containing four light treatments created us-
262 ing shade cloth that reduced incoming radiation by either 0 (full sun), 30, 50,
263 or 80%. Two weeks post-germination, individuals were randomly placed in the
264 four light treatments in each block. Individuals received one of four nitrogen fer-
265 tilization doses as 100ml of a modified Hoagland solution (Hoagland and Arnon
266 1950) equivalent to either 0, 70, 210, or 630 ppm N twice per week within each
267 light treatment. Nitrogen fertilization doses were received as topical agents to
268 the soil surface. Each Hoagland solution was modified to keep concentrations of
269 other macro- and micronutrients equivalent (Supplementary Table S1). Plants
270 were routinely well watered to eliminate water stress.

271 2.2.2 *Plant measurements and calculations*

272 Each individual was harvested after 5 weeks of treatment, and biomass
273 was separated by organ type (leaves, stems, and roots). Nodules on *G. max*
274 roots were also harvested. Except for the 0% shade cover and 630 ppm N treat-
275 ment combination, all treatment combinations in both species had lower average
276 dry biomass:pot volume ratios than the 1:1 ratio recommended by Poorter et al.
277 (2012) to minimize the likelihood of pot volume-induced growth limitation (Sup-
278 plementary Tables S2, S3; Supplementary Fig. S1). All harvested material was
279 dried, weighed, and ground by organ type. Carbon and nitrogen content (g g^{-1})
280 was determined by subsampling from ground and homogenized biomass of each
281 organ type using an elemental analyzer (Costech 4010; Costech, Inc., Valencia,
282 CA, USA). We scaled these values to total leaf, stem, and root carbon and ni-
283 trogen biomass (g) by multiplying dry biomass of each organ type by carbon or
284 nitrogen content of each corresponding organ type. Whole-plant nitrogen biomass
285 (g) was calculated as the sum of total leaf (g), stem (g), and root (g) nitrogen
286 biomass. Root nodule carbon biomass was not included in the calculation of root
287 carbon biomass; however, relative plant investment toward root or root nodule
288 standing stock was estimated as the ratio of root biomass to root nodule biomass
289 (g g^{-1}), following similar metrics to those adopted by Dovrat et al. (2018) and
290 Dovrat et al. (2020).

291 Carbon costs to acquire nitrogen (N_{cost} ; gC gN^{-1}) were estimated as the
292 ratio of total root carbon biomass (C_{bg} ; gC) to whole-plant nitrogen biomass
293 (N_{wp} ; gN). This calculation quantifies the relationship between carbon spent on
294 nitrogen acquisition and whole-plant nitrogen acquisition by using root carbon

295 biomass as a proxy for estimating the magnitude of carbon allocated toward ni-
296 trogen acquisition. This calculation therefore assumes that the magnitude of root
297 carbon standing stock is proportional to carbon transferred to root nodules or my-
298 corrhizae, or lost through root exudation or turnover. The assumption has been
299 supported in species that associate with ectomycorrhizal fungi (Hobbie 2006; Hob-
300 bie and Hobbie 2008), but is less clear in species that acquire nitrogen through
301 non-symbiotic active uptake or symbiotic nitrogen fixation. It is also unclear
302 whether relationships between root carbon standing stock and carbon transfer to
303 root nodules are similar in magnitude to carbon lost through exudation or when
304 allocated toward other active uptake pathways. Thus, because of the way mea-
305 surements were calculated, proximal values of carbon costs to acquire nitrogen are
306 underestimates.

307 2.2.3 *Statistical analyses*

308 I explored the effects of light and nitrogen availability on carbon costs to ac-
309 quire nitrogen using separate linear mixed-effects models for each species. Models
310 included shade cover, nitrogen fertilization, and interactions between shade cover
311 and nitrogen fertilization as continuous fixed effects, and also included block as a
312 random intercept term. Three separate models for each species were built with
313 this independent variable structure for three different dependent variables: (i)
314 carbon costs to acquire nitrogen (gC gN^{-1}); (ii) whole plant nitrogen biomass (de-
315 nominator of carbon cost to acquire nitrogen; gN); and (iii) belowground carbon
316 biomass (numerator of carbon cost to acquire nitrogen; gC). I constructed two
317 additional models for *G. max* with the same model structure described above to

318 investigate the effects of light availability and nitrogen fertilization on root nodule
319 biomass (g) and the ratio of root nodule biomass to root biomass (unitless).

320 I used Shapiro–Wilk tests of normality to determine whether species spe-
321 cific linear mixed-effects model residuals followed a normal distribution. None of
322 our models satisfied residual normality assumptions when models were fit using
323 untransformed data (Shapiro–Wilk: $p < 0.05$ in all cases). I attempted to satisfy
324 residual normality assumptions by first fitting models using dependent variables
325 that were natural-log transformed. If residual normality assumptions were still
326 not met (Shapiro–Wilk: $p < 0.05$), then models were fit using dependent variables
327 that were square root transformed. All residual normality assumptions were satis-
328 fied when models were fit with either a natural-log or square root transformation
329 (Shapiro–Wilk: $p > 0.05$ in all cases). Specifically, I natural-log transformed *G.*
330 *hirsutum* carbon costs to acquire nitrogen and *G. hirsutum* whole-plant nitrogen
331 biomass. I also square root transformed *G. max* carbon costs to acquire nitrogen,
332 *G. max* whole-plant nitrogen biomass, root carbon biomass in both species, *G.*
333 *max* root nodule biomass, and the *G. max* ratio of root nodule biomass to root
334 biomass. I used the ‘lmer’ function in the ‘lme4’ R package (Bates et al. 2015) to
335 fit each model and the ‘Anova’ function in the ‘car’ R package (Fox and Weisberg
336 2019) to calculate Wald’s χ^2 to determine the significance ($\alpha = 0.05$) of each fixed
337 effect coefficient. Finally, I used the ‘emmeans’ R package (Lenth 2019) to conduct
338 post-hoc comparisons of our treatment combinations using Tukey’s tests. Degrees
339 of freedom for all Tukey’s tests were approximated using the Kenward–Roger ap-
340 proach (Kenward and Roger 1997). All analyses and plots were conducted in R
341 version 4.0.1 (R Core Team 2021).

342 2.3 Results

343 2.3.1 *Carbon costs to acquire nitrogen*

344 Carbon costs to acquire nitrogen in *G. hirsutum* increased with increasing
345 light availability ($p < 0.001$; Table 2.1; Fig. 2.1) and decreased with increasing
346 nitrogen fertilization ($p < 0.001$; Table 2.1; Fig. 2.1). There was no interaction
347 between light availability and nitrogen fertilization ($p = 0.486$, Table 2.1; Fig.
348 2.1).

349 Carbon costs to acquire nitrogen in *G. max* also increased with increasing
350 light availability ($p < 0.001$, Table 2.1; Fig. 2.1) and decreased with increasing
351 nitrogen fertilization ($p < 0.001$; Table 2.1; Fig. 2.1). There was no interaction
352 between light availability and nitrogen fertilization ($p = 0.261$, Table 2.1; Fig.
353 2.1).

Table 2.1. Analysis of variance results exploring species-specific effects of light availability, nitrogen fertilization, and their interactions on carbon costs to acquire nitrogen (N_{cost}), whole-plant nitrogen biomass (N_{wp}), and root carbon biomass (C_{bg})

	df	N_{cost}			N_{wp}			C_{bg}		
		Coefficient	χ^2	p	Coefficient	χ^2	p	Coefficient	χ^2	p
<i>G. hirsutum</i>										
Intercept		1.594	-	-	-3.232	-	-	0.432	-	-
Light (L)	1	-1.09E-02	56.494	<0.001	-6.41E-03	91.275	<0.001	-2.62E-03	169.608	<0.001
Nitrogen (N)	1	-1.34E-03	54.925	<0.001	1.83E-03	118.784	<0.001	1.15E-04	2.901	0.089
L*N	1	3.88E-06	0.485	0.486	-1.34E-05	10.721	0.001	-1.67E-06	3.140	0.076
<i>G. max</i>										
Intercept		1.877	-	-	0.239	-	-	0.438	-	-
Light (L)	1	-7.67E-03	174.156	<0.001	-6.72E-04	39.799	<0.001	-2.55E-03	194.548	<0.001
Nitrogen (N)	1	-2.35E-04	21.948	<0.001	1.55E-04	70.771	<0.001	2.52E-04	19.458	<0.001
L*N	1	-2.89E-06	1.262	0.261	-6.32E-07	1.435	0.231	-3.16E-06	10.803	0.001

354 *Significance determined using Wald's χ^2 tests ($P = 0.05$). P -values < 0.05 are in bold and p -values between 0.05 and
 355 0.1 are italicized. Negative coefficients for light treatments indicate a positive effect of increasing light availability
 356 on all response variables, as light availability is treated as percent shade cover in all linear mixed-effects models.

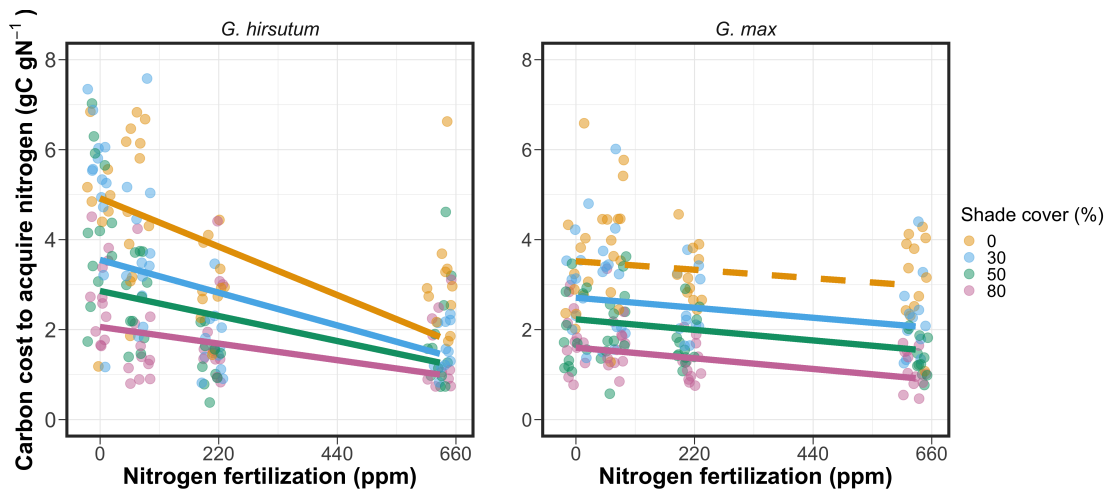


Figure 2.1. Relationships between soil nutrient fertilization and light availability on carbon costs to acquire nitrogen in *G. hirsutum* and *G. max*. Nitrogen fertilization treatments are represented on the x-axis. Shade cover treatments are represented through colored points and trendlines. Trendlines were created by back-transforming marginal mean slopes and intercepts from species-specific linear mixed-effects models. These values were calculated using the ‘emtrends’ and ‘emmmeans’ functions in the ‘emmeans’ R package (Lenth, 2019). Points are jittered for visibility. Yellow points and trendlines represent the 0% shade cover treatment, blue points and trendlines represent the 30% shade cover treatment, green points and trendlines represent the 50% shade cover treatment, and purple points and trendlines represent the 80% shade cover treatment. Solid trendlines indicate slopes that are significantly different from zero (Tukey: $p < 0.05$), while dashed trendlines indicate slopes that are not statistically different from zero.

357 2.3.2 *Whole plant nitrogen biomass*

358 Whole-plant nitrogen biomass in *G. hirsutum* was driven by an interaction
359 between light availability and nitrogen fertilization ($p = 0.001$; Table 2.1; Fig.
360 2.2). This interaction indicated a greater stimulation of whole-plant nitrogen
361 biomass by nitrogen fertilization as light levels increased (Table 2.1; Fig. 2.2).

362 Whole-plant nitrogen biomass in *G. max* increased with increasing light
363 availability ($p < 0.001$) and nitrogen fertilization ($p < 0.001$), with no interaction
364 between light availability and nitrogen fertilization ($p = 0.231$; Table 2.1; Fig.
365 2.2).

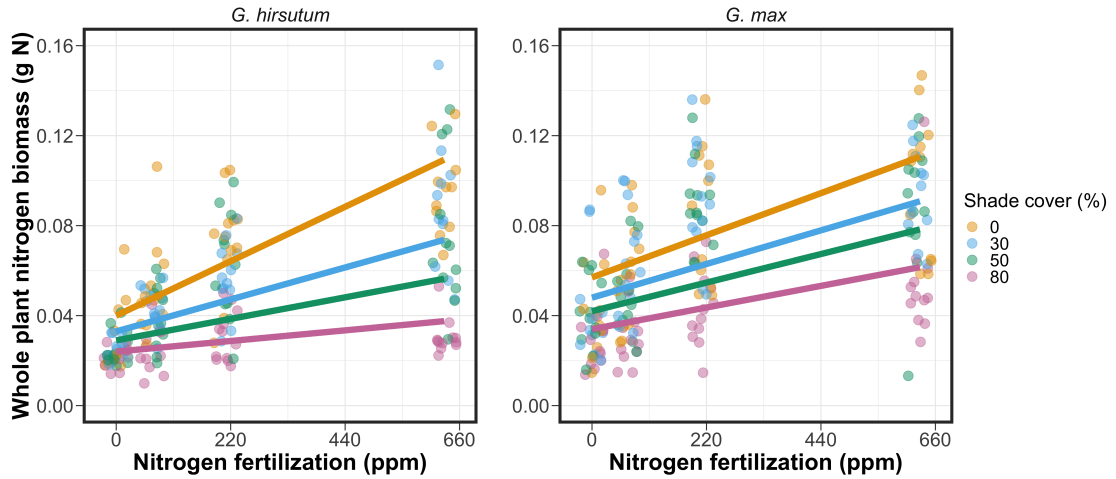


Figure 2.2. Relationships between soil nutrient fertilization and light availability on whole-plant nitrogen biomass in *G. hirsutum* and *G. max*. Whole-plant nitrogen biomass is the denominator of the carbon cost to acquire nitrogen calculation. Nitrogen fertilization treatments are represented on the x-axis. Shade cover treatments are represented through colored points and trendlines. Trendlines were created by back-transforming marginal mean slopes and intercepts from species-specific linear mixed-effects models. These values were calculated using the ‘emtrends’ and ‘emmmeans’ functions in the ‘emmeans’ R package (Lenth 2019). Points are jittered for visibility. Yellow points and trendlines represent the 0% shade cover treatment, blue points and trendlines represent the 30% shade cover treatment, green points and trendlines represent the 50% shade cover treatment, and purple points and trendlines represent the 80% shade cover treatment. Solid trendlines indicate slopes that are significantly different from zero (Tukey: $P < 0.05$), while dashed trendlines indicate slopes that are not statistically different from zero.

366 2.3.3 *Root carbon biomass*

367 Root carbon biomass in *G. hirsutum* significantly increased with increasing
368 light availability ($p < 0.001$; Table 2.1; Fig. 2.3) and marginally increased with
369 nitrogen fertilization ($p = 0.089$; Table 2.1; Fig. 2.3). There was also a marginal
370 interaction between light availability and nitrogen fertilization ($p = 0.076$; Table
371 2.1), driven by an increase in the positive response of root carbon biomass to
372 increasing nitrogen fertilization as light availability increased. This resulted in
373 significantly positive trends between root carbon biomass and nitrogen fertilization
374 in the two highest light treatments (Tukey: $p < 0.05$ in both cases; Table 2.3;
375 Fig. 2.3) and no effect of nitrogen fertilization in the two lowest light treatments
376 (Tukey: $p > 0.05$ in both cases; Table 2.3; Fig. 2.3).

377 There was an interaction between light availability and nitrogen fertiliza-
378 tion on root carbon biomass in *G. max* ($p = 0.001$; Table 2.1; Fig. 2.3). Post-hoc
379 analyses indicated that the positive effects of nitrogen fertilization on *G. max* root
380 carbon biomass increased with increasing light availability (Table 2.3; Fig. 2.3).
381 There were also positive individual effects of increasing nitrogen fertilization ($p <$
382 0.001) and light availability ($p < 0.001$) on *G. max* root carbon biomass (Table
383 2.1; Fig. 2.3).

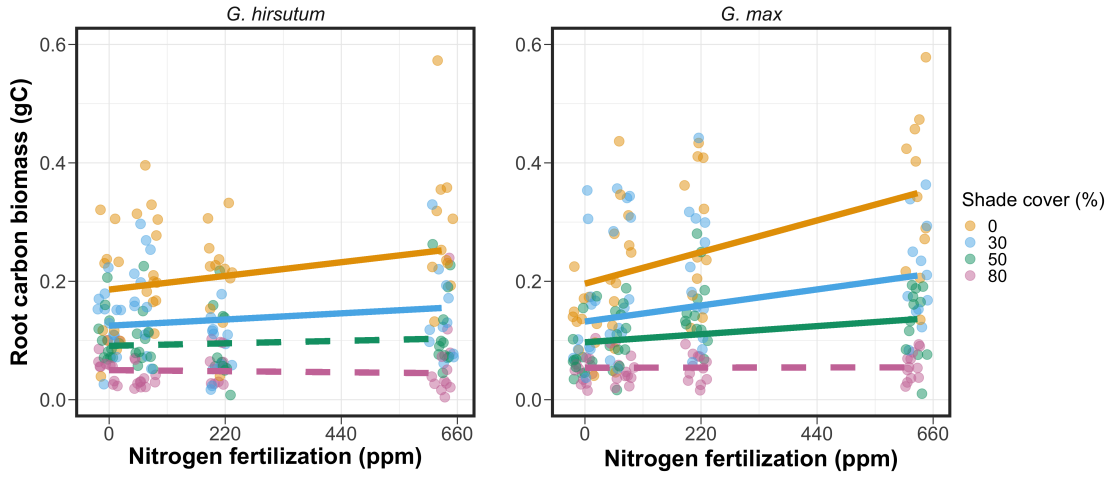


Figure 2.3. Relationships between soil nutrient fertilization and light availability on root carbon biomass in *G. hirsutum* and *G. max*. Root carbon biomass is the numerator of the carbon cost to acquire nitrogen calculation. Nitrogen fertilization treatments are represented on the x-axis. Shade cover treatments are represented through colored points and trendlines. Trendlines were created by back-transforming marginal mean slopes and intercepts from species-specific linear mixed-effects models. These values were calculated using the ‘emtrends’ and ‘emmmeans’ functions in the ‘emmeans’ R package (Lenth 2019). Points are jittered for visibility. Yellow points and trendlines represent the 0% shade cover treatment, blue points and trendlines represent the 30% shade cover treatment, green points and trendlines represent the 50% shade cover treatment, and purple points and trendlines represent the 80% shade cover treatment. Solid trendlines indicate slopes that are significantly different from zero (Tukey: $p < 0.05$), while dashed trendlines indicate slopes that are not statistically different from zero.

384 2.3.4 *Root nodule biomass*

385 Root nodule biomass in *G. max* increased with increasing light availability
386 ($p < 0.001$; Table 2.2; Fig. 2.4A) and decreased with increasing nitrogen fertiliza-
387 tion ($p < 0.001$; Table 2.2; Fig. 2.4A). There was no interaction between nitrogen
388 fertilization and light availability ($p = 0.133$; Table 2.2; Fig. 2.4A). The ratio of
389 root nodule biomass to root biomass did not change in response to light avail-
390 ability ($p = 0.481$; Table 2.2; Fig. 2.4B) but decreased with increasing nitrogen
391 fertilization ($p < 0.001$; Table 2.2; Fig. 2.4B). There was no interaction between
392 nitrogen fertilization and light availability on the ratio of root nodule biomass to
393 root biomass ($p = 0.621$; Table 2.2; Fig. 2.4B).

Table 2.2. Analysis of variance results exploring effects of light availability, nitrogen fertilization, and their interactions on *G. max* root nodule biomass and the ratio of root nodule biomass to root biomass*

	Nodule biomass			Nodule biomass: root biomass			<i>p</i>
	df	Coefficient	χ^2	<i>p</i>	Coefficient	χ^2	
(Intercept)		0.302	-	-	0.448	-	-
Light (L)	1	-1.81E-03	72.964	<0.001	-8.76E-05	0.496	0.481
Nitrogen (N)	1	-2.83E-04	115.377	<0.001	-5.09E-04	156.476	<0.001
L*N	1	1.14E-06	2.226	0.133	-7.30E-07	0.244	0.621

394 *Significance determined using Wald's χ^2 tests ($\alpha = 0.05$). *P*-values less than 0.05 are in bold. Negative coefficients
 395 for light treatments indicate a positive effect of increasing light availability on all response variables, as light avail-
 396 ability is treated as percent shade cover in all linear mixed-effects models. Root nodule biomass and nodule biomass:
 397 root biomass models were only constructed for *G. max* because *G. hirsutum* was not inoculated with *B. japonicum*
 398 and is not capable of forming root nodules.

Table 2.3. Slopes of the regression line describing the relationship between each dependent variable and nitrogen fertilization at each light level*

Shade cover	Carbon cost to acquire nitrogen	Whole plant N biomass	Belowground C biomass	Root nodule biomass	Nodule biomass: root biomass
<i>G. hirsutum</i>					
0%	-1.34E-03^a	1.83E-03^a	1.15E-04^b	-	-
30%	-1.22E-03^a	1.43E-03^a	1.17E-04^b	-	-
50%	-1.14E-03^a	1.17E-03^a	3.12E-05 ^b	-	-
80%	-1.02E-03^a	7.66E-04^a	-1.89E-06 ^b	-	-
<i>G. max</i>					
0%	-2.35E-04 ^b	1.55E-05^b	2.51E-04^b	-2.83E-04^b	-5.09E-04^b
30%	-3.22E-04^b	1.35E-05^b	1.57E-04^b	-2.49E-04^b	-5.31E-04^b
50%	-3.80E-04^b	1.23E-05^b	9.37E-05^b	-2.26E-04^b	-5.45E-04^b
80%	-4.66E-04^b	1.04E-05^b	-9.95E-07 ^b	-1.92E-04^b	-5.67E-04^b

25

399 *Slopes represent estimated marginal mean slopes from linear mixed-effects models described in the Methods. Slopes
 400 were calculated using the ‘emmeans’ R package (Lenth 2019). Superscripts indicate slopes fit to natural-log (^a) or
 401 square root (^b) transformed data. Slopes statistically different from zero (Tukey: $p < 0.05$) are indicated in bold.
 402 Marginally significant slopes (Tukey: $0.05 < p < 0.1$) are italicized.

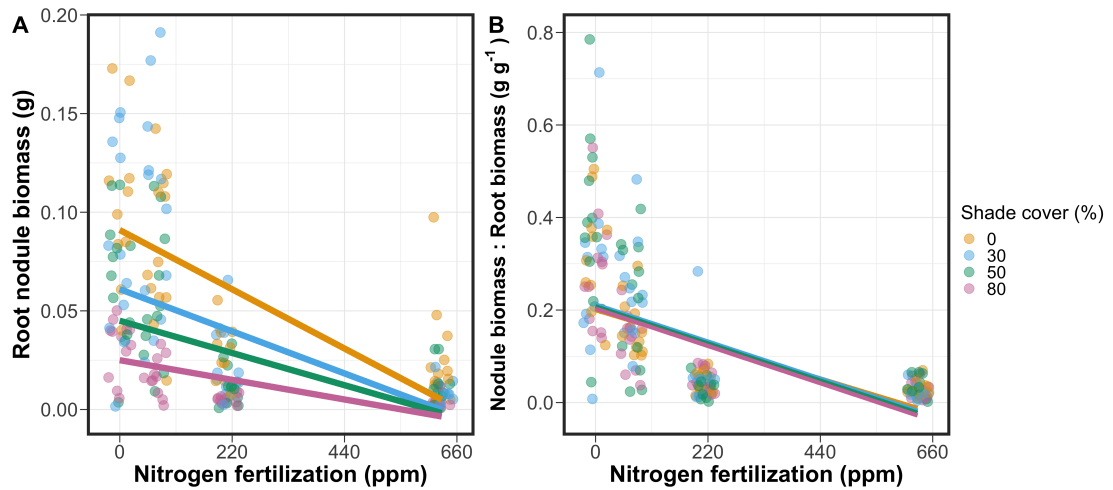


Figure 2.4. Effects of shade cover and nitrogen fertilization on root nodule biomass (A) and the ratio of root nodule biomass to root biomass (B) in *G. max*. Nitrogen fertilization treatments are represented on the x-axis. Shade cover treatments are represented through colored points and trendlines. Trendlines were created by back-transforming marginal mean slopes and intercepts from species-specific linear mixed-effects models. These values were calculated using the ‘emtrends’ and ‘emmeans’ functions in the ‘emmeans’ R package (Lenth 2019). Points are jittered for visibility. Yellow points and trendlines represent the 0% shade cover treatment, blue points and trendlines represent the 30% shade cover treatment, green points and trendlines represent the 50% shade cover treatment, and purple points and trendlines represent the 80% shade cover treatment. Solid trendlines indicate slopes that are significantly different from zero (Tukey: $p < 0.05$), while dashed trendlines indicate slopes that are not statistically different from zero.

403 2.4 Discussion

404 In this chapter, I determined the effects of light availability and soil ni-
405 trogen fertilization on root mass carbon costs to acquire nitrogen in *G. hirsutum*
406 and *G. max*. In support of my hypotheses, I found that carbon costs to acquire
407 nitrogen generally increased with increasing light availability and decreased with
408 increasing soil nitrogen fertilization in both species. These findings suggest that
409 carbon costs to acquire nitrogen are determined by factors that influence plant
410 nitrogen demand and soil nitrogen availability. In contrast to my second hypothe-
411 sis, root nodulation data suggested that *G. max* and *G. hirsutum* achieved similar
412 directional carbon cost responses to nitrogen fertilization despite a likely shift in
413 *G. max* allocation from nodulation to root biomass along the nitrogen fertilization
414 gradient (Fig. 2.4B).

415 Both *G. max* and *G. hirsutum* experienced an increase in carbon costs to
416 acquire nitrogen due to increasing light availability. These patterns were driven by
417 a larger increase in root carbon biomass than whole-plant nitrogen biomass. In-
418 creases in root carbon biomass due to factors that increase plant nitrogen demand
419 are a commonly observed pattern, as carbon allocated belowground provides sub-
420 strate needed to produce and maintain structures that satisfy aboveground plant
421 nitrogen demand (Nadelhoffer and Raich 1992; Giardina et al. 2005; Raich et al.
422 2014). Findings suggest that plants allocate relatively more carbon for acquiring
423 nitrogen when demand increases over short temporal scales, which may cause a
424 temporary state of diminishing return due to asynchrony between belowground
425 carbon and whole-plant nitrogen responses to plant nitrogen demand (Kulmatiski
426 et al. 2017; Noyce et al. 2019). These responses might be attributed to a temporal

427 lag associated with producing structures that enhance nitrogen acquisition. For
428 example, fine roots (Matamala and Schlesinger 2000; Norby et al. 2004; Arndal
429 et al. 2018) and root nodules (Parvin et al. 2020) take time to build and first
430 require the construction of coarse roots. Thus, full nitrogen returns from these
431 investments may not occur immediately (Kayler et al. 2010; Kayler et al. 2017),
432 and may vary by species acquisition strategy. I speculate that increases in ni-
433 trogen acquisition from a given carbon investment may occur beyond the 5-week
434 scope of this experiment. A similar study conducted over a longer temporal scale
435 would address this.

436 Increasing soil nitrogen fertilization generally decreased carbon costs to
437 acquire nitrogen in both species. These patterns were driven by a larger increase
438 in whole-plant nitrogen biomass than root carbon biomass. In *G. hirsutum*, re-
439 ductions in carbon costs to acquire nitrogen may have been due to an increase in
440 per-root nitrogen uptake, allowing individuals to maximize the amount of nitro-
441 gen acquired from a belowground carbon investment. Interestingly, increased soil
442 nitrogen fertilization increased whole-plant nitrogen biomass in *G. max* despite
443 reductions in root nodule biomass that likely reduced the nitrogen-fixing capac-
444 ity of *G. max* (Andersen et al. 2005; Muñoz et al. 2016). While reductions in
445 root nodulation due to increased soil nitrogen availability are commonly observed
446 (Gibson and Harper 1985; Fujikake et al. 2003), root nodulation responses were
447 observed in tandem with increased root carbon biomass, implying that *G. max*
448 shifted relative carbon allocation from nitrogen fixation to soil nitrogen acquisi-
449 tion (Markham and Zekveld 2007; Dovrat et al. 2020). This was likely because
450 there was a reduction in the carbon cost advantage of acquiring fixed nitrogen

451 relative to soil nitrogen, and suggests that species capable of associating with
452 symbiotic nitrogen-fixing bacteria shift their relative nitrogen acquisition path-
453 way to optimize nitrogen uptake (Rastetter et al. 2001). Future studies should
454 further investigate these patterns with a larger quantity of phylogenetically re-
455 lated species, or different varieties of a single species that differ in their ability to
456 form associations with symbiotic nitrogen-fixing bacteria to more directly test the
457 impact of nitrogen fixation on the patterns observed in this study.

458 Carbon costs to acquire nitrogen are subsumed in the general discussion of
459 economic analogies to plant resource uptake (Bloom et al. 1985; Rastetter et al.
460 2001; Vitousek et al. 2002; Phillips et al. 2013; Terrer et al. 2018; Henneron et al.
461 2020). Despite this, terrestrial biosphere models rarely include costs of nitrogen
462 acquisition within their framework for predicting plant nitrogen uptake. There
463 is currently one plant resource uptake model, FUN, that quantitatively predicts
464 carbon costs to acquire nitrogen within a framework for predicting plant nitrogen
465 uptake for different nitrogen acquisition strategies (Fisher et al. 2010; Brzostek
466 et al. 2014). Iterations of FUN are currently coupled to two terrestrial biosphere
467 models: the Community Land Model 5.0 and the Joint UK Land Environment
468 Simulator (Shi et al. 2016; Lawrence et al. 2019; Clark et al. 2011). Recent work
469 suggests that coupling FUN to CLM 5.0 caused a large overprediction of plant
470 nitrogen uptake associated with nitrogen fixation (Davies-Barnard et al. 2020)
471 compared to other terrestrial biosphere model products. Thus, empirical data
472 from manipulative experiments that explicitly quantify carbon costs to acquire
473 nitrogen in species capable of associating with nitrogen-fixing bacteria across dif-
474 ferent environmental contexts is an important step toward identifying potential

475 biases in models such as FUN.

476 My findings broadly support the FUN formulation of carbon costs to ac-
477 quire nitrogen in response to soil nitrogen availability. FUN calculates carbon
478 costs to acquire nitrogen based on the sum of carbon costs to acquire nitrogen
479 via nitrogen fixation, mycorrhizal active uptake, non-mycorrhizal active uptake,
480 and retranslocation (Fisher et al. 2010; Brzostek et al. 2014). Carbon costs to
481 acquire nitrogen via mycorrhizal or non-mycorrhizal active uptake pathways are
482 derived as a function of nitrogen availability, root biomass, and two parameterized
483 values based on nitrogen acquisition strategy (Brzostek et al. 2014). Due to this,
484 FUN simulates a net decrease in carbon costs to acquire nitrogen with increasing
485 nitrogen availability for mycorrhizal and non-mycorrhizal active uptake pathways,
486 assuming constant root biomass. This was a pattern I observed in *G. hirsutum*
487 regardless of light availability. In contrast, FUN would not simulate a net change
488 in carbon costs to acquire nitrogen via nitrogen fixation due to nitrogen avail-
489 ability. This is because carbon costs to acquire nitrogen via nitrogen fixation are
490 derived from a well established function of soil temperature, which is independent
491 of soil nitrogen availability (Houlton et al. 2008; Fisher et al. 2010). I observed
492 a net reduction in carbon costs to acquire nitrogen in *G. max*, except when in-
493 dividuals were grown under 0% shade cover (Fig. 2.1). While a net reduction of
494 carbon costs in response to nitrogen fertilization runs counter to nitrogen fixa-
495 tion carbon costs simulated by FUN, these patterns were likely because *G. max*
496 individuals switched their primary mode of nitrogen acquisition from symbiotic
497 nitrogen fixation to a non-symbiotic active uptake pathway (Fig. 2.4B).

498 It should be noted that the metric used in this study to determine carbon

499 costs to acquire nitrogen has several limitations. Most notably, this metric uses
500 root carbon biomass as a proxy for estimating the amount of carbon spent on
501 nitrogen acquisition. While it is true that most carbon allocated belowground has
502 at least an indirect structural role in acquiring soil resources, it remains unclear
503 whether this assumption holds true for species that acquire nitrogen via symbi-
504 otic nitrogen fixation. I also cannot quantify carbon lost through root exudates
505 or root turnover, which may increase due to factors that increase plant nitrogen
506 demand (Tingey et al. 2000; Phillips et al. 2011), and can increase the magni-
507 tude of available nitrogen from soil organic matter through priming effects on soil
508 microbial communities (Uselman et al. 2000; Bengtson et al. 2012). It is also not
509 clear whether these assumptions hold under all environmental conditions, such
510 as those that shift belowground carbon allocation toward a different mode of ni-
511 trogen acquisition (Taylor and Menge 2018; Friel and Friesen 2019) or between
512 species with different acquisition strategies. In this study, increasing soil nitrogen
513 fertilization increased carbon investment to roots relative to carbon transferred
514 to root nodules (Fig. 2.4B). By assuming that carbon allocated to root carbon
515 was proportional to carbon allocated to root nodules across all treatment com-
516 binations, these observed responses to soil nitrogen fertilization were likely to be
517 overestimated in *G. max*. I encourage future research to quantify these carbon
518 fates independently.

519 Researchers conducting pot experiments must carefully choose pot volume
520 to minimize the likelihood of growth limitations induced by pot volume (Poorter
521 et al. 2012). Poorter et al. (2012) indicate that researchers are likely to avoid
522 growth limitations associated with pot volume if measurements are collected when

523 the plant biomass:pot volume ratio is less than 1 g L⁻¹. In this experiment, all
524 treatment combinations in both species had biomass:pot volume ratios less than
525 1 g L⁻¹ except for *G. max* and *G. hirsutum* that were grown under 0% shade
526 cover and had received 630 ppm N. Specifically, *G. max* and *G. hirsutum* had
527 average respective biomass:pot volume ratios of 1.24±0.07 g L⁻¹ and 1.34±0.13 g
528 L⁻¹, when grown under 0% shade cover and received 630 ppm N (Supplementary
529 Tables S2, S3; Supplementary Fig. S1). If growth in this treatment combination
530 was limited by pot volume, then individuals may have had larger carbon costs
531 to acquire nitrogen than would be expected if they were grown in larger pots.
532 This pot volume induced growth limitation could cause a reduction in per-root
533 nitrogen uptake associated with more densely packed roots, which could reduce
534 the positive effect of nitrogen fertilization on whole-plant nitrogen biomass relative
535 to root carbon biomass (Poorter et al. 2012).

536 Growth limitation associated with pot volume provides a possible explana-
537 tion for the marginally insignificant effect of increasing nitrogen fertilization on *G.*
538 *max* carbon costs to acquire nitrogen when grown under 0% shade cover (Table
539 2.3; Fig. 2.1). This is because the regression line describing the relationship be-
540 tween carbon costs to acquire nitrogen and nitrogen fertilization in *G. max* grown
541 under 0% shade cover would have flattened if growth limitation had caused larger
542 than expected carbon costs to acquire nitrogen in the 0% shade cover, 630 ppm
543 N treatment combination. This may have been exacerbated by the fact that *G.*
544 *max* likely shifted relative carbon allocation from nitrogen fixation to soil nitrogen
545 acquisition, which could have increased the negative effect of more densely packed
546 roots on nitrogen uptake. These patterns could have also occurred in *G. hirsutum*

547 grown under 0% shade cover; however, there was no change in the effect of nitro-
548 gen fertilization on *G. hirsutum* carbon costs to acquire nitrogen grown under 0%
549 shade cover relative to other shade cover treatments. Regardless, the possibility
550 of growth limitation due to pot volume suggests that effects of increasing nitro-
551 gen fertilization on carbon costs to acquire nitrogen in both species grown under
552 0% shade cover could have been underestimated. Follow-up studies using a simi-
553 lar experimental design with a larger pot volume would be necessary in order to
554 determine whether these patterns were impacted by pot volume-induced growth
555 limitation.

556 In conclusion, this chapter provides empirical evidence that carbon costs to
557 acquire nitrogen are influenced by light availability and soil nitrogen fertilization
558 in a species capable of acquiring nitrogen via symbiotic nitrogen fixation and a
559 species not capable of forming such associations. We show that carbon costs to
560 acquire nitrogen generally increase with increasing light availability and decrease
561 with increasing nitrogen fertilization. This chapter provides important empirical
562 data needed to evaluate the formulation of carbon costs to acquire nitrogen in
563 terrestrial biosphere models, particularly carbon costs to acquire nitrogen that
564 are associated with symbiotic nitrogen fixation. My findings broadly support the
565 general formulation of these carbon costs in the FUN biogeochemical model in
566 response to shifts in nitrogen availability. However, there is a need for future
567 studies to explicitly quantify carbon costs to acquire nitrogen under different en-
568 vironmental contexts, over longer temporal scales, and using larger selections of
569 phylogenetically related species. In addition, I suggest that future studies mini-
570 mize the limitations associated with the metric used here by explicitly measuring

571 belowground carbon fates independently.

572

Chapter 3

573 Soil nitrogen availability modifies leaf nitrogen economies in mature
574 temperate deciduous forests: a direct test of photosynthetic least-cost
575 theory

576 3.1 Introduction

Photosynthesis represents the largest carbon flux between the atmosphere and land surface (IPCC 2021), and plays a central role in biogeochemical cycling at multiple spatial and temporal scales (Vitousek and Howarth 1991; LeBauer and Treseder 2008; Kaiser et al. 2015; Wieder et al. 2015). Therefore, carbon and energy fluxes simulated by terrestrial biosphere models are sensitive to the formulation of photosynthetic processes (Ziehn et al. 2011; Bonan et al. 2011; Booth et al. 2012; Smith et al. 2016; Smith et al. 2017) and must be represented using robust, empirically tested processes (Prentice et al. 2015; Wieder et al. 2019). Current formulations of photosynthesis vary across terrestrial biosphere models (Smith and Dukes 2013; Rogers et al. 2017), which causes variation in modeled ecosystem processes (Knorr 2000; Knorr and Heimann 2001; Bonan et al. 2011; Friedlingstein et al. 2014) and casts uncertainty on the ability of these models to accurately predict terrestrial ecosystem responses and feedbacks to global change (Zaehle et al. 2005; Schaefer et al. 2012; Davies-Barnard et al. 2020).

Terrestrial biosphere models commonly represent C₃ photosynthesis through variants of the Farquhar et al. (1980) biochemical model (Smith and Dukes 2013; Rogers 2014; Rogers et al. 2017). This well-tested photosynthesis model estimates leaf-level carbon assimilation, or photosynthetic capacity, as a function of the maximum rate of Ribulose-1,5-bisphosphate carboxylase-oxygenase (Ru-

596 bisco) carboxylation (V_{cmax}) and the maximum rate of Ribulose-1,5-bisphosphate
597 (RuBP) regeneration (J_{max}) (Farquhar et al. 1980). Many terrestrial biosphere
598 models predict these model inputs based on plant functional group specific linear
599 relationships between leaf nutrient content and V_{cmax} (Smith and Dukes 2013;
600 Rogers 2014; Rogers et al. 2017) under the tenet that a large fraction of leaf
601 nutrients, and nitrogen (N) in particular, are partitioned toward building and
602 maintaining enzymes that support photosynthetic capacity, such as Rubisco (Brix
603 1971; Gulmon and Chu 1981; Evans 1989; Kattge et al. 2009; Walker et al. 2014).
604 Terrestrial biosphere models also predict leaf nutrient content from soil nutrient
605 availability based on the assumption that increasing soil nutrients generally in-
606 creases leaf nutrients (Firn et al. 2019; Li et al. 2020; Liang et al. 2020) which, in
607 the case of N, generally corresponds with an increase in photosynthetic processes
608 (Li et al. 2020; Liang et al. 2020).

609 Recent work calls the generality of relationships between soil nutrient avail-
610 ability, leaf nutrient content, and photosynthetic capacity into question, suggest-
611 ing instead that leaf nutrients and photosynthetic capacity are better predicted as
612 an integrated product of aboveground climate, leaf traits, and soil nutrient avail-
613 ability, rather than soil nutrient availability alone (Dong et al. 2017; Dong et al.
614 2020; Dong et al. 2022; Firn et al. 2019; Smith et al. 2019; Peng et al. 2021).
615 It has been reasoned that this result is because plants allocate added nutrients to
616 growth and storage rather than alterations in leaf chemistry (Smith et al. 2019),
617 perhaps as a result of nutrient limitation of primary productivity (LeBauer and
618 Treseder 2008; Fay et al. 2015). Additionally, recent work suggests that relation-
619 ships between leaf nutrient content and photosynthesis vary across environments,

620 and that the proportion of leaf nutrient content allocated to photosynthetic tis-
621 sue varies over space and time with plant acclimation and adaptation responses
622 to light availability, vapor pressure deficit, soil pH, soil nutrient availability, and
623 environmental factors that influence leaf mass per area (Pons and Pearcy 1994;
624 Niinemets and Tenhunen 1997; Evans and Poorter 2001; Hikosaka and Shigeno
625 2009; Ghimire et al. 2017; Onoda et al. 2017; Luo et al. 2021). The use of linear
626 relationships between leaf nutrient content and Vcmax to predict photosynthetic
627 capacity, as commonly used in terrestrial biosphere models (Rogers 2014), is not
628 capable of detecting such responses.

629 Photosynthetic least-cost theory provides an alternative framework for un-
630 derstanding relationships between soil nutrient availability, leaf nutrient content,
631 and photosynthetic capacity (Harrison et al. 2021). Leveraging a two-input mi-
632 croeconomics approach (Wright et al. 2003), the theory posits that plants accli-
633 mate to a given environment by optimizing leaf photosynthesis rates at the lowest
634 summed cost of using nutrients and water (Prentice et al. 2014; Wang et al. 2017;
635 Smith et al. 2019; Paillassa et al. 2020). Across resource availability gradients,
636 the theory predicts that optimal photosynthetic rates can be achieved by trading
637 less efficient use of a resource that is less costly to acquire (or more abundant)
638 for more efficient use of a resource more costly to acquire (or less abundant). For
639 example, an increase in soil nutrient availability should reduce the cost of acquir-
640 ing and using nutrients (Bae et al. 2015; Eastman et al. 2021; Perkowski et al.
641 2021), which could increase leaf nutrient investments in photosynthetic proteins to
642 allow similar photosynthetic rates to be achieved with higher nutrient use (lower
643 nutrient use efficiency) but lower water use (greater water use efficiency). The

644 theory suggests similar tradeoffs in response to increasing soil pH (Paillassa et al.
645 2020), specifically, that increasing soil pH should reduce the cost of acquiring soil
646 nutrients due to an increase in plant-available nutrient concentration (Paillassa
647 et al. 2020; Dong et al. 2022). The theory is also capable of reconciling dynamic
648 leaf nutrient-photosynthesis relationships at global scales (Luo et al. 2021).

649 Patterns expected from photosynthetic least-cost theory have recently re-
650 ceived empirical support both in global environmental gradient (Smith et al.
651 2019; Paillassa et al. 2020; Luo et al. 2021; Querejeta et al. 2022; Wester-
652 band et al. 2023) and local manipulative invasion (Bialic-Murphy et al. 2021)
653 studies. However, nutrient addition experiments that directly examine nutrient-
654 water use tradeoffs expected from the theory are rare (Guerrieri et al. 2011), and
655 only global gradient studies testing the theory have considered soil pH in their
656 analyses. As a result, there is a need to use nutrient addition and soil pH manu-
657 lation experiments to test mechanisms driving responses predicted by the theory.
658 Such experiments would also be useful to detect whether patterns expected from
659 theory translate to finer spatial scales.

660 In this study, we measured leaf responses to soil N availability in five decid-
661 uous tree species growing in the upper canopy of mature closed canopy temperate
662 forests in the northeastern United States. Soil N availability and pH were manipu-
663 lated through an N-by-pH field manipulation experiment with treatments applied
664 since 2011, eight years prior to measurement. Two different soil N treatments
665 were applied to increase N availability with opposing effects on soil pH. An addi-
666 tional N-free acidifying treatment was expected to decrease soil pH. I hypothesized
667 that increased soil N availability would enable plants to increase nutrient uptake

668 and create more photosynthetic enzymes per leaf, allowing similar photosynthetic
669 rates achieved with lower leaf C_i:C_a and increased leaf N content allocated to
670 photosynthetic leaf tissue. I expected that this response would be driven by a
671 reduction in the cost of acquiring N, which would cause trees to sacrifice efficient
672 N use to enable more efficient use of other limiting resources (i.e., water). Finally,
673 I hypothesized similar leaf responses to increasing soil pH.

674 3.2 Methods

675 3.2.1 *Study site description*

676 We conducted this study in summer 2019 at three stands located within
677 a 20-km radius of Ithaca, NY, USA (42.444 °N, 76.502 °W). All stands contain
678 mature, closed-canopy forests dominated by deciduous tree species. Stands con-
679 tained abundant sugar maple (*Acer saccharum* Marshall), American beech (*Fagus*
680 *grandifolia* Ehrh.), and white ash (*Fraxinus americana* L.), accounting for 43%,
681 15%, and 17% of the total aboveground biomass across the three stands, respec-
682 tively, with less frequent red maple (*Acer rubrum* L.; 9% of total aboveground
683 biomass) and red oak occurrences (*Quercus rubra* L.; 10% of total aboveground
684 biomass). Soils at each site were broadly classified as a channery silt loam Incep-
685 tisols using the USDA NRCS Web Soil Survey data product (Soil Survey Staff
686 2022). Between 2006 and 2020, study sites averaged 972 mm of precipitation per
687 year and had an average temperature of 7.9 °C per a weather station located near
688 the Cornell University campus (42.449 °N, 76.449 °W) part of the NOAA NCEI
689 Global Historical Climatology Network (Menne et al. 2012).

690 3.2.2 *Experimental design*

691 Four 40 m x 40 m plots were set up at each site in 2009, each with an
692 additional 10 m buffer along plot perimeters (60 m x 60 m total). The plots
693 were set up as a nitrogen-by-pH field manipulation experiment, with one each of
694 four treatments at each site. Two nitrogen treatments were applied, both at 50
695 kg N ha⁻¹ yr⁻¹, as either sodium nitrate (NaNO₃) to raise soil pH, or ammonium
696 sulfate ((NH₄)₂SO₄) to acidify; an elemental sulfur treatment was selected to acid-
697 ify without N, applied at the same rate of S addition (57 kg S ha⁻¹ yr⁻¹); and
698 control plots received no additions. All amendments were added in pelletized form
699 using hand-held fertilizer spreaders to both the main plots and buffers. Amend-
700 ments were divided into three equal doses distributed across the growing season
701 from 2011-2017 and added as a single dose from 2018 onward. During 2019, plots
702 were fertilized during the week of May 20.

703 3.2.3 *Leaf gas exchange and trait measurements*

704 We sampled one leaf each from 6 to 10 individuals per plot between June
705 25 and July 12, 2019 for gas exchange measurements (Table S1). Leaves were
706 collected from deciduous broadleaf trees represented across all sites and plots
707 and were replicated in efforts to mimic the species abundance of each plot at
708 each site. We also attempted to collect leaves from the upper canopy to reduce
709 differential shading effects on leaf physiology. Leaves were accessed by pulling
710 down small branches using an arborist's slingshot and weighted beanbag attached
711 to a throw line. Branches were immediately recut under deionized water and
712 remained submerged to reduce stomatal closure and avoid xylem embolism (as in

713 Smith & Dukes, 2018) until gas exchange data were collected.

714 Randomly selected leaves with little to no visible external damage were
715 attached to a Li-COR LI-6800 (Li-COR Bioscience, Lincoln, Nebraska, USA)
716 portable photosynthesis machine to measure net photosynthesis (A_{net} ; $\mu\text{mol m}^{-2}$
717 s^{-1}), stomatal conductance (g_{sw} ; $\text{mol m}^{-2} \text{s}^{-1}$), and intercellular CO_2 concentra-
718 tion (C_i ; $\mu\text{mol mol}^{-1}$) at different reference CO_2 concentrations (C_a ; $\mu\text{mol mol}^{-1}$)
719 concentrations (i.e., an A_{net}/C_i curve) under saturating light conditions (2,000
720 $\mu\text{mol m}^{-2} \text{s}^{-1}$). Reference CO_2 concentrations followed the sequence: 400, 300,
721 200, 100, 50, 400, 400, 600, 800, 1000, 1200, 1500, and 2000 $\mu\text{mol mol}^{-1} \text{CO}_2$. Leaf
722 temperatures were not controlled in the cuvette and ranged from 21.8 °C to 31.7
723 °C (mean±SD: 27.2 ± 2.2 °C). A linear and second order log-polynomial nonlinear
724 regression suggested no effect of temperature on stomatal conductance measured
725 at 400 $\mu\text{mol mol}^{-1} \text{CO}_2$ or net photosynthesis measured at $\mu\text{mol mol}^{-1} \text{CO}_2$ (Ta-
726 ble S2-3; Fig. S1). All A_{net}/C_i curves were generated within one hour of branch
727 severance.

728 Leaf morphological and chemical traits were collected on the same leaf used
729 to generate each A_{net}/C_i curve. Images of each leaf were taken using a flat-bed
730 scanner to determine fresh leaf area using the ‘LeafArea’ R package (Katabuchi
731 2015), which automates leaf area calculations using ImageJ software (Schneider
732 et al. 2012). Each leaf was dried at 65°C for at least 48 hours, weighed, and
733 ground using a Retsch MM200 ball mill grinder (Verder Scientific, Inc., Newtown,
734 PA, USA) until homogenized. Leaf mass per area (M_{area} , g m^{-2}) was calculated
735 as the ratio of dry leaf biomass to fresh leaf area. Using a subsample of ground and
736 homogenized leaf biomass, leaf N content (N_{mass} ; gN g^{-1}) and leaf $\delta^{13}\text{C}$ (‰, rela-

737 tive to VPDB) were measured at the Cornell Stable Isotope Lab with an elemental
 738 analyzer (NC 2500, CE Instruments, Wigan, UK) interfaced to an isotope ratio
 739 mass spectrometer (Delta V Isotope Ratio Mass Spectrometer, ThermoFisher Sci-
 740 entific, Waltham, MA, USA). Leaf N content per unit leaf area (N_{area} ; gN m⁻²)
 741 was calculated by multiplying N_{mass} by M_{area} .

742 We used leaf $\delta^{13}\text{C}$ values to estimate χ (unitless), which is an isotope-
 743 derived estimate of the leaf $C_i:C_a$ ratio. While intercellular and atmospheric CO₂
 744 concentrations were directly measured during each A_{net}/C_i curve, deriving χ from
 745 $\delta^{13}\text{C}$ provides a more integrative estimate of the $C_i:C_a$ over an individual leaf's
 746 lifespan. We derived χ following the approach of Farquhar et al. (1989) described
 747 in Cernusak et al. (2013):

$$\chi = \frac{\Delta^{13}C - a}{b - a} \quad (3.1)$$

748 where $\Delta^{13}\text{C}$ represents the relative difference between leaf $\delta^{13}\text{C}$ (‰) and air $\delta^{13}\text{C}$
 749 (‰), and is calculated from the following equation:

$$\Delta^{13}C = \frac{\delta^{13}C_{\text{air}} - \delta^{13}C_{\text{leaf}}}{1 + \delta^{13}C_{\text{leaf}}} \quad (3.2)$$

750 where $\delta^{13}C_{\text{air}}$ is assumed to be -8‰ (Keeling et al. 1979; Farquhar et al. 1989), a
 751 represents the fractionation between ¹²C and ¹³C due to diffusion in air, assumed
 752 to be 4.4‰, and b represents the fractionation caused by Rubisco carboxylation,
 753 assumed to be 27‰ (Farquhar et al. 1989).

754 3.2.4 A_{net}/C_i curve-fitting and parameter estimation

755 We fit A_{net}/C_i curves of each individual using the ‘fitaci’ function in the
756 ‘plantecophys’ R package (Duursma 2015). This function estimates the maxi-
757 mum rate of Rubisco carboxylation (V_{cmax} ; $\mu\text{mol m}^{-2} \text{s}^{-1}$) and maximum rate
758 of electron transport for RuBP regeneration (J_{max} ; $\mu\text{mol m}^{-2} \text{s}^{-1}$) based on the
759 Farquhar, von Caemmerer, and Berry biochemical model of C₃ photosynthesis
760 (Farquhar et al. 1980). For each curve fit, we included triose phosphate uti-
761 lization (TPU) limitation to avoid underestimating J_{max} (Gregory et al. 2021).
762 Curves were visually examined to confirm the likely presence of TPU limitation.

763 We determined Michaelis-Menten coefficients for Rubisco affinity to CO₂
764 (K_c ; $\mu\text{mol mol}^{-1}$) and O₂ (K_o ; $\mu\text{mol mol}^{-1}$), and the CO₂ compensation point
765 (Γ^* ; $\mu\text{mol mol}^{-1}$) using leaf temperature and equations described in Medlyn et al.
766 (2002) and derived in Bernacchi et al. (2001). Specifically, K_c and K_o were
767 calculated as:

$$K_c = 404.9 * \exp^{\frac{79430(T_k - 298)}{298RT_k}} \quad (3.3)$$

768 and

$$K_o = 278.4 * \exp^{\frac{36380(T_k - 298)}{298RT_k}} \quad (3.4)$$

769 while Γ^* was calculated as:

$$\Gamma^* = 42.75 * \exp^{\frac{37830(T_k - 298)}{298RT_k}} \quad (3.5)$$

770 In all three equations, T_k is the leaf temperature (in Kelvin) during each A_{net}/C_i

771 curve and R is the universal gas constant ($8.314 \text{ J mol}^{-1} \text{ K}^{-1}$).

772 We standardized V_{cmax} and J_{max} estimates to 25°C using a modified Ar-

773 rhenius equation (Kattge and Knorr 2007):

$$k_{25} = \frac{k_{\text{obs}}}{e^{\frac{H_a(T_{\text{obs}} - T_{\text{ref}})}{T_{\text{ref}}RT_{\text{obs}}}} * \frac{1+e^{\frac{T_{\text{ref}}\Delta S - H_d}{T_{\text{obs}}}}}{1+e^{\frac{T_{\text{obs}}\Delta S - H_d}{T_{\text{obs}}}}}} \quad (3.6)$$

774 k_{25} represents the standardized V_{cmax} or J_{max} rate at 25°C , k_{obs} represents

775 the V_{cmax} or J_{max} estimate at the average leaf temperature measured inside the

776 cuvette during the A_{net}/C_i curve. H_a is the activation energy of V_{cmax} ($71,513$

777 J mol^{-1}) Kattge and Knorr (2007) or J_{max} ($49,884 \text{ J mol}^{-1}$) (Kattge and Knorr

778 2007). H_d represents the deactivation energy of both V_{cmax} and J_{max} ($200,000 \text{ J}$

779 mol^{-1}) (Medlyn et al. 2002), and R represents the universal gas constant (8.314

780 $\text{J mol}^{-1} \text{ K}^{-1}$). T_{ref} represents the standardized temperature of 298.15 K (25°C)

781 and T_{obs} represents the mean leaf temperature (in K) during each A_{net}/C_i curve.

782 ΔS is an entropy term that (Kattge and Knorr 2007) derived as a linear relation-

783 ship with average growing season temperature (T_g ; $^\circ\text{C}$), where:

$$\Delta S_{v_{\text{cmax}}} = -1.07 T_g + 668.39 \quad (3.7)$$

784 and

$$\Delta S_{j_{\text{max}}} = -0.75 T_g + 659.70 \quad (3.8)$$

785 We estimated T_g in Equations 3.7 and 3.8 based on mean daily (24-hour) air
786 temperature of the 30 days leading up to the day of each sample collection using
787 the same weather station reported in the site description. We then used V_{cmax25}
788 and J_{max25} estimates to calculate the ratio of J_{max25} to V_{cmax25} ($J_{max25}:V_{cmax25}$;
789 unitless).

790 3.2.5 *Proportion of leaf nitrogen allocated to photosynthesis and structure*

791 We used equations from Niinemets and Tenhunen (1997) to estimate the
792 proportion of leaf N content allocated to Rubisco and bioenergetics. The propor-
793 tion of leaf N allocated to Rubisco (ρ_{rub} ; gN gN $^{-1}$) was calculated as a function
794 of V_{cmax25} and N_{area} :

$$\rho_{rubisco} = \frac{V_{cmax25} N_r}{V_{cr} N_{area}} \quad (3.9)$$

795 where N_r is the amount of nitrogen in Rubisco, set to 0.16 gN (gN in Rubisco) $^{-1}$
796 and V_{cr} is the maximum rate of RuBP carboxylation per unit Rubisco protein,
797 set to 20.5 μ mol CO $_2$ (g Rubisco) $^{-1}$. The proportion of leaf nitrogen allocated to
798 bioenergetics (ρ_{bioe} ; gN gN $^{-1}$) was similarly calculated as a function of J_{max25} and
799 N_{area} :

$$\rho_{bioe} = \frac{J_{max25} N_b}{J_{mc} N_{area}} \quad (3.10)$$

800 where N_b is the amount of nitrogen in cytochrome f, set to 0.12407 gN (μ mol
801 cytochrome f) $^{-1}$ assuming a constant 1: 1: 1.2 cytochrome f: ferredoxin NADP
802 reductase: coupling factor molar ratio (Evans and Seemann 1989; Niinemets and

803 Tenhunen 1997), and J_{mc} is the capacity of electron transport per cytochrome f,
804 set to $156 \mu\text{mol electron} (\mu\text{mol cytochrome f})^{-1}\text{s}^{-1}$.

805 We estimated the proportion of leaf N content allocated to photosynthetic
806 tissue (ρ_{photo} ; gN gN^{-1}) as the sum of ρ_{rub} and ρ_{bioe} . This calculation is an un-
807 derestimate of the proportion of leaf N allocated to photosynthetic tissue because
808 it does not include N allocated to light harvesting proteins. This leaf N pool was
809 not included because we did not perform chlorophyll extractions on focal leaves.
810 However, the proportion of leaf N content allocated to light harvesting proteins
811 tends to be small relative to ρ_{rub} and ρ_{bioe} , and may scale with changes in ρ_{rub}
812 and ρ_{bioe} (Niinemets and Tenhunen 1997).

813 Finally, we estimated the proportion of leaf N content allocated to struc-
814 tural tissue (ρ_{str} ; gN gN^{-1}) using an empirical equation from Onoda et al. (2017):

$$N_{cw} = 0.000355 * M_{area}^{1.39} \quad (3.11)$$

815 where N_{cw} is the leaf N content allocated to cell walls (gN m^{-2}). ρ_{str} was estimated
816 by dividing N_{cw} by N_{area} .

817 3.2.6 *Tradeoffs between nitrogen and water use*

818 Photosynthetic nitrogen use efficiency (PNUE; $\mu\text{mol CO}_2 \text{ mol}^{-1} \text{ N s}^{-1}$)
819 was calculated by dividing A_{net} by N_{area} , first converting N_{area} to mol N m^{-2}
820 using the molar mass of N (14 g mol^{-1}). We used χ as an indicator of water
821 use efficiency, which exploratory analyses suggest had similar responses to soil N
822 availability and pH as intrinsic water use efficiency measured from gas exchange

823 (A_{net}/g_s). Tradeoffs between nitrogen and water use were determined by cal-
824 culating the ratio of N_{area} to χ ($N_{\text{area}}:\chi$; g N m⁻²) and V_{cmax25} to χ ($V_{\text{cmax25}}:\chi$;
825 $\mu\text{mol m}^{-2} \text{s}^{-1}$). This approach is similar to tradeoff calculations in which nitrogen-
826 water use tradeoffs are measured as the ratio of N_{area} or V_{cmax25} to g_s (Paillassa
827 et al. 2020; Bialic-Murphy et al. 2021). In this study, we quantify these re-
828 lationships using χ in lieu of g_s because g_s rapidly changes with environmental
829 conditions and therefore may have been altered by recent tree branch severance
830 and/or placement in the cuvette.

831 3.2.7 *Soil nitrogen availability and pH*

832 To characterize soil N availability at the time of our leaf gas exchange
833 measurements, we used mixed bed resin bags to quantify mobile ammonium-N
834 and nitrate-N concentrations in each plot. Lycra mesh bags were filled with 5 g
835 of Dowex® Marathon MR-3 hydrogen and hydroxide form resin (MilliporeSigma,
836 Burlington, MA USA) and sealed with a zip tie. Each bag was activated by
837 soaking in 0.5 M HCl for 20 minutes, then in 2 M NaCl until pH of the saline
838 solution stabilized, as described in Allison et al. (2008). Five resin bags were
839 inserted about 10 cm below the soil surface at each plot on June 25, 2019: one
840 near each of the four plot corners and one near the plot center. All resin bags
841 were collected 24 days later on July 19, 2019 and were frozen until extracted.

842 Prior to anion and cation extraction, each resin bag was rinsed with ul-
843 trapure water (MilliQ IQ 7000; Millipore Sigma, Burlington, MA) to remove any
844 surface soil residues. Anions and cations were extracted from surface-cleaned resin
845 bags by individually soaking and shaking each bag in 100 mL of a 0.1 M HCl/2.0

846 M NaCl matrix for one hour. Using a microplate reader (Biotek Synergy H1;
847 Biotek Instruments, Winooski, VT USA), nitrate-N concentrations were quanti-
848 fied spectrophotometrically at 540 nm with the end product of a single reagent
849 vanadium (III) chloride reaction (Doane and Horwáth 2003), and ammonium-N
850 concentrations quantified at 650 nm with the end product of a modified phenol-
851 hypochlorite reaction (Weatherburn 1967; Rhine et al. 1998). Both the single
852 reagent vanadium (III) chloride and modified phenol-hypochlorite methodologies
853 have been well established for determining nitrate-N and ammonium-N concen-
854 trations in resin bag extracts (Arnone 1997; Allison et al. 2008). We used a
855 series of negative and positive controls throughout each well plate to verify the
856 accuracy and precision of our measurements, assaying each resin bag extract and
857 control in triplicate. Soil N availability was estimated as the sum of the nitrate-N
858 and ammonium-N concentration in each resin bag, normalized per g of resin and
859 duration in the field ($\mu\text{g N g}^{-1} \text{ resin d}^{-1}$), then subsequently averaged across all
860 resin bags in a plot for a plot-level mean.

861 Soil pH was measured on 0-10 cm mineral soil samples collected prior to
862 fertilization in 2019. Near each of the four plot corners, three 5.5 cm diameter soil
863 cores were collected after first removing the forest floor where present. Each set
864 of three cores was placed in a plastic bag, and later composited by hand mixing
865 and sieved to 4mm. Soil pH was determined for a 1:2 soil:water slurry (10 g field-
866 moist soil to 20 mL DI water) of each sample using an Accumet AB15 pH meter
867 with flushable junction probe (Fisher Scientific; Hampton, NH, USA), and was
868 estimated at the plot level as the mean soil pH within each plot.

869 3.2.8 *Statistical analyses*

870 We built two separate series of linear mixed-effects models to explore effects
871 of soil N availability, soil pH, species, and leaf N content on leaf physiological
872 traits. In the first series of linear mixed-effects models, we explored the effect
873 of soil N availability, soil pH, and species on leaf N content, leaf photosynthesis,
874 stomatal conductance, and nitrogen-water use tradeoffs. Models included plot-
875 level soil N availability and plot-level soil pH as continuous fixed effects, species
876 as a categorical fixed effect, and site as a categorical random intercept term.
877 Interaction terms between fixed effects were not included due to the small number
878 of experimental plots. We built a series of separate models with this independent
879 variable structure to quantify individual effects of soil N availability, soil pH,
880 and species on N_{area} , M_{area} , N_{mass} , A_{net} , V_{cmax25} , J_{max25} , $J_{\text{max25}}:V_{\text{cmax25}}$, ρ_{rubisco} ,
881 $\rho_{\text{bioenergetics}}$, ρ_{photo} , $\rho_{\text{structure}}$, χ , PNUE, $N_{\text{area}}:\chi$, and $V_{\text{cmax25}}:\chi$.

882 A second series of linear mixed-effects models were built to investigate
883 relationships between leaf N content and photosynthetic parameters. Statistical
884 models included N_{area} as a single continuous fixed effect with species and site des-
885 ignated as individual random intercept terms. We used this independent variable
886 structure to quantify individual effects of leaf N content on A_{net} , V_{cmax25} , J_{max25} ,
887 $J_{\text{max25}}:V_{\text{cmax25}}$, and χ .

888 For all linear mixed-effects models, we used Shapiro-Wilk tests of normal-
889 ity to determine whether linear mixed-effects models satisfied residual normality
890 assumptions. If residual normality assumptions were not met, then models were
891 fit using dependent variables that were natural log transformed. If residual nor-
892 mality assumptions were still not met (Shapiro-Wilk: $p < 0.05$), then models were

893 fit using dependent variables that were square root transformed. All residual nor-
894 mality assumptions for both sets of models that did not originally satisfy residual
895 normality assumptions were met with either a natural log or square root data
896 transformation (Shapiro-Wilk: $p > 0.05$ in all cases).

897 In the first series of models, models for N_{area} , M_{area} , N_{mass} , V_{cmax25} , J_{max25} ,
898 χ , $N_{\text{area}}:\chi$, and $V_{\text{cmax25}}:\chi$, ρ_{rubisco} , $\rho_{\text{bioenergetics}}$, ρ_{photo} , $\rho_{\text{structure}}$ satisfied residual
899 normality assumptions without data transformations (Shapiro-Wilk: $p > 0.05$ in
900 all cases). The model for $J_{\text{max25}}:V_{\text{cmax25}}$ satisfied residual normality assumptions
901 with a natural log data transformation, while models for A_{net} and PNUE each
902 satisfied residual normality assumptions with square root data transformations.
903 In the second series of models, models for V_{cmax25} , J_{max25} , χ , and $V_{\text{cmax25}}:\chi$ satisfied
904 residual normality assumptions without data transformations (Shapiro-Wilk: p
905 > 0.05 in all cases). The model for $J_{\text{max25}}:V_{\text{cmax25}}$ required a natural log data
906 transformation and the model for A_{net} required a square root data transformation
907 (Shapiro-Wilk: $p > 0.05$ in both cases).

908 In all models, we used the ‘lmer’ function in the ‘lme4’ R package (Bates
909 et al. 2015) to fit each model and the ‘Anova’ function in the ‘car’ R package (Fox
910 and Weisberg 2019) to calculate Type II Wald’s χ^2 and determine the significance
911 level ($\alpha = 0.05$) of each fixed effect coefficient. Finally, we used the ‘emmeans’
912 R package (Lenth, 2019) to conduct post-hoc comparisons using Tukey’s tests,
913 where degrees of freedom were approximated using the Kenward-Roger approach
914 (Kenward and Roger 1997). All analyses and plots were conducted in R version
915 4.1.1 (R Core Team 2021). All figure regression lines and associated 95% confi-
916 dence interval error bars were plotted using predictions generated across the soil

917 nitrogen availability gradient using the ‘emmeans’ R package (Lenth 2019).

918 3.3 Results

919 3.3.1 *Leaf N content*

920 Increasing soil N availability generally increased N_{area} (Table 3.1; Fig.
921 3.1a). This pattern was driven by an increase in N_{mass} (Table 3.1; Fig. 3.1c)
922 and a marginal increase in M_{area} (Table 3.1; Fig. 3.1e) with increasing soil N
923 availability. There was no effect of soil pH on N_{area} , N_{mass} , or M_{area} (Table 3.1);
924 however, we did observe strong differences in N_{area} (Fig. 3.1b), N_{mass} (Fig. 3.1d),
925 and M_{area} (Fig. 3.1e) between species (Table 3.1).

Table 3.1. Effects of soil N availability, soil pH, and species on leaf N content per unit leaf area (N_{area}), leaf N content per unit leaf mass (N_{mass}), and leaf mass per unit leaf area (M_{area})

	N_{area}			N_{mass}			M_{area}			
	df	Coefficient	χ^2	p	Coefficient	χ^2	p	Coefficient	χ^2	p
Intercept	-	9.03E-01	-	-	1.68E+00	-	-	4.60E+01	-	-
Soil N	1	1.68E-02	11.990	0.001	1.25E-02	6.902	0.009	4.87E-01	4.143	0.042
Soil pH	1	9.28E-02	0.836	0.361	8.08E-02	0.663	0.415	4.05E+00	0.653	0.419
Species	4	-	72.128	<0.001	-	35.074	<0.001	-	29.869	<0.001

926 *Significance determined using Type II Wald χ^2 tests ($\alpha = 0.05$). P-values < 0.05 are in bold.

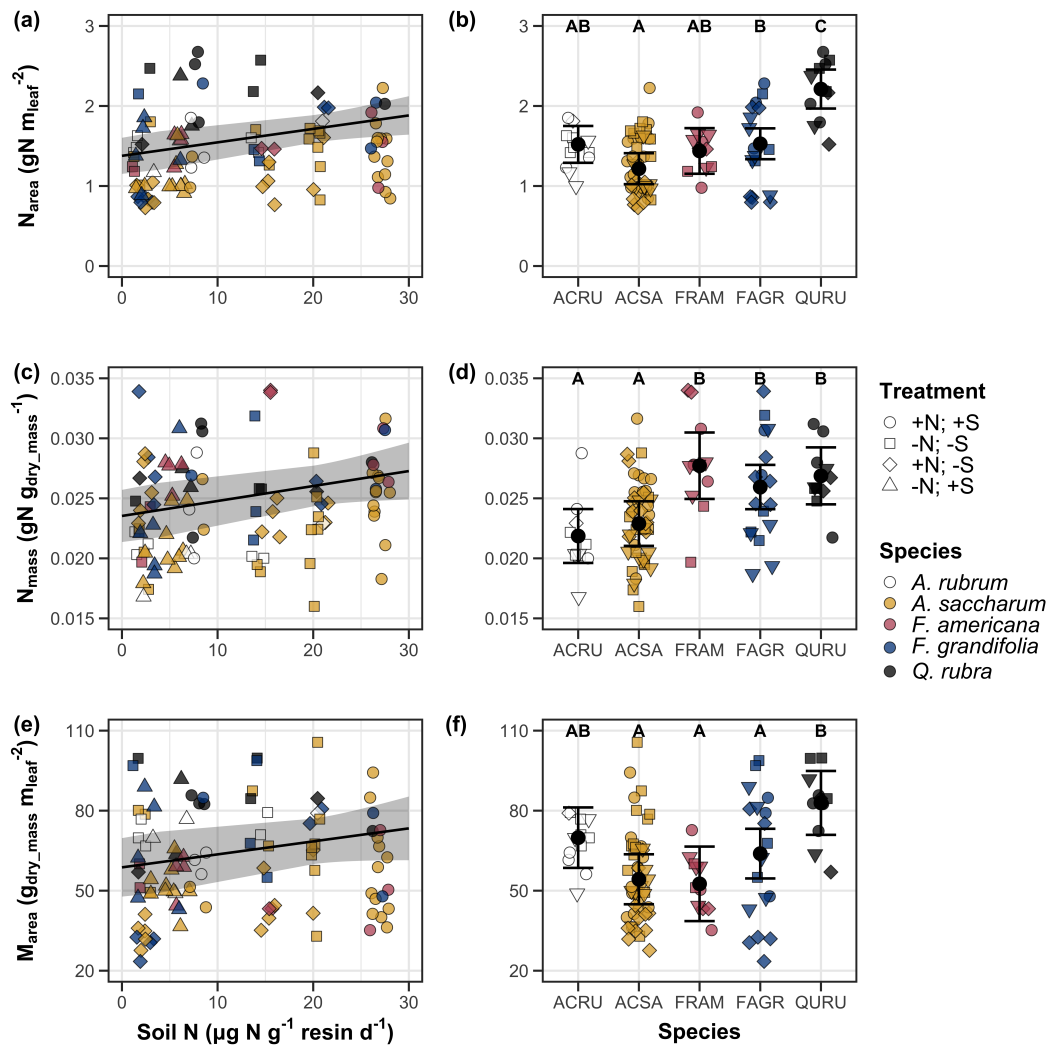


Figure 3.1. Effects of soil N availability and species on leaf N content per unit leaf area (a-b), leaf nitrogen content per unit leaf biomass (c-d), and leaf mass per leaf area (e-f). Soil N availability is represented on the x-axis in the left column of panels, while species is represented on the x-axis in the right column of panels. Tree species are represented as colored points and treatment plots are represented as shaped points, jittered for visibility. Species are abbreviated in the right column of panels through their assigned NRCS PLANTS Database symbol (USDA NRCS 2022), grouped along the x-axis per common mycorrhizal association, where the first three species commonly associate with arbuscular mycorrhizae (ACRU, ASCA, FAGR) and the second two species with ectomycorrhizae (FAGR, QURU). Trendlines are only included when the regression slope is statistically different from zero ($p < 0.05$).

927 3.3.2 *Net photosynthesis and leaf biochemistry*

928 Increasing soil N availability generally had no effect on A_{net} , V_{cmax25} , J_{max25} ,
929 or $J_{\text{max25}}:V_{\text{cmax25}}$ (Table 3.2, Figs. 3.2a, 3.2d, 3.2g). We also observed strong
930 species effects on all measured leaf photosynthetic traits (Table 3.2; Figs. 3.2b,
931 3.2e, 3.2h). Increasing soil pH had a marginal negative effect on A_{net} , but had no
932 effect on V_{cmax25} , J_{max25} , or $J_{\text{max25}}:V_{\text{cmax25}}$ (Table 3.2). There was a weak positive
933 effect of increasing N_{area} on A_{net} (Fig. 3.2c), but quite strong positive effects of
934 increasing N_{area} on V_{cmax25} and J_{max25} (Table 3.2; Fig. 3.2f and 3.2i).

Table 3.2. Effects of soil N availability, soil pH, species, and N_{area} on leaf biochemistry

	A_{net}			V_{cmax25}			J_{max25}			
	df	Coefficient	χ^2	p	Coefficient	χ^2	p	Coefficient	χ^2	p
(Intercept)	-	3.29E+00 ^b	-	-	6.38E+01	-	-	1.12E+02	-	-
Soil N	1	-1.23E-03 ^b	1.798	0.180	-3.84E-01	1.745	0.187	-6.70E-01	2.172	0.141
Soil pH	1	-3.09E-01 ^b	3.312	0.069	-4.91E+00	0.655	0.418	-8.18E+00	0.742	0.389
Species	4	-	11.838	0.019	-	31.748	<0.001	-	27.291	<0.001
(N_{area} int.)	-	6.59E-01 ^b	-	-	1.45E-01	-	-	2.86E+01	-	-
N_{area}	4	3.13E-01 ^b	4.790	0.029	2.43E+01	22.616	<0.001	4.04E+01	28.259	<0.001

	$J_{\text{max25}}:V_{\text{cmax25}}$			
	df	Coefficient	χ^2	p
(Intercept)	-	6.59E-01 ^a	-	-
Soil N	1	7.04E-04 ^a	0.088	0.767
Soil pH	1	-7.84E-03 ^a	0.025	0.874
Species	4	-	12.745	0.013
(N_{area} int.)	-	6.69E-01 ^a	-	-
N_{area}	4	-4.69E-02 ^a	1.142	0.285

935 *Significance determined using Type II Wald χ^2 tests ($\alpha = 0.05$). P-values < 0.05 are in bold, while p-values between
 936 0.05 and 0.1 are italicized. Superscript letters indicate model coefficients fit to natural-log (^a) or square-root (^b)
 937 transformed data. Relationships between N_{area} and each response variable were fit using the second series of bivariate
 938 mixed-effects models, so model coefficients and results are independent of model coefficients and results reported
 939 for relationships between soil N, soil pH, and species for each response variable. Key: A_{net} – light saturated net
 940 photosynthesis rate; V_{cmax25} – maximum rate of Rubisco carboxylation at 25°C; J_{max25} – maximum rate of electron
 941 transport for RuBP regeneration at 25°C, $J_{\text{max25}}:V_{\text{cmax25}}$ – the ratio of J_{max25} to V_{cmax25} .

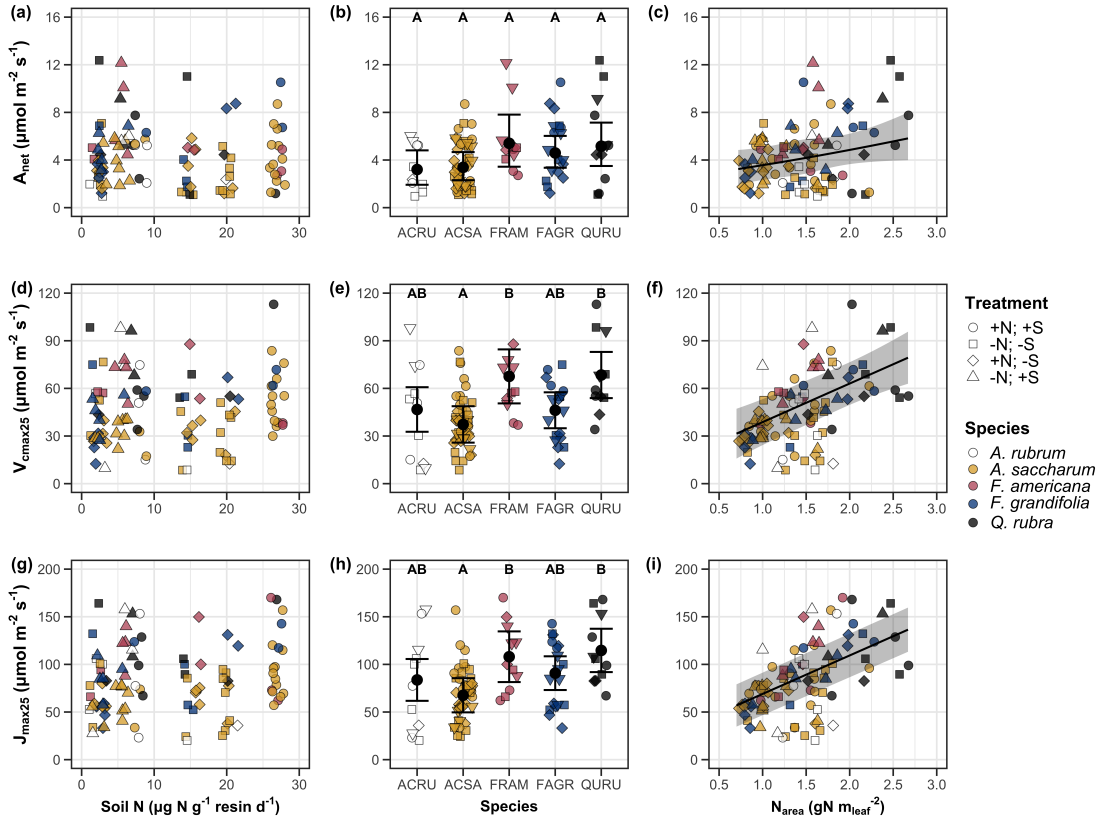


Figure 3.2. Effects of soil N availability (left column of panels), species (middle column of panels), and leaf N content per unit leaf area (right column of panels) on net photosynthesis (a-c), maximum Rubisco carboxylation rate (d-f), and maximum RuBP regeneration rate (g-i). Soil N availability is represented on the x-axis in the left column of panels, species is represented on the x-axis in the middle column of panels, and leaf N content per unit leaf area is represented continuously on the x-axis in the right column of panels. Species abbreviations and position along the x-axis in the middle column of panels, colored points, shapes, and trendlines are as explained in Figure 3.1.

942 3.3.3 *Leaf N allocation*

943 Neither soil N availability nor soil pH affected the proportion of leaf N
944 allocated to Rubisco or bioenergetics (Table 3.3; Fig. 3.3a, Fig. 3.3c), nor was
945 there any subsequent effect on the proportion of leaf N allocated to photosynthesis
946 (Table 3.3; Fig. 3.3f). We also found no effect of soil N availability or soil pH on
947 the proportion of leaf N allocated to structure (Table 3.3; Fig 3.3g). Species varied
948 in the proportion of leaf N allocated to Rubisco, photosynthesis, and structure (Fig
949 3.3b, Fig. 3.3d, Fig 3.3h), with no detectable species effect on the proportion of
950 leaf N allocated to bioenergetics (Table 3.3).

Table 3.3. Effects of soil N availability, soil pH, and species on the proportion of leaf nitrogen content allocated to photosynthesis, Rubisco, bioenergetics, and structure

	ρ_{photo}			ρ_{rub}			ρ_{bioe}			
	df	Coefficient	χ^2	p	Coefficient	χ^2	p	Coefficient	χ^2	p
Intercept	-	4.93E-01	-	-	4.17E-01	-	-	7.64E-02	-	-
Soil N	1	-1.23E-03	0.521	0.470	-1.04E-03	0.501	0.479	-1.77E-04	0.557	0.455
Soil pH	1	-4.37E-02	1.581	0.209	-3.70E-02	1.511	0.219	-6.84E-03	1.941	0.164
Species	4	-	13.106	0.011	-	14.152	0.007	-	7.300	0.121

	ρ_{str}			
	df	Coefficient	χ^2	p
Intercept	-	9.77E-02	-	-
Soil N	1	-2.29E-04	1.165	0.280
Soil pH	1	-1.87E-03	0.179	0.672
Species	4	-	16.428	0.002

58

951 *Significance determined using Type II Wald χ^2 tests ($\alpha = 0.05$). P-values < 0.05 are in bold. Key: ρ_{photo} -
 952 proportion of leaf nitrogen content allocated to photosynthesis; ρ_{rub} - proportion of leaf nitrogen content allocated
 953 to Rubisco; ρ_{bioe} - proportion of leaf nitrogen content allocated to bioenergetics; ρ_{str} - proportion of leaf nitrogen
 954 content allocated to structure.

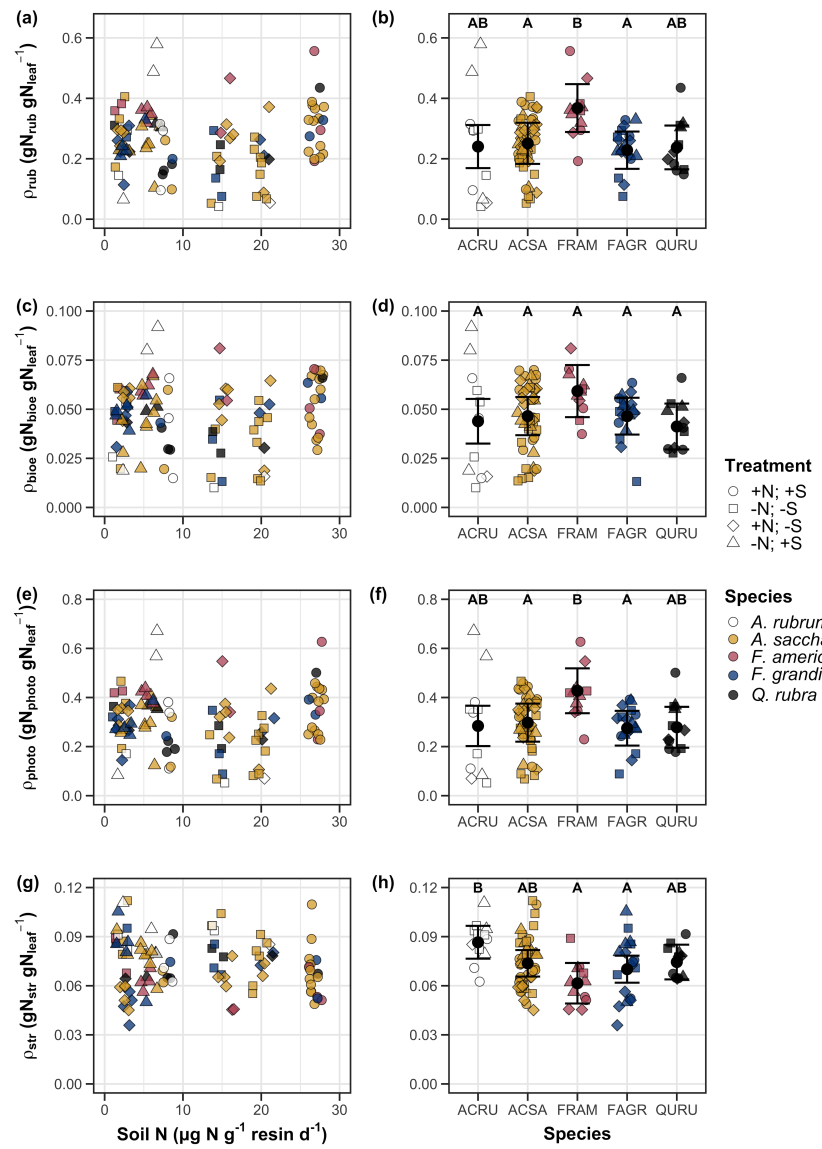


Figure 3.3. Effects of soil nitrogen availability and species on the proportion of leaf nitrogen content allocated to Rubisco (a-b), bioenergetics (c-d), photosynthesis (e-f), and structure (g-h). Soil nitrogen availability is represented on the x-axis in the left column of panels and species are represented on the x-axis in the right column of panels. Species abbreviations and position along the x-axis in the middle column of panels, colored points, shapes, trendlines, error bars, and compact lettering are as explained in Figure 3.1.

955 3.3.4 *Tradeoffs between nitrogen and water use*

956 Although soil N availability did not affect χ (Table 3.4; Fig. 3.4a), increasing
957 soil N availability decreased PNUE (Table 3.4; Fig. 3.4d) and increased the
958 ratio of $N_{\text{area}}:\chi$ (Table 3.4; Fig. 3.4f). Specifically, this response yielded a 26%
959 reduction in PNUE and 37% stimulation in $N_{\text{area}}:\chi$ across the soil nitrogen avail-
960 ability gradient. There was no apparent effect of soil N availability on $V_{\text{cmax25}}:\chi$
961 (Table 3.4; Fig. 3.4h). Increasing soil pH had a weak marginal negative effect
962 on PNUE, but did not influence χ , $N_{\text{area}}:\chi$, or $V_{\text{cmax25}}:\chi$ (Table 3.4). We also
963 observed differences in χ (Fig. 3.4b), PNUE (Fig. 3.4e), $N_{\text{area}}:\chi$ (Fig. 3.4g), and
964 $V_{\text{cmax25}}:\chi$ (Fig. 3.4i) between species (Table 3.4). Finally, increasing N_{area} had a
965 strong negative effect on χ (Table 3.4; Fig. 3.4c) and a strong positive effect on
966 $V_{\text{cmax25}}:\chi$ (Table 3.4; Fig. 3.4j).

Table 3.4. Effects of soil N availability, soil pH, species, and N_{area} on tradeoffs between nitrogen and water use

	χ	PNUE				$N_{\text{area}}:\chi$				
	df	Coefficient	χ^2	p	Coefficient	χ^2	p	Coefficient	χ^2	p
(Intercept)	-	8.12E-01	-	-	9.57E+00	-	-	9.19E-01	-	-
Soil N	1	-1.14E-03	1.698	0.193	-6.63E-02	6.396	0.011	2.60E-02	9.533	0.002
Soil pH	1	-1.91E-02	1.087	0.297	-9.25E-01	2.843	<i>0.092</i>	2.03E-01	1.321	0.250
Species	4	-	18.843	0.001	-	13.454	0.009	-	52.983	<0.001
$(N_{\text{area}} \text{ int.})$	-	8.93E-01	-	-	-	-	-	-	-	-
N_{area}	1	-1.11E-01	80.606	<0.001	-	-	-	-	-	-

	$V_{\text{cmax25}}:\chi$			
	df	Coefficient	χ^2	p
(Intercept)	-	7.20E+01	-	-
Soil N	1	3.99E-01	0.963	0.326
Soil pH	1	-3.12E+00	0.138	0.711
Species	4	-	31.450	<0.001
$(N_{\text{area}} \text{ int.})$	-	1.18E+01	-	-
N_{area}	4	3.87E+01	32.797	<0.001

967 *Significance determined using Type II Wald χ^2 tests ($\alpha = 0.05$). P-values < 0.05 are in bold, while p-values
 968 between 0.05 and 0.1 are italicized. Superscript letters indicate model coefficients fit to natural-log ^(a) or square-root
 969 ^(b) transformed data. Relationships between N_{area} and each response variable were fit using the second series of
 970 bivariate mixed-effects models, so model coefficients and results are independent of model coefficients and results
 971 reported for relationships between soil N, soil pH, and species for each response variable. Key: χ - isotope-derived
 972 estimate of the $C_i:C_a$; PNUE - photosynthetic N use efficiency, ratio of net photosynthesis to leaf N content per unit
 973 leaf area; $N_{\text{area}}:\chi$ - ratio of N_{area} to χ ; $V_{\text{cmax25}}:\chi$ - ratio of V_{cmax25} to χ .

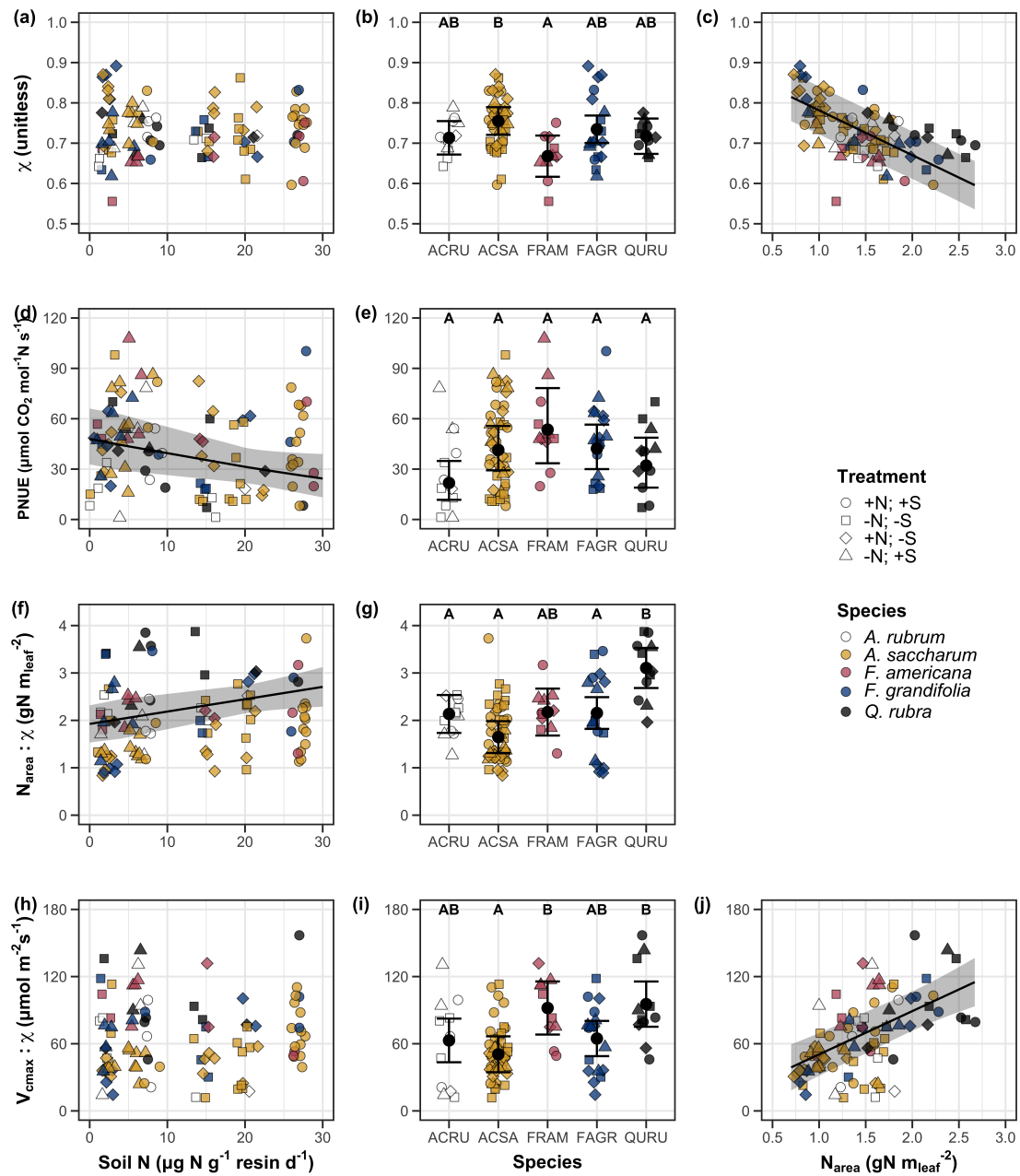


Figure 3.4. Effects of soil nitrogen availability and species on the proportion of leaf nitrogen content allocated to Rubisco (a-b), bioenergetics (c-d), photosynthesis (Rubisco + bioenergetics; e-f), and structure (g-h). Soil nitrogen availability is represented on the x-axis in the left column of panels and species are represented on the x-axis in the right column of panels. Species abbreviations and position along the x-axis in the middle column of panels, colored points, shapes, trendlines, error bars, and compact lettering are as explained in Figure 3.1.

974 3.4 Discussion

975 Photosynthetic least-cost theory provides an explanation for understand-
976 ing relationships between soil nutrient availability, leaf nutrient allocation, and
977 photosynthetic capacity. The theory suggests that plants acclimate to a given
978 environment by optimizing leaf photosynthesis rates at the lowest summed cost
979 of using nutrients and water Prentice et al. (2014), Wang et al. (2017), Smith
980 et al. (2019), Paillassa et al. (2020). The theory predicts that an increase in
981 soil nutrient availability should allow similar photosynthesis rates to be achieved
982 with increased leaf nutrient content and photosynthetic capacity (i.e., V_{cmax25} and
983 J_{max25}) at lower leaf $C_i:C_a$ (χ), resulting in an increase in water use efficiency,
984 decrease in nutrient use efficiency, and increase in both leaf nutrient content and
985 photosynthetic capacity per unit χ . The theory predicts similar leaf responses to
986 increasing soil pH under acidic conditions, presumably due to generally faster nu-
987 trient cycle dynamics and consequent reductions in the cost of acquiring nutrients
988 relative to water with increasing soil pH (Wang et al. 2017; Paillassa et al. 2020;
989 Dong et al. 2020).

990 Supporting the theory, we showed that increasing soil N availability was
991 associated with increased leaf N content (Fig 3.1a, 3.1c), a pattern that reduced
992 photosynthetic N use efficiency (Fig 3.4d) and increased leaf N content per unit
993 χ (Fig 3.4f). Increasing soil N coincided with slight, but non-significant decreases
994 in χ and increases in V_{cmax25} and J_{max25} ($p < 0.2$, Table 3.2). The positive trend
995 between soil N availability and photosynthetic capacity was supported by the con-
996 current strong increase in leaf N content with increasing soil N availability, which
997 resulted in no change in the proportion of leaf N content allocated to photosynthe-

998 sis across the soil N availability gradient. Additionally, leaf N content exhibited a
999 strong negative correlation with χ , indicative of strong nitrogen-water use trade-
1000 offs at the leaf level. Responses tended to vary more due to soil N availability
1001 than soil pH. Overall, these findings are consistent with the nutrient-water use
1002 tradeoffs predicted from theory.

1003 3.4.1 *Soil nitrogen availability modifies tradeoffs between nitrogen and water use*

1004 In support of expected least-cost outcomes and past environmental gradient
1005 studies (Dong et al. 2017; Paillassa et al. 2020), we found that increasing soil N
1006 availability was associated with increased leaf N content. Soil N availability had
1007 smaller impacts on measures of net photosynthesis and χ , which led to reductions
1008 in PNUE and increases in leaf N content per unit χ , as expected from theory.
1009 Photosynthetic least-cost theory suggests that reductions in PNUE should be
1010 driven by an increase in the proportion of leaf N allocated to photosynthetic tissue,
1011 a pattern that should allow plants to achieve optimal photosynthetic rates with
1012 greater photosynthetic capacity to make better use of available light. Contrasting
1013 theory predictions, we found no effect of soil N availability on photosynthetic
1014 capacity. However, photosynthetic capacity did tend to increase with increasing
1015 soil N availability ($p < 0.20$; Table 3.2) resulting in no effect of soil N availability on
1016 the relative fraction of leaf N allocated to photosynthesis, Rubisco, or bioenergetics
1017 (Fig. 3.3). These lines of evidence support the idea that trees use additional N
1018 to support increased leaf N allocation toward photosynthetic tissue and enhance
1019 photosynthetic capacity (Wright et al. 2003).

1020 Soil N availability had a stronger effect on leaf N than photosynthetic ca-

1021 pacity. This pattern suggests that additional plant N uptake due to increased
1022 soil N availability was also being used to support non-photosynthetic N pools,
1023 possibly to structural tissue or stress-induced amino acid and polyamine synthe-
1024 sis (Minocha et al. 2000; Onoda et al. 2004; Bubier et al. 2011). While we
1025 found no change in the proportion of leaf N allocated to leaf structural tissue, the
1026 overall stimulation in leaf N content with increasing soil N availability suggests an
1027 increase in the net amount of N invested in leaf structural tissue along the N avail-
1028 ability gradient. Importantly, leaf N allocated to structure was calculated using
1029 an empirical relationship between M_{area} and the amount of leaf N allocated to cell
1030 walls (Onoda et al. 2017). As the generality of relationships between M_{area} and
1031 the amount of leaf N allocated to cell walls has been called into question (Harrison
1032 et al. 2009), future work should consider explicitly measuring N allocation to cell
1033 wall tissue and stress-induced amino acid synthesis to confirm these patterns.

1034 In opposition to patterns expected from least-cost theory, increasing soil
1035 N availability had no apparent effect on χ (Fig. 3.4a). Interestingly, despite
1036 the null effect of soil N availability on χ , we observed a strong negative effect of
1037 increasing N_{area} on χ (Fig. 3.4c), consistent with the nitrogen-water use tradeoffs
1038 expected from theory. The null response of χ to increasing soil N availability may
1039 have been due to a lack of water limitation in the system, given that the area
1040 received approximately 20% more precipitation (1167 mm) during the 12-month
1041 period leading up to our measurement period than normally expected (972 mm).
1042 However, droughts can and do occur in temperate forests of the northeastern
1043 United States (Sweet et al. 2017), so the observed increase in leaf N content
1044 with increasing soil N availability could be a strategy that allows trees to hedge

1045 bets against drier than normal growing seasons (Onoda et al. 2004; Onoda et al.
1046 2017; Hallik et al. 2009). As was suggested in Paillassa et al. (2020), and more
1047 recently by Querejeta et al. (2022), negative effects of soil N availability on χ may
1048 increase with increasing aridity. This strategy would be especially advantageous if
1049 it allows individuals growing in arid regions to maintain carbon assimilation rates
1050 with reduced water loss. Future work should attempt to quantify interactive roles
1051 of climate and soil nitrogen availability on nitrogen-water use tradeoffs, which
1052 could be done by leveraging coordinated and multifactor nutrient (Borer et al.
1053 2014) and water (Knapp et al. 2017) manipulation experiments across broad
1054 climatic gradients.

1055 3.4.2 *Soil pH did not modify tradeoffs between nitrogen and water usage*

1056 While the primary purpose of this study was to examine the role of soil N
1057 availability on nitrogen-water use tradeoffs, our experimental design manipulated
1058 both soil N and pH, providing an opportunity to isolate the roles of these variables.
1059 Previous correlational studies along environmental gradients identified soil pH as
1060 a particularly important factor that can modify tradeoffs between nutrient and
1061 water use (Smith et al. 2019; Paillassa et al. 2020; Westerband et al. 2023)
1062 and the proportion of leaf nitrogen allocated to photosynthesis (Luo et al. 2021).
1063 Such studies implied that these patterns may be driven by reductions in the cost of
1064 acquiring nutrients relative to water with increasing pH, which may be exacerbated
1065 in acidic soils.

1066 Consistent with theory (Wright et al. 2003; Prentice et al. 2014), our
1067 results indicate that increasing soil pH was negatively associated with PNUE.

1068 However, there was no effect of soil pH on leaf N content, χ , or leaf N content per
1069 unit χ , most likely because the experimental N additions increased soil N sup-
1070 ply while both increasing (sodium nitrate) and decreasing (ammonium sulfate)
1071 soil pH. These results suggest that soil pH did not play a major role in modify-
1072 ing expected photosynthetic least-cost theory patterns, contrasting findings from
1073 Paillassa et al. (2020) and other gradient studies that note positive effects of in-
1074 creasing soil pH on leaf N content, Rubisco carboxylation, and χ (Viet et al. 2013;
1075 Cornwell et al. 2018; Luo et al. 2021). Instead, null responses to soil pH show
1076 that leaf photosynthetic parameters depend more on soil N availability than pH
1077 per se, and that inferences from gradient studies might be confounding covariation
1078 between N availability and soil acidity.

1079 3.4.3 *Species identity explains a large amount of variation in leaf and whole*
1080 *plant traits*

1081 Species generally explained a larger amount of variation in measured leaf
1082 traits than soil N availability or soil pH. Interspecies variation is an important
1083 factor to consider when deducing mechanisms that drive photosynthetic least-
1084 cost theory, particularly for species that form distinct mycorrhizal associations or
1085 have different photosynthetic pathways, growth forms, or leaf habit (Espelta et al.
1086 2005; Adams et al. 2016; Bialic-Murphy et al. 2021; Scott and Smith 2022). The
1087 need to consider species may also be important when comparing nutrient-water
1088 use tradeoffs in early and late successional species, or in species with different
1089 resource economic strategies (Abrams and Mostoller 1995; Ellsworth and Reich
1090 1996; Wright et al. 2004; Reich 2014; Onoda et al. 2017; Ziegler et al. 2020).

1091 A strength of the study design and sampling effort is that it controls for
1092 many species differences that should modify nitrogen-water use tradeoffs expected
1093 from theory. All tree species measured in this study shared the leaf habit of decid-
1094 uous broadleaves, were growing in forests of similar successional stage, but differed
1095 in mycorrhizal association and consequent resource economic strategies. As stands
1096 tended to be dominated by trees that associate with arbuscular mycorrhizae (*Frax-*
1097 *inus* and both *Acer* species made up 70% of total aboveground biomass across
1098 stands), ecosystem biogeochemical cycle dynamics may be more closely aligned
1099 to the inorganic nutrient economy proposed in Phillips et al. (2013), which may
1100 promote stronger nitrogen-water use tradeoffs in tree species that associate with
1101 arbuscular mycorrhizae. This result was not observed here, as photosynthetic
1102 properties varied as much within as across the two mycorrhizal associations rep-
1103 resented. Given the high variability in measured photosynthetic traits within
1104 and across species, effects of mycorrhizal association likely require more intensive
1105 sampling efforts to detect than were possible here.

1106 3.4.4 *Implications for photosynthetic least-cost theory model development*

1107 In the field, soil nutrient availability is heterogeneous across time and space
1108 (Table S4). Unaccounted within-plot heterogeneity may have contributed to the
1109 low amount of variation explained by soil N availability in our statistical mod-
1110 els, as resin bags are a coarse surrogate for soil N availability. Despite this, we
1111 still observed evidence for nutrient-water use tradeoffs, suggesting that observed
1112 responses reported here may be an underestimate toward the net effect of soil
1113 N availability on these tradeoffs. While we urge caution in the interpretation of

1114 these results, they do provide a promising baseline for future studies investigating
1115 patterns expected from photosynthetic least-cost theory at finer spatiotemporal
1116 resolutions.

1117 The general stronger relationship between leaf N content and photosynthetic parameters versus between leaf N content and soil N availability suggests
1119 that leaf N content is more directly tied to photosynthesis than soil N availability. While this could be due to the high spatiotemporal heterogeneity of soil N
1121 availability, principles from photosynthetic least-cost theory suggest that leaf N
1122 content is the downstream product of leaf nutrient demand to build and maintain
1123 photosynthetic machinery, which is set by aboveground environmental conditions
1124 such as light availability, CO₂, temperature, or vapor pressure deficit (Smith
1125 et al. 2019; Paillassa et al. 2020; Peng et al. 2021; Westerband et al. 2023). The
1126 stronger relationship between leaf N and photosynthetic parameters paired with
1127 the strong negative relationship between leaf N and χ could indicate a relatively
1128 stronger effect of climate on leaf N-photosynthesis relationships than soil resource
1129 availability. However, the short distance between plots and across sites limited
1130 our ability to test this mechanism.

1131 Variation in soil pH affected least cost responses less than variations in
1132 soil N availability, in part because experimental treatments directly increased soil
1133 N and affected soil pH in opposite directions. While soil pH has been shown
1134 to drive nitrogen-water tradeoffs in global gradient analyses (Viet et al. 2013;
1135 Paillassa et al. 2020), these responses may be due to covariations between soil pH
1136 and nutrient cycling rather than a role of pH per se. The direct manipulations
1137 of soil pH and soil N availability in this study allowed us to partly disentangle

1138 these factors and show that variation in N availability matters more for least-cost
1139 tradeoffs than pH alone.

1140 3.4.5 *Conclusions*

1141 Increasing soil N availability generally increased leaf N content (both area-
1142 and mass-based), but did not significantly influence χ . This shift in leaf N led
1143 to a reduction in PNUE, and an increase in leaf N per unit χ with increasing
1144 soil N availability. Despite null effects of soil N availability on χ , we observed a
1145 strong negative relationship between leaf N content and χ . These results provide
1146 empirical support for the nutrient-water use tradeoffs expected from photosyn-
1147 thetic least-cost theory in response to soil nutrient availability, but suggest that
1148 all tenets of the theory may not hold in every environment. These results exper-
1149 imentially test previous work suggesting that leaf water-nitrogen economies vary
1150 across gradients of soil nutrient availability and pH, and show that variations in
1151 nutrient availability matter more for determining variation in leaf photosynthetic
1152 traits than soil pH.

1153

Chapter 4

1154 The relative cost of resource use for photosynthesis drives variance in
1155 leaf nitrogen content across climate and soil resource availability
1156 gradients

1157 4.1 Introduction

1158 Terrestrial biosphere models, which comprise the land surface component of
1159 Earth system models, are sensitive to the formulation of photosynthetic processes
1160 (Knorr 2000; Ziehn et al. 2011; Booth et al. 2012). This is because photosynthe-
1161 sis is the largest carbon flux between the atmosphere and terrestrial biosphere,
1162 and is constrained by ecosystem carbon and nutrient cycles (Hungate et al. 2003;
1163 LeBauer and Treseder 2008; IPCC 2021; Fay et al. 2015). Many terrestrial bio-
1164 sphere models formulate photosynthesis by parameterizing photosynthetic capac-
1165 ity within plant functional groups through empirical linear relationships between
1166 area-based leaf nitrogen content (N_{area}) and the maximum carboxylation rate
1167 of Ribulose-1,5-bisphosphate carboxylase/oxygenase (Kattge et al. 2009; Rogers
1168 2014; Rogers et al. 2017). Models are also beginning to include connected carbon-
1169 nitrogen cycles (Wieder et al. 2015; Shi et al. 2016; Davies-Barnard et al. 2020;
1170 Braghieri et al. 2022), which allows leaf photosynthesis to be predicted directly
1171 through changes in N_{area} and indirectly through changes in soil nitrogen avail-
1172 ability (e.g., LPJ-GUESS, Smith et al., 2014; CLM5.0, Lawrence et al., 2019).
1173 Despite recent model developments, open questions remain regarding the gen-
1174 erality of ecological relationships between soil nitrogen availability, leaf nitrogen
1175 content, and leaf photosynthesis across edaphic and climatic gradients.
1176 Empirical support for positive relationships between soil nitrogen avail-

ability and N_{area} is abundant (Firn et al. 2019; Liang et al. 2020), and is a result often attributed to the high nitrogen cost of building and maintaining Rubisco (Evans 1989; Evans and Seemann 1989; Onoda et al. 2004; Onoda et al. 2017; Dong et al. 2020). Such patterns imply that positive relationships between soil nitrogen availability and N_{area} should cause an increase in leaf photosynthesis and photosynthetic capacity by increasing the maximum rate of Rubisco carboxylation through increased investments to Rubisco construction and maintenance. This integrated N_{area} -photosynthesis response to soil nitrogen availability has been observed both in manipulative experiments and across environmental gradients (Field and Mooney 1986; Evans 1989; Walker et al. 2014; Li et al. 2020), and is thought to be driven by ecosystem nitrogen limitation, which limits its primary productivity globally (LeBauer and Treseder 2008; Fay et al. 2015). However, this response is not consistently observed, as recent studies note variable N_{area} -photosynthesis relationships across soil nitrogen availability gradients (Liang et al. 2020; Luo et al. 2021) and that aboveground growing conditions (e.g., light availability, temperature, vapor pressure deficit) or species identity traits (e.g., photosynthetic pathway, nitrogen acquisition strategy) may be more important for explaining variance in N_{area} and photosynthetic capacity across time and space (Adams et al. 2016; Dong et al. 2017; Dong et al. 2020; Dong et al. 2022; Smith et al. 2019; Peng et al. 2021; Westerband et al. 2023).

One hypothesized mechanism to explain variance in N_{area} across environmental gradients has been proposed via photosynthetic least-cost theory (Wright et al. 2003; Prentice et al. 2014; Paillassa et al. 2020; Harrison et al. 2021). The theory predicts that plants acclimate to environments by optimizing photo-

1201 synthetic assimilation rates at the lowest summed cost of nitrogen and water use
1202 (Wright et al. 2003; Prentice et al. 2014). In a given environment, the theory
1203 proposes that nitrogen and water use can be substituted for each other to main-
1204 tain the lowest summed cost to satisfy leaf resource demand, such that optimal
1205 photosynthetic rates are achieved with less efficient use of the more abundant
1206 and less costly resource to acquire in exchange for more efficient use of the less
1207 abundant and more costly resource to acquire.

1208 Photosynthetic least-cost theory predicts that, all else equal, an increase
1209 in soil nitrogen availability should decrease the cost of acquiring and using nitro-
1210 gen relative to water (β), resulting in optimal photosynthetic rates achieved with
1211 greater N_{area} at lower stomatal conductance and lower leaf $C_i:C_a$ (χ) (Wright et al.
1212 2003; Prentice et al. 2014). Alternatively, an increase in soil moisture should re-
1213 duce costs of water acquisition and use, increasing β , stomatal conductance, and
1214 χ , resulting in optimal photosynthetic rates achieved with decreased N_{area} . The
1215 theory also predicts variability in stomatal conductance and N_{area} in response to
1216 climatic factors, suggesting that the optimal response to increased vapor pressure
1217 deficit (VPD) should be a reduction in stomatal conductance and χ that is coun-
1218 terbalanced by an increase in N_{area} to support the higher photosynthetic capacity
1219 needed to maintain high assimilation at lower conductance (Grossiord et al. 2020;
1220 Dong et al. 2020; Westerband et al. 2023).

1221 Leaf nitrogen allocation responses to changing climates or soil resource
1222 availability may also depend on their mode of nutrient acquisition or photo-
1223 synthetic pathway. For example, species that form associations with symbiotic
1224 nitrogen-fixing bacteria (referred as “N-fixing species” from this point forward)

1225 should, in theory, have access to a less finite nitrogen supply, which may result in
1226 lower β values than species not capable of forming such associations (referred as
1227 “non-fixing species” from this point forward). This result was previously shown
1228 in a greenhouse experiment, where a leguminous species generally had lower costs
1229 of nitrogen acquisition compared to a non-leguminous species, although these dif-
1230 ferences were generally stronger under increased nitrogen limitation (Fig. 2.1)
1231 (Perkowski et al. 2021). Lower β values could be a possible explanation for
1232 why N-fixing species commonly have higher leaf nitrogen content than non-fixing
1233 species (Adams et al. 2016; Dong et al. 2017).

1234 Similarly, leaf nitrogen allocation patterns across environmental gradients
1235 may be dependent on photosynthetic pathway. General lower χ values in C₄
1236 species suggests that C₄ species should have lower β values than C₃ species, a
1237 pattern that could be the result of increased costs associated with water acquisition
1238 and use or reduced costs associated with nutrient acquisition and use relative to
1239 C₃ species. No study to date has directly quantified χ in C₄ species aside from the
1240 dataset used to initially parameterize an optimality model for C₄ species (Scott
1241 and Smith 2022).

1242 While photosynthetic least-cost theory provides a unified hypothesis for
1243 understanding effects of climate and soil resource availability on N_{area} , empiri-
1244 cal tests of the theory are sparse. Increasing soil nitrogen availability has been
1245 previously shown to decrease the cost of acquiring nutrients (Bae et al. 2015; Lu
1246 et al. 2022; Eastman et al. 2021), which can induce predictable nutrient-water use
1247 tradeoffs expected from the theory across broad environmental gradients (Paillassa
1248 et al. 2020; Querejeta et al. 2022; Westerband et al. 2023) and in manipulation

1249 experiments (Bialic-Murphy et al. 2021). Additionally, increasing VPD has been
1250 shown to have a positive effect on N_{area} (Dong et al. 2017; Dong et al. 2020; Firn
1251 et al. 2019). However, studies have been restricted to exploring these patterns
1252 with C₃ species and, while previous studies have shown that variance in N_{area}
1253 across environmental gradients is driven by strong negative relationships with χ
1254 (Fig 3.4c)(Dong et al. 2017; Paillassa et al. 2020; Westerband et al. 2023),
1255 no study to date has explicitly investigated effects of soil resource availability or
1256 plant functional group on N_{area} using β as a direct predictor of χ . Additionally, as
1257 N_{area} can be broken down into structural (leaf mass per area; M_{area} ; g m⁻²) and
1258 metabolic (mass-based leaf nitrogen content; N_{mass} ; gN g⁻¹) components (Dong et
1259 al. 2017), no study has investigated which component of N_{area} drives the hypothe-
1260 sized response of N_{area} to χ , which would be useful for detecting whether changes
1261 in N_{area} due to χ are driven by changes in leaf morphology or stoichiometry.

1262 Here, I measured N_{area} , N_{mass} , M_{area} , leaf δ¹³C-derived estimates of χ , and
1263 leaf δ¹³C-derived estimates of β in 520 individuals spanning 57 species scattered
1264 across 24 grassland sites in Texas, USA (Table S1). Texas contains a diverse
1265 climatic gradient, indicated by 2006-2020 mean annual precipitation totals ranging
1266 from 204 to 1803 mm and 2006-2020 mean annual temperature ranging from
1267 11.8° to 24.6°C. Variability in soil nitrogen availability and soil moisture was
1268 expected across sites, owing to differences in soil texture and aboveground climate
1269 that would drive differential rates of water retention and nitrogen transformations
1270 to plant-available substrate. I leveraged the expected climatic and soil resource
1271 variability across sites to test the following hypotheses:

1272 1. Soil nitrogen availability will decrease β through a reduction in costs of

1273 nitrogen acquisition and use, while soil moisture will increase β through a
1274 reduction in costs of water acquisition and use. We expected that N-fixing
1275 species would have lower β values due to their ability to minimize costs
1276 of nitrogen acquisition under low nitrogen availability and that C₄ species
1277 would have lower β values due to increased costs of water acquisition and
1278 use or reduced costs of nitrogen acquisition and use.

1279 2. χ will be positively related to β , a pattern that will result in a negative
1280 indirect effect of increasing soil nitrogen availability, positive indirect effect
1281 of increasing soil moisture on χ , and lower χ in both N-fixing species and
1282 C₄ species. We also expected that χ would be negatively related to VPD,
1283 as increasing atmospheric dryness should cause plants to close stomata to
1284 minimize water loss.

1285 3. N_{area} will be negatively related to χ . This response will result in an indi-
1286 rect positive effect of increasing soil nitrogen availability, a negative effect of
1287 increasing soil moisture on N_{area} , and generally larger N_{area} values in both N-
1288 fixing species. We expected these patterns to be mediated through a positive
1289 relationship between β and χ . While theory predicts that negative relation-
1290 ships between N_{area} and χ should yield generally larger N_{area} in C₄ species,
1291 we expected that C₄ species would have lower N_{area} due to generally greater
1292 nitrogen use efficiency in C₄ species than C₃ species. Additionally, VPD
1293 was expected to increase N_{area} , a pattern that would be directly mediated
1294 through the reduction in χ with increasing VPD.

1295 4.2 Methods

1296 4.2.1 *Site descriptions and sampling methodology*

1297 I collected leaf and soil samples from 24 open grassland sites across cen-
1298 tral and eastern Texas in summer 2020 and summer 2021 (Fig. 4.1). Twelve
1299 sites were visited between June and July 2020 and 14 sites (11 unique from 2020)
1300 were visited between May and June 2021 (Table 1). I explicitly chose sites that
1301 maximized variability in precipitation and edaphic variability between sites while
1302 minimizing temperature variability across the environmental gradient (Table 1).
1303 No site with personally communicated or anecdotal evidence of grazing or distur-
1304 bance (e.g., mowing, feral hog activity, etc.) were used. I collected leaf material
1305 from three individuals each of the five most abundant species at random locations
1306 at each site, only selecting species that were broadly classified as graminoid or
1307 forb/herb growth habits per the USDA PLANTS database (USDA NRCS 2022).
1308 All collected leaves were fully expanded with no visible herbivory or other external
1309 damage and also free from shading by nearby shrubs or trees. Five soil samples
1310 were collected from 0-15cm below the soil surface at each site near the leaf collec-
1311 tion sample locations. Soil samples were later mixed together by hand to create
1312 one composite soil sample per site.

1313 4.2.2 *Leaf trait measurements*

1314 Images of each leaf were taken immediately following each site visit using
1315 a flat-bed scanner. Fresh leaf area was determined from each image using the
1316 'LeafArea' R package (Katabuchi 2015), which automates leaf area calculations
1317 using ImageJ software (Schneider et al. 2012). Each leaf was dried at 65°C for at

1318 least 48 hours to a constant mass, weighed, and manually ground in a mortar and
1319 pestle until homogenized. Leaf mass per area (M_{area} ; g m⁻²) was calculated as the
1320 ratio of dry leaf biomass to fresh leaf area. Subsamples of dried and homogenized
1321 leaf tissue were used to measure leaf nitrogen content (N_{mass} ; gN g⁻¹) through el-
1322 emental combustion analysis (Costech-4010, Costech Instruments, Valencia, CA).
1323 Leaf nitrogen content per unit leaf area (N_{area} ; gN m⁻²) was then calculated as
1324 the product of N_{mass} and M_{area} .

1325 Subsamples of dried and homogenized leaf tissue were sent to the University
1326 of California-Davis Stable Isotope Facility to determine leaf $\delta^{13}\text{C}$. Leaf $\delta^{13}\text{C}$ values
1327 were determined using an elemental analyzer (PDZ Europa ANCA-GSL; Sercon
1328 Ltd., Chestshire, UK) interfaced to an isotope ratio mass spectrometer (PDZ
1329 Europa 20-20 Isotope Ratio Mass Spectrometer, Sercon Ltd., Chestshire, UK).
1330 I used leaf $\delta^{13}\text{C}$ values (‰; relative to Vienna Pee Dee Belemnite international
1331 reference standard) to estimate the ratio of intercellular (C_i) to extracellular (C_a)
1332 CO₂ ratio (leaf $C_i:C_a$, χ ; unitless) following the approach of Farquhar et al. (1989)
1333 described in Cernusak et al. (2013). Specifically, I derived χ as:

$$\chi = \frac{C_i}{C_a} = \frac{\Delta^{13}\text{C} - a}{b - a} \quad (4.1)$$

1334 where $\Delta^{13}\text{C}$ represents the relative difference between leaf $\delta^{13}\text{C}$ (‰) and air $\delta^{13}\text{C}$
1335 (‰), and is calculated as:

$$\Delta^{13}\text{C} = \frac{\delta^{13}\text{C}_{\text{air}} - \delta^{13}\text{C}_{\text{leaf}}}{1 + \delta^{13}\text{C}_{\text{leaf}}} \quad (4.2)$$

1336 $\delta^{13}\text{C}_{\text{air}}$, traditionally assumed to be -8‰ (Keeling et al. 1979; Farquhar et al.

1337 1989), was calculated as a function of calendar year t using an empirical equation
1338 derived in Feng (1999):

$$\delta^{13}C_{air} = -6.429 - 0.006e^{0.0217(t-1740)} \quad (4.3)$$

1339 This calculation resulted in $\delta^{13}C_{air}$ values for 2020 and 2021 as -9.04 and -9.09,
1340 respectively. a represents the fractionation between ^{12}C and ^{13}C due to diffusion
1341 in air, assumed to be 4.4‰, and b represents the fractionation caused by Rubisco
1342 carboxylation, assumed to be 27‰ (Farquhar et al. 1989). For C_4 species, b in
1343 Eqn. 4.1 was set to 6.3‰, and was derived from:

$$b = c + (d \cdot \phi) \quad (4.4)$$

1344 Where c was set to -5.7‰ and d was set to 30‰ (Farquhar et al. 1989). ϕ , which
1345 is the bundle sheath leakiness term, was set to 0.4. All χ values less than 0.2 and
1346 greater than 1.0 were assumed to be incorrect and removed.

1347 I derived the unit cost of resource use (β) using leaf χ and site climate data
1348 with equations first described in Prentice et al. (2014) and simplified in Lavergne
1349 et al. (2020):

$$\beta = 1.6\eta^*D \frac{\chi - (\frac{\Gamma^*}{C_a})^2}{(1 - \chi)^2(K_m + \Gamma^*)} \quad (4.5)$$

1350 where η^* is the viscosity of water relative to 25°C, calculated using elevation and
1351 mean air temperature of the seven days leading up to each site visit following
1352 equations in Huber et al. (2009). D represents vapor pressure deficit (Pa), set

1353 to the mean vapor pressure deficit of the seven days leading up to each site visit,
1354 C_a represents atmospheric CO₂ concentration, arbitrarily set to 420 $\mu\text{mol mol}^{-1}$
1355 CO². K_m (Pa) is the Michaelis-Menten coefficient for Rubisco affinity to CO₂ and
1356 O₂, calculated as:

$$K_m = K_c \cdot \left(1 + \frac{O_i}{K_o}\right) \quad (4.6)$$

1357 where K_c (Pa) and K_o (Pa) are the Michaelis-Menten coefficients for Rubisco
1358 affinity to CO₂ and O₂, respectively, and O_i is the intercellular O₂ concentration.
1359 Γ^* (Pa) is the CO₂ compensation point in the absence of dark respiration. K_c , K_o ,
1360 and Γ^* were determined using equations described in Medlyn et al. (2002) and
1361 derived in Bernacchi et al. (2001), invoking an elevation correction for atmospheric
1362 pressure as explained in Stocker et al. (2020).

Table 4.1. Site locality information, sampling year(s), 2006-2020 mean annual precipitation (MAP; mm), mean annual temperature (MAT; °C), and water holding capacity (WHC; mm)*

Site	Latitude	Longitude	Sampling year	MAP	MAT	WHC
Edwards_2019_17	29.95	-100.36	2020	563.5	19.0	224.7
Uvalde_2020_02	29.59	-100.09	2020, 2021	648.5	19.5	224.7
Menard_2020_01	30.91	-99.59	2020	641.9	18.3	220.2
Kerr_2020_03	30.06	-99.34	2021	672.4	18.3	237.5
Bandera_2020_03	29.85	-99.30	2021	789.4	18.8	235.1
Sansaba_2020_01	31.29	-98.62	2020	733.0	18.8	234.3
Comal_2020_21	29.79	-98.43	2020	878.5	19.9	220.7
Blanco_2019_16	29.99	-98.43	2020	833.0	19.2	222.2
Bexar_2019_13	29.24	-98.43	2020	759.3	21.5	206.0
Burnet_2020_14	30.84	-98.34	2021	763.3	19.5	217.8
Comal_2020_19	30.01	-98.32	2021	845.0	19.3	220.4
Hays_2020_54	29.96	-98.17	2021	861.3	20.0	225.6
Burnet_2020_12	30.82	-98.06	2021	815.1	19.4	245.3
Williamson_2019_09	30.71	-97.86	2020	867.7	19.7	270.2
Williamson_2019_10	30.54	-97.77	2020	819.5	19.9	239.8
Bell_2021_08	31.06	-97.55	2021	937.3	19.6	232.3
Fayette_2021_12	29.86	-97.21	2021	985.7	20.4	165.6
Fayette_2019_04	30.09	-96.78	2020	1017.4	20.6	226.9
Fayette_2020_09	29.86	-96.71	2021	1002.7	20.8	187.6
Washington_2020_08	30.28	-96.41	2021	1077.4	20.4	203.9
Austin_2020_03	29.78	-96.24	2021	1108.7	20.6	253.0
Brazos_2020_16	30.93	-96.23	2021	1078.0	20.1	202.2
Brazos_2020_18	30.52	-96.21	2020, 2021	1099.4	20.4	233.5
Harris_2020_03	29.88	-95.31	2020, 2021	1492.0	21.6	265.6

1363 *Rows are arranged by longitude to visualize precipitation variability across sites

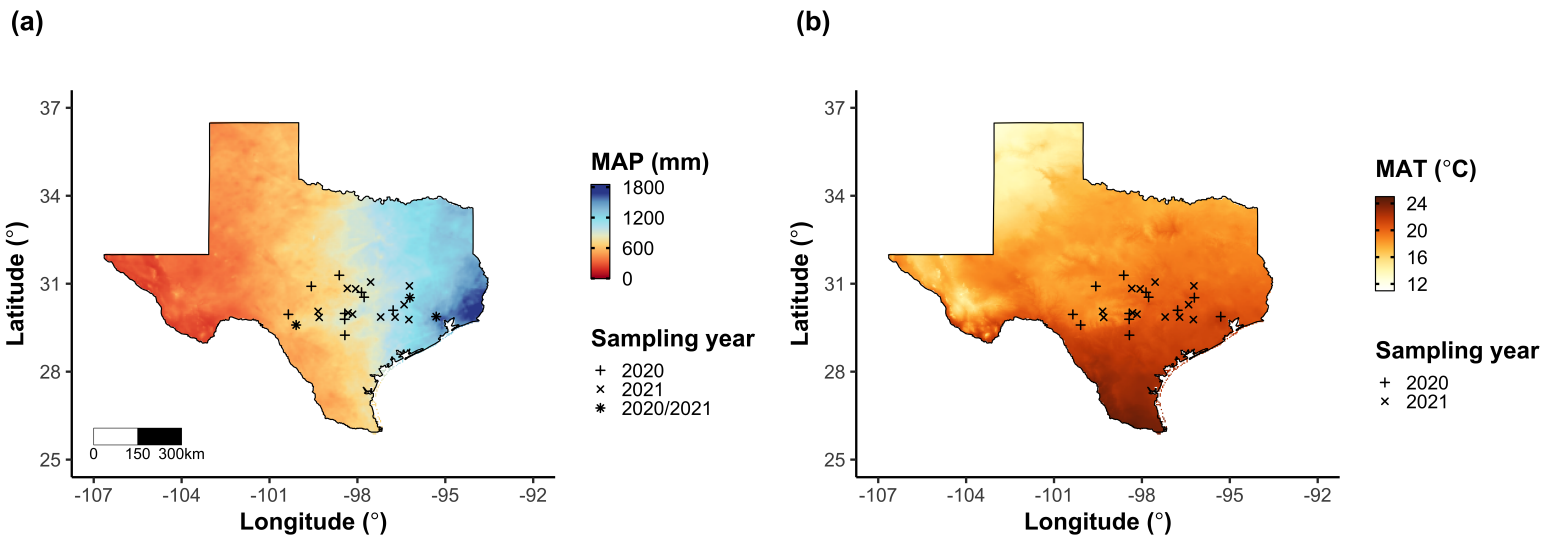


Figure 4.1. Maps that detail site locations along 2006-2020 mean annual precipitation (a) and mean annual temperature (b) gradients in Texas, USA. Precipitation and temperature data were plotted at a 4-km grid resolution and are masked to include only grid cells that occur in the Texas state boundary in the United States. In both panels, open circles refer to sites visited in 2020, open triangles to sites visited in 2021, and closed circles to sites visited in 2020 and 2021. The scale bar in panel A also applies to panel B.

1364 4.2.3 *Site climate data*

1365 I used the Parameter-elevation Regressions on Independent Slopes Model
1366 (PRISM) (Daly et al. 2008)climate product to access gridded daily temperature
1367 and precipitation data for the coterminous United States at a 4-km grid resolution
1368 between January 1, 2006 and July 31, 2021 (PRISM Climate Group, Oregon State
1369 University, <https://prism.oregonstate.edu>, data created 4 Feb 2014, accessed 24
1370 Mar 2022). Daily mean air temperature, mean VPD, and total precipitation
1371 data were extracted from the grid cell that contained the latitude and longitude
1372 of each property using the ‘extract’ function in the ‘terra’ R package (Hijmans
1373 2022). PRISM data were used in lieu of local weather station data because several
1374 rural sites did not have a local weather station present within a 20-km radius of
1375 the site. Daily site climate data were used to estimate mean annual precipitation
1376 and mean annual temperature for each site between 2006 and 2020 (Table 1). I
1377 calculated total precipitation and mean daily VPD for the prior 1, 2, 3, 4, 5, 6, 7,
1378 8, 9, 10, 15, 20, 25, 30, 60, and 90 days leading up to each site visit.

1379 4.2.4 *Site edaphic characteristics*

1380 Subsamples of composited soil samples were sent to the Texas A & M
1381 Soil, Water and Forage Laboratory to quantify soil nitrate concentration (NO₃-N;
1382 ppm). Soil NO₃-N was determined by extracting composite soil samples in 1 M
1383 KCl, measuring absorbance values of extracts at 520 nm using the end product of
1384 a NO₃-N to NO₂-N cadmium reduction reaction (Kachurina et al. 2000). Soil tex-
1385 ture data from 0-15cm below the soil surface were accessed using the SoilGrids2.0
1386 data product (Poggio et al. 2021) through the ‘fetchSoilGrids’ function in the

1387 ‘soilDB’ R package (Beaudette et al. 2022). I used SoilGrids2.0 to access soil
1388 texture data in lieu of analyses using the collected composite soil sample due to
1389 a lack of soil material from some sites after sending samples for soil NO₃-N.

1390 Soil moisture was not measured in the field, but was estimated using
1391 the ‘Simple Process-Led Algorithms for Simulating Habitats’ model (‘SPLASH’)
1392 (Davis et al. 2017). This model, derived from the STASH model (Cramer and
1393 Prentice 1988), spins up a bucket model using Priestley-Taylor equations (Priest-
1394 ley and Taylor 1972) to calculate daily soil moisture (W_n ; mm) as a function
1395 of the previous day’s soil moisture (W_{n-1} ; mm), daily precipitation (P_n ; mm),
1396 condensation (C_n ; mm), actual evapotranspiration (E_n^a ; mm), and runoff (RO;
1397 mm):

$$W_n = W_{n-1} + P_n + C_n - E_n^a - RO \quad (4.7)$$

1398 Models were spun up by equilibrating the previous day’s soil moisture using
1399 successive model iterations with daily mean air temperature, daily precipitation
1400 total, the number of daily sunlight hours, and latitude as model inputs (Davis et al.
1401 2017). Daily sunlight hours were estimated for each day at each site using the
1402 ‘getSunlightTimes’ function in the ‘suncalc’ R package, which estimated sunrise
1403 and sunset times of each property using date and site coordinates (Thieurmel and
1404 Elmarhraoui 2019). Water holding capacity (mm), or bucket size, was estimated
1405 as a function of soil texture using pedotransfer equations explained in Saxton and
1406 Rawls (2006), as done in Stocker et al. (2020) and Bloomfield et al. (2023). A
1407 summary of these equations is included in the Supplemental Information.

1408 Daily soil moisture outputs from the SPLASH model for each site were
1409 used to calculate mean daily soil moisture for the prior 1, 2, 3, 4, 5, 6, 7, 8, 9,
1410 10, 15, 20, 25, 30, 60, and 90 days leading up to each site visit. Mean daily
1411 soil moisture values were then expressed as a fraction of water holding capacity
1412 to normalize across sites with different bucket depths, as done in Stocker et al.
1413 (2018).

1414 4.2.5 *Plant functional group assignments*

1415 Plant functional group was assigned to each species and used as the pri-
1416 mary descriptor of species identity. Specifically, I assigned plant functional groups
1417 based on photosynthetic pathway (C_3 , C_4) and ability to form associations with
1418 symbiotic nitrogen-fixing bacteria. The ability to form associations with symbi-
1419 otic nitrogen-fixing bacteria was assigned based on whether species were in the
1420 *Fabaceae* family, and photosynthetic pathway of each species was determined from
1421 past literature and confirmed through leaf $\delta^{13}C$ values. We chose these plant func-
1422 tional groups based on *a priori* hypotheses regarding the functional role of nitrogen
1423 fixation and photosynthetic pathway on the sensitivity of plant nitrogen uptake
1424 and leaf nitrogen allocation to soil nutrient availability and aboveground growing
1425 conditions. These plant functional group classifications resulted in three distinct
1426 plant functional groups within our dataset: C_3 legumes ($n = 53$), C_3 non-legumes
1427 ($n = 350$), and C_4 non-legumes ($n = 117$).

1428 4.2.6 *Data analysis*

1429 All analyses and plotting were conducted in R version 4.1.1 (R Core Team
1430 2021). I constructed a series of separate linear mixed-effects models to investigate
1431 environmental drivers of β , χ , N_{area} , N_{mass} , and M_{area} , followed by a path analysis
1432 using a piecewise structural equation model to investigate direct and indirect
1433 effects of climate and soil resource availability on N_{area} .

1434 To explore environmental drivers of β , I built a linear mixed-effects model
1435 that included soil moisture, soil nitrogen availability, and plant functional group
1436 as fixed effect coefficients. Species were designated as a random intercept term.
1437 Interaction coefficients between all possible combinations of the three fixed effect
1438 coefficients were also included. β was natural log transformed to linearize data.
1439 I used an information-theoretic model selection approach to determine whether
1440 90-, 60-, 30-, 20-, 15-, 10-, 9-, 8-, 7-, 6-, 5-, 4-, 3-, 2-, or 1-day mean daily soil
1441 moisture conferred the best model fit for β . To do this, I constructed 16 separate
1442 linear mixed-effects models where log-transformed β was included as the response
1443 variable and each soil moisture time step was separately included as a single
1444 continuous fixed effect. Species were included as a random intercept term for all
1445 models. I used corrected Akaike Information Criterion (AICc) to select the soil
1446 moisture timescale that conferred the best model fit, indicated by the model with
1447 the lowest AICc score (Table S2; Fig. S2).

1448 To explore environmental drivers of χ , I constructed a second linear mixed
1449 effects model that included VPD, soil moisture, soil nitrogen availability, and plant
1450 functional group as fixed effect coefficients. Two-way interactions between plant
1451 functional group and VPD, soil nitrogen availability, or soil moisture were also

1452 included as fixed effect coefficients, in addition to a three-way interaction between
1453 soil moisture, soil nitrogen availability, and plant functional group. Species were
1454 included as a random intercept term. I used an information-theoretic model se-
1455 lection approach to determine whether 90-, 60-, 30-, 20-, 15-, 10-, 9-, 8-, 7-, 6-,
1456 5-, 4-, 3-, 2-, or 1-day mean daily VPD conferred the best model fit for χ using
1457 the same approach explained above for the soil moisture effect on β . The soil
1458 moisture timescale was set to the same timescale that conferred the best fit for β .

1459 To explore environmental drivers of N_{area} , N_{mass} , and M_{area} , I constructed
1460 three separate linear mixed effects model that each included χ , soil nitrogen avail-
1461 ability, soil moisture, and plant functional group as fixed effect coefficients. Two-
1462 way interactions between plant functional group and β , χ , soil nitrogen availability,
1463 or soil moisture were included as additional fixed effect coefficients, in addition to
1464 a three-way interaction between soil nitrogen availability, soil moisture, and plant
1465 functional group. Species were included as a random intercept term, with the soil
1466 moisture timescale set to the same timescale that conferred the best fit for β .

1467 In all linear mixed-effects models explained above, including those to select
1468 relevant timescales, I used the 'lmer' function in the 'lme4' R package (Bates et al.
1469 2015) to fit each model and the 'Anova' function in the 'car' R package (Fox and
1470 Weisberg 2019) to calculate Type II Wald's χ^2 and determine the significance
1471 level ($\alpha = 0.05$) of each fixed effect coefficient. I used the 'emmeans' R package
1472 (Lenth 2019) to conduct post-hoc comparisons using Tukey's tests, where degrees
1473 of freedom were approximated using the Kenward-Roger approach (Kenward and
1474 Roger 1997). Trendlines and error ribbons for all plots were drawn using a series
1475 of 'emmeans' outputs across the range in plotted x-axis values.

Finally, I conducted a path analysis using a piecewise structural equation model to examine direct and indirect pathways that determined variance in N_{area} . Seven separate linear mixed effects models were loaded into the piecewise structural equation model. Models were constructed per our *a priori* hypotheses following patterns expected from photosynthetic least-cost theory. The first model regressed N_{area} against χ , N_{mass} , and M_{area} . The second model regressed M_{area} against χ . The third model regressed N_{mass} against χ and M_{area} (Dong et al. 2017; Dong et al. 2020). The fourth model regressed χ against β and VPD. The fifth model regressed β against soil nitrogen availability, soil moisture, ability to associate with symbiotic nitrogen-fixing bacteria, and photosynthetic pathway. The sixth model regressed soil nitrogen availability against soil moisture, while the seventh model regressed VPD against soil moisture (Novick et al. 2016; Sulman et al. 2016). All models included the relevant timescale selected in the individual linear mixed effect models explained above (2-day soil moisture, 4-day vapor pressure deficit). Models also included species as a random intercept term, were built using the ‘lme’ function in the ‘nlme’ R package (Pinheiro and Bates 2022), and subsequently loaded into the piecewise structural equation model using the ‘psem’ function in the ‘piecewiseSEM’ R package (Lefcheck 2016).

4.3 Results

4.3.1 Cost to acquire nitrogen relative to water

Model selection indicated that 2-day soil moisture was the timescale that conferred the best model fit for β ($\text{AICc} = 1227.83$; Table S2; Fig. S1). Increasing soil nitrogen availability generally decreased β ($p < 0.001$; Table 4.2), a pattern

1499 driven by a negative effect of increasing soil nitrogen availability on β in C₃ non-
1500 legumes (Tukey: $p < 0.001$) and C₃ legumes (Tukey: $p = 0.004$; Fig. 4.2a). C₄
1501 nonlegumes also demonstrated a negative trend in the effect of increasing soil ni-
1502 trogen availability on β , but this pattern was not significantly different from zero
1503 (Tukey: $p = 0.307$; Fig. 4.2a). There was no apparent effect of soil moisture on
1504 β ($p = 0.264$; Table 4.2; Fig. 4.2b). A functional group effect ($p < 0.001$; Table
1505 4.2) indicated that C₄ nonlegumes generally had lower β values than both C₃
1506 legumes and C₃ non-legumes when averaged across soil moisture and soil nitrogen
1507 availability values (Tukey: $p < 0.001$ in both cases), while average β values in C₃
1508 legumes did not differ from C₃ nonlegumes (Tukey: $p = 0.691$).

Table 4.2. Effects of soil moisture, soil nitrogen availability, and plant functional group on β

	df	Coefficient	χ^2	p
Intercept	-	3.20E+00	-	-
Soil moisture (SM_2)	1	2.19E-01	1.244	0.265
Soil N (N)	1	-1.70E-02	26.823	<0.001
PFT	2	-	199.617	<0.001
SM_2*N	1	1.77E-03	0.438	0.508
SM_2*PFT	2	-	2.038	0.361
$N*PFT$	2	-	7.668	0.022
$SM_2*N*PFT$	2	-	0.127	0.939

1509 *Significance determined using Type II Wald χ^2 tests ($\alpha = 0.05$). P-values < 0.05

1510 are in bold. Model coefficients are expressed on the natural-log scale and are only

1511 included for continuous fixed effects. Key: df = degrees of freedom, χ^2 = Wald

1512 Type II chi-square test statistic

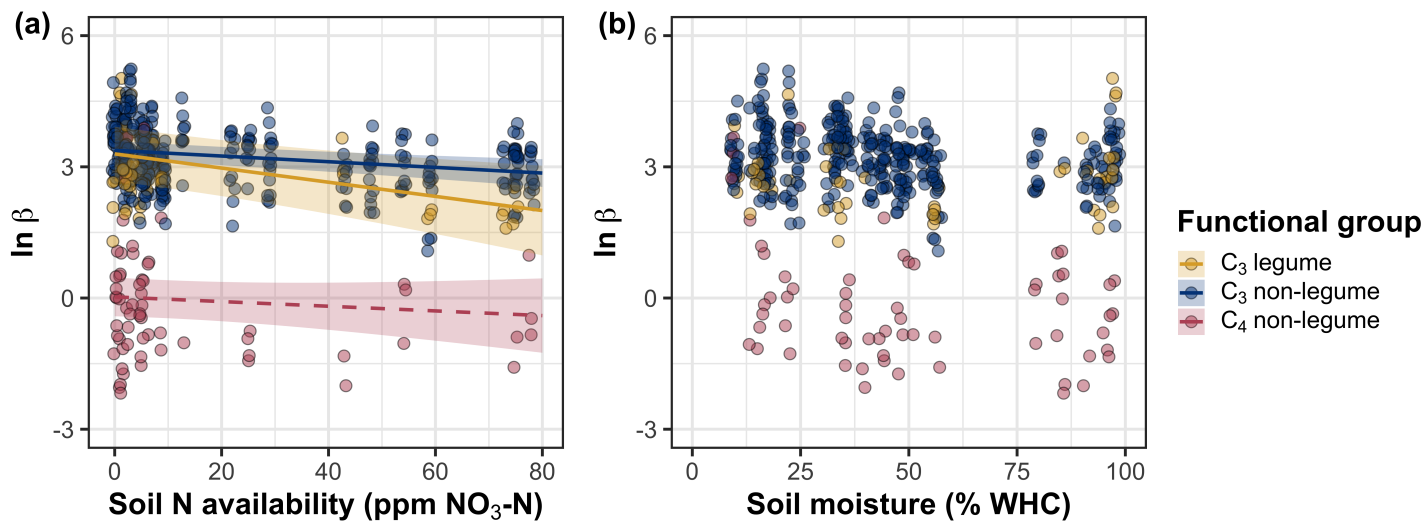


Figure 4.2. Effects of soil nitrogen availability (a) and soil moisture (b) on the unit cost ratio β . In (b), soil moisture is represented as a percent of site water holding capacity. Yellow shading and trendlines indicate C₃ legumes, blue shading and trendlines indicate C₃ non-legumes, and red shading and trendlines indicate C₄ non-legumes. Points are jittered for visibility. Variably colored trendlines are only included if there is an interaction between the x-axis and plant functional group, where solid trendlines indicate slopes that are different from zero ($p < 0.05$) and dashed trendlines indicate slopes that are not different from zero ($p > 0.05$). Error ribbons represent the upper and lower 95% confidence intervals of each fitted trendline.

1513 4.3.2 *Leaf C_i:C_a*

1514 Model selection indicated that 4-day daily VPD was the timescale that
1515 conferred the best model fit for χ (AICc = -883.97; Table S1; Fig. S2).

1516 Variance in χ was driven by a series of two-way interactions between func-
1517 tional group and VPD ($p = 0.006$; Table 3), soil moisture ($p = 0.033$, Table 3.3),
1518 and soil nitrogen availability ($p = 0.022$; Table 3). The interaction between 4-day
1519 VPD and functional group revealed that the general negative effect of increasing
1520 VPD ($p < 0.001$; Table 3) was driven by a negative effect of increasing VPD
1521 on χ in C₃ nonlegumes (Tukey: $p < 0.001$) and marginal negative effect in C₃
1522 legumes (Tukey: $p = 0.074$) paired with a positive trending, but insignificant
1523 effect of increasing VPD in C₄ nonlegumes (Tukey: $p = 0.130$; Fig. 3a). The
1524 interaction between 2-day soil moisture and functional group indicated that the
1525 general negative effect of increasing soil moisture on χ was driven by a positive
1526 effect of increasing soil moisture on χ in C₄ nonlegumes (Tukey: $p = 0.009$) de-
1527 spite a positive trending but insignificant effect of increasing soil moisture on χ
1528 in C₃ legumes (Tukey: $p = 0.116$) and a null effect of soil moisture on χ in C₃
1529 nonlegumes (Tukey: $p = 0.693$; Fig. 3c). The interaction between soil nitrogen
1530 availability and plant functional group revealed a weak negative effect of increas-
1531 ing soil nitrogen availability on χ in C₃ legumes (Tukey: $p = 0.045$), with no
1532 apparent effect in C₃ nonlegumes (Tukey: $p = 0.706$) or C₄ nonlegumes (Tukey:
1533 $p = 0.757$). Finally, an individual effect of functional group ($p < 0.001$; Table 3)
1534 revealed that C₄ nonlegumes generally had lower χ than C₃ legumes and C₃ non-
1535 legumes (Tukey: $p < 0.001$ in both cases), with no apparent difference between
1536 C₃ legumes and C₃ nonlegumes (Tukey: $p = 0.831$).

Table 4.3. Effects of soil moisture, soil nitrogen availability, and plant functional group on χ^*

	df	Coefficient	χ^2	p
Intercept	-	9.33E-01	-	-
Vapor pressure deficit (VPD_4)	1	-1.78E-01	20.792	<0.001
Soil moisture (SM_2)	1	4.53E-02	1.972	0.160
Soil N (N)	1	-1.30E-03	0.168	0.682
PFT	2	-	172.624	<0.001
SM_2^*N	1	7.40E-04	0.849	0.357
VPD_4^*PFT	2	-	10.241	0.006
SM_2^*PFT	2	-	6.806	0.033
N^*PFT	2	-	7.602	0.022
$SM_2^*N^*PFT$	2	-	0.732	0.694

1537 *Significance determined using Type II Wald χ^2 tests ($\alpha = 0.05$). *P*-values less

1538 than 0.05 are in bold and *p*-values where $0.05 < p < 0.1$ are italicized. χ was

1539 not transformed prior to model fitting, so model coefficients are reported on the

1540 response scale. Model coefficients are only included for continuous fixed effects.

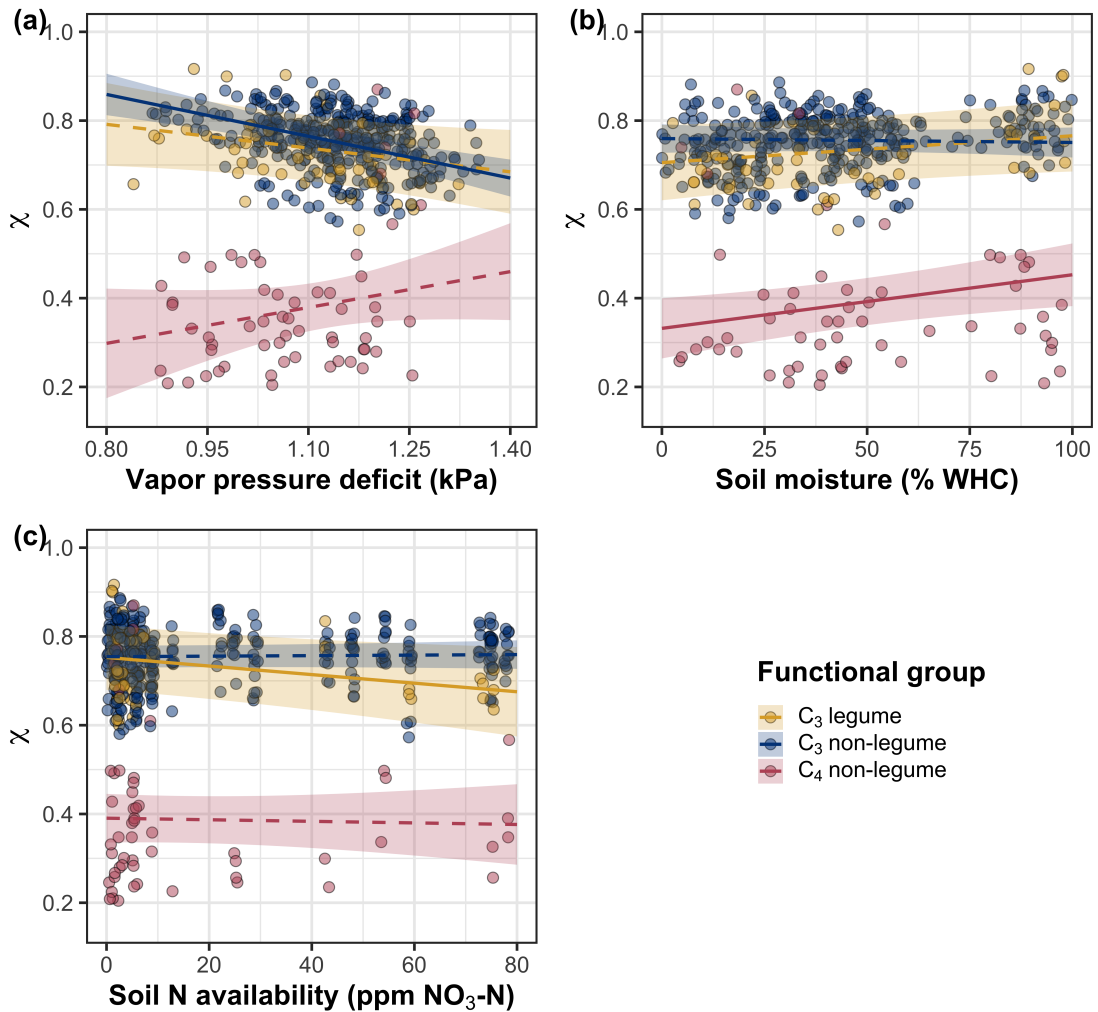


Figure 4.3. Effects of 4-day mean vapor pressure deficit (a), 2-day soil moisture (per water holding capacity; b), and soil nitrogen availability (c) on χ . Shading and trendlines are as explained in Figure 2. Points are jittered for visibility. Variably colored trendlines are only included if there is an interaction between the x-axis and plant functional group, where solid trendlines indicate slopes that are different from zero ($p < 0.05$) and dashed trendlines indicate slopes that are not different from zero ($p < 0.05$). Error ribbons represent the upper and lower 95% confidence intervals of each fitted trendline.

1541 4.3.3 *Leaf nitrogen content*

1542 An interaction between χ and plant functional group ($p < 0.001$; Table
1543 4) revealed that the general negative effect of increasing χ on N_{area} ($p < 0.001$;
1544 Table 4) was driven by a negative effect of increasing χ on N_{area} in C₃ nonlegumes
1545 (Tukey: $p < 0.001$) and C₃ legumes (Tukey: $p = 0.002$) despite a null effect of χ
1546 on N_{area} in C₄ nonlegumes (Tukey: $p = 0.795$; Fig. 4a). An interaction between
1547 soil nitrogen availability and soil moisture ($p = 0.028$; Table 4) indicated that the
1548 marginal positive effect of increasing soil nitrogen availability on N_{area} ($p = 0.091$;
1549 Table 4) decreased with increasing soil moisture, despite no apparent individual
1550 effect of soil moisture on N_{area} ($p = 0.692$; Table 4). Finally, a plant functional
1551 group effect ($p < 0.001$; Table 4) indicated that C₄ nonlegumes had lower N_{area}
1552 values on average compared to C₃ legumes (Tukey: $p < 0.001$) and C₃ nonlegumes
1553 (Tukey: $p = 0.001$), while C₃ legumes had lower average N_{area} values compared
1554 to C₃ nonlegumes (Tukey: $p = 0.012$).

1555 A marginal interaction between χ and plant functional group ($p = 0.088$;
1556 Table 4) revealed that, despite no apparent general effect of χ on N_{mass} ($p = 0.273$;
1557 Table 4), increasing χ decreased N_{mass} in C₃ nonlegumes (Tukey: $p = 0.021$), but
1558 this effect was not apparent in C₄ nonlegumes (Tukey: $p = 0.693$) or C₃ legumes
1559 (Tukey: $p = 0.477$). An interaction between soil nitrogen availability and soil
1560 moisture ($p < 0.001$; Table 4) indicated that the general positive effect of increas-
1561 ing soil nitrogen availability on N_{mass} ($p < 0.001$; Table 4) generally decreased
1562 with increasing soil moisture, despite an apparent general positive effect of in-
1563 creasing soil moisture on N_{mass} ($p < 0.001$; Table 4). This interaction indicated
1564 that the positive effect of increasing soil nitrogen availability on N_{mass} was only

1565 apparent when soil moisture was less than 70% the maximum water holding ca-
1566 pacity (Tukey: $p < 0.05$ in all cases) despite a positive effect of increasing soil
1567 moisture on N_{mass} ($p < 0.001$; Table 4). Finally, a plant functional group effect
1568 ($p < 0.001$; Table 4) indicated that C₄ nonlegumes had lower N_{mass} values on
1569 average compared to C₃ legumes (Tukey: $p = 0.002$) and C₃ nonlegumes (Tukey:
1570 $p = 0.019$), while N_{mass} did not differ between C₃ legumes and C₃ nonlegumes
1571 (Tukey: $p = 0.149$).

1572 An interaction between χ and functional group ($p = 0.005$; Table 4) indi-
1573 cated that the general negative effect of increasing χ on M_{area} ($p < 0.001$; Table
1574 4; Fig. 4c) was driven by a negative effect of increasing χ on M_{area} in C₃ legumes
1575 and C₃ nonlegumes (Tukey: $p < 0.001$ in both cases) despite a nonsignificant
1576 effect of increasing χ on M_{area} in C₄ nonlegumes (Tukey: $p = 0.724$). An in-
1577 teraction between soil nitrogen and soil moisture ($p < 0.001$; Table 4) indicated
1578 that the general negative effect of increasing soil nitrogen availability on M_{area} (p
1579 < 0.001 ; Table 4) decreased with increasing soil moisture, despite an apparent
1580 general negative effect of increasing soil moisture on M_{area} ($p = 0.002$; Table 4).
1581 Specifically, the negative effect of increasing soil nitrogen availability on M_{area} was
1582 only apparent when soil moisture was less than 65% the maximum water holding
1583 capacity (Tukey: $p < 0.05$ in all cases). An additional interaction between soil
1584 nitrogen availability and functional group ($p = 0.034$; Table 4) indicated that the
1585 general negative effect of increasing soil nitrogen availability on M_{area} was driven
1586 by decreases in C₃ nonlegumes (Tukey: $p < 0.001$) and C₄ nonlegumes (Tukey:
1587 $p = 0.003$), with no apparent effect of soil nitrogen availability on M_{area} in C₃
1588 legumes (Tukey: $p = 0.997$).

Table 4.4. Effects of soil nitrogen fertilization, inoculation, and CO₂ treatments on N_{area} , N_{mass} , and M_{area}

	df	N_{area}			N_{mass}			M_{area}		
		Coefficient	χ^2	p	Coefficient	χ^2	p	Coefficient	χ^2	p
(Intercept)	-	2.78E+00	-	-	4.42E-01	-	-	6.97E+00	-	-
χ	1	-2.53E+00	15.771	<0.001	4.56E-01	1.201	0.273	-3.10E+00	20.620	<0.001
Soil N (N)	1	1.08E-02	2.855	<i>0.091</i>	1.37E-02	54.531	<0.001	-2.87E-03	29.759	<0.001
Soil moisture (SM ₂)	1	3.61E-01	0.157	0.692	5.04E-01	16.255	<0.001	-1.26E-01	9.282	0.002
PFT	1	-	60.641	<0.001	-	21.539	<0.001	-	11.520	0.003
SM ₂ *N	1	-1.09E-02	4.779	0.029	-1.76E-02	41.784	<0.001	6.35E-03	14.111	<0.001
χ^*PFT	1	-	15.188	<0.001	-	4.864	<i>0.088</i>	-	17.032	0.025
N*PFT	1	-	2.289	<i>0.318</i>	-	0.914	0.633	-	6.760	0.034
SM ₂ *PFT	1	-	0.978	0.613	-	0.128	0.938	-	2.121	0.346
SM ₂ *N*PFT	1	-	1.289	0.525	-	2.180	0.336	-	0.629	0.730

989 *Significance determined using Type II Wald χ^2 tests ($\alpha = 0.05$). P -values less than 0.05 are in bold and p -values
 1590 where $0.05 < p < 0.1$ are italicized. Coefficients are reported on the natural-log scale and are only included for
 1591 continuous fixed effects.

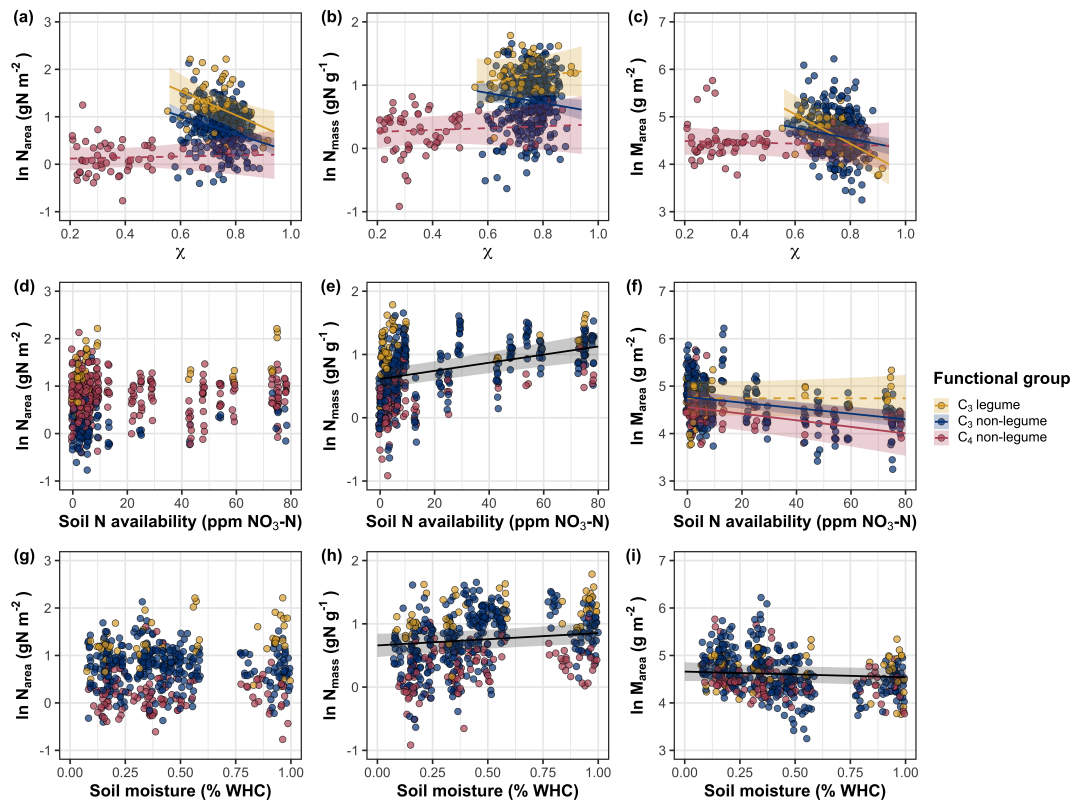


Figure 4.4. Effects of χ (a-c), soil nitrogen availability (d-f), and soil moisture (g-i) on leaf nitrogen content per unit leaf area (a, d, g), leaf nitrogen content per unit leaf biomass (b, e, h), and leaf mass per area (c, f, i). A solid black trendline indicates the bivariate relationship between the fixed effect the x-axis and response variable on the y-axis and is only included when there is no interaction between the x-axis and plant functional group.

1592 4.3.4 *Structural equation model*

1593 The piecewise structural equation model explained 90%, 54%, 80%, 92%,
1594 and 41% of variance in N_{area} , N_{mass} , M_{area} , χ , and β , respectively (Table 5; Fig.
1595 5). Variance in N_{area} was driven by a negative effect of increasing χ ($p < 0.001$;
1596 Table 5) paired with positive effects of increasing N_{mass} and M_{area} ($p < 0.001$ in
1597 both cases; Table 5; Fig. 5). Model results indicated that the negative effect
1598 of χ on N_{area} was driven by a strong reduction in M_{area} with increasing χ ($p <$
1599 0.001; Table 5) paired with no change in χ due to N_{mass} ($p = 0.150$; Table 5).
1600 However, there was a strong negative effect of increasing M_{area} on N_{mass} ($p <$
1601 0.001; Table 5; Fig. 5). χ generally increased with increasing β ($p < 0.001$; Table
1602 5) and decreased with increasing VPD ($p < 0.001$; Table 5; Fig. 5). Variance in β
1603 was driven by a negative effect of increasing soil nitrogen availability ($p < 0.001$;
1604 Table 5) and was generally higher in C₃ species ($p < 0.001$; Table 5; Fig. 5).
1605 However, β did not change with soil moisture ($p = 0.332$; Table 5) or with ability
1606 to acquire nitrogen via symbiotic nitrogen fixation ($p = 0.546$; Table 5). Finally,
1607 soil nitrogen availability was positively associated with increasing soil moisture (p
1608 < 0.001 ; Table 5; Fig. 5), while VPD was negatively associated with increasing
1609 soil moisture ($p < 0.001$; Table 5; Fig. 5).

Table 4.5. Structural equation model results investigating direct effects of climatic and soil resource availability on N_{area} , N_{mass} , M_{area} , χ , and β

Predictor	Coefficient	<i>p</i>
$N_{\text{area}} (R^2_c) = 0.90$		
χ	-0.140	<0.001
M_{area}	0.807	<0.001
N_{mass}	0.795	<0.001
$N_{\text{mass}} (R^2_c) = 0.54$		
χ	0.097	<0.001
$M_{\text{area}} (R^2_c) = 0.80$		
χ	-0.372	0.150
M_{area}	-0.303	<0.001
$\chi (R^2_c) = 0.92$		
β	0.261	<0.001
VPD_4	-0.122	<0.001
$\beta (R^2_c) = 0.41$		
Soil N	-0.201	<0.001
SM_2	-0.048	0.332
Photo. pathway	0.490	<0.001
N-fixing ability	-0.053	0.546
Soil N (R^2_c) = 0.39		
SM_2	0.410	<0.001

1610 *Reported coefficients are standardized across the structural equation model. *P*-
1611 values less than 0.05 are noted in bold. Positive coefficients for photosynthetic
1612 pathway indicate generally larger values in C₃ species, while positive coefficients
1613 for N-fixing ability indicate generally larger values in N-fixing species. Key:
1614 N_{area} =leaf nitrogen content per unit leaf area, M_{area} =leaf mass per unit leaf dry
1615 biomass, N_{mass} =leaf nitrogen content per unit leaf dry biomass, β =cost of acquiring
1616 nitrogen relative to water, χ =isotope-derived estimate of the leaf Ci:Ca ratio,
1617 VPD_4 = 4-day mean vapor pressure deficit, SM_2 =2-day mean soil moisture, R^2_c
1618 = conditional R² value

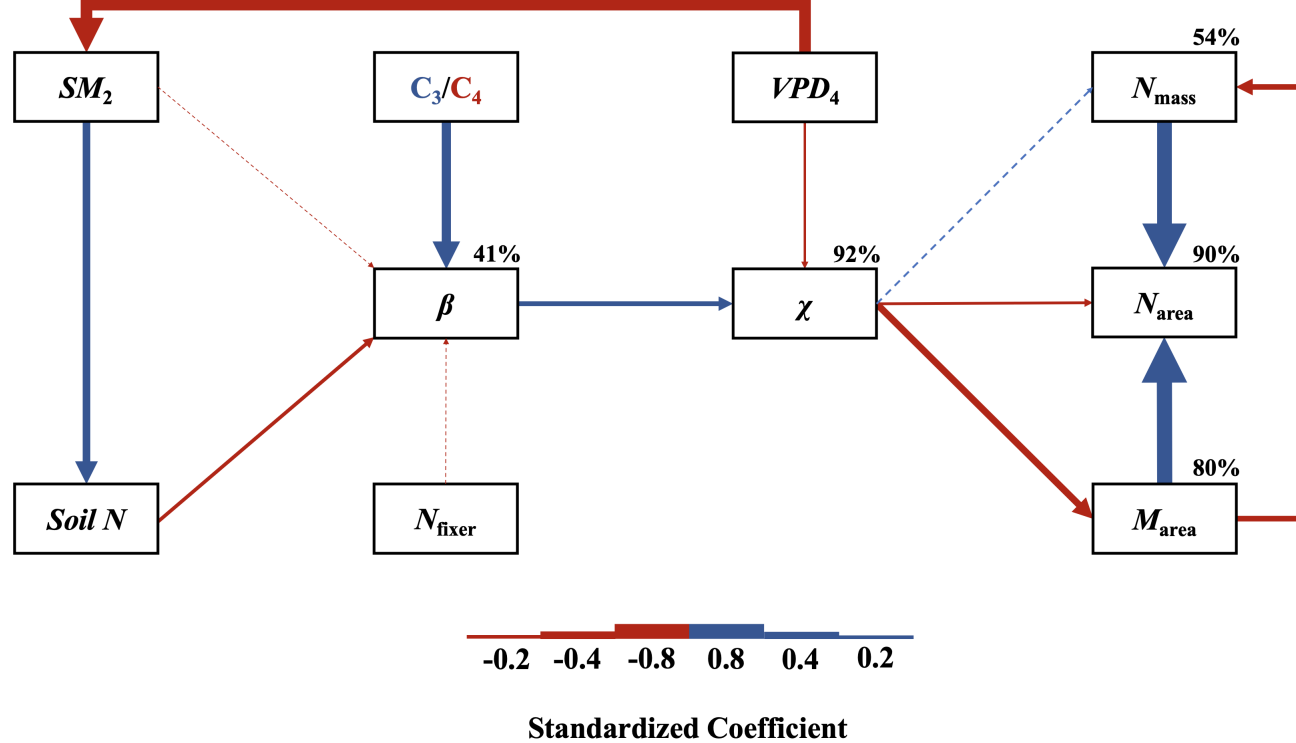


Figure 4.5. Structural equation model results exploring direct and indirect drivers of N_{area} . Boxes indicate measured edaphic factors, climatic factors, and leaf traits. Percentages above boxes indicate conditional R^2 values of each respective leaf trait. Solid arrows indicate bivariate relationships where $p < 0.05$, while dashed arrows indicate bivariate relationships where $p > 0.05$. Positive model coefficients are indicated through blue arrows, while negative model coefficients are indicated through red arrows. Arrow thickness scales with the standardized model coefficient of each bivariate relationship. A positive coefficient for photosynthetic pathway indicates generally larger values in C_3 species, while a positive coefficient for N_{fixer} indicates generally larger values in N-fixing species. Standardized model coefficients and associated p -values are reported in Table 5.

1619 4.4 Discussion

1620 In this chapter, I quantified direct and indirect effects of soil resource avail-
1621 ability, climate, β , and χ on N_{area} and components of N_{area} (N_{mass} and M_{area}) in
1622 520 individuals spanning across a soil resource availability and climate gradient
1623 in Texas, USA. We found consistent support for patterns expected from photo-
1624 synthetic least-cost theory, a result driven by a strong direct negative effect of
1625 increasing χ on N_{area} (Fig. 4.4a; Fig. 4.5) and a positive relationship between χ
1626 and β (Fig. 4.5). In further support of patterns expected from theory, increasing
1627 soil nitrogen availability had a strong negative effect on β (Fig. 4.2a), resulting in
1628 an indirect stimulation in N_{area} (Fig. 4.5) despite a marginal positive direct asso-
1629 ciation between increasing soil nitrogen availability and N_{area} ($p = 0.092$; Table
1630 4.4; Fig. 4.4d). Increasing VPD also indirectly increased N_{area} through a direct
1631 negative effect of increasing VPD on χ (Fig. 4.3a; Fig. 4.5). Interestingly, we
1632 found no effect of soil moisture on β (Fig. 1b; Fig. 4.5), though a strong posi-
1633 tive association between soil moisture and soil nitrogen availability resulted in an
1634 indirect positive effect of increasing soil moisture on N_{area} (Fig. 4.5) despite an
1635 apparent null direct effect of soil moisture on N_{area} (Fig. 4.4g). Overall, results
1636 provide strong and consistent support for patterns expected from photosynthetic
1637 least-cost theory, showing that χ is a dynamic driver of variance in N_{area} and is
1638 capable of unifying expected responses of N_{area} to shifts in soil resource availability
1639 and climate.

1640

Chapter 5

1641 Optimal resource investment to photosynthetic capacity maximizes
1642 nutrient allocation to whole plant growth under elevated CO₂

1643 5.1 Introduction

1644 Terrestrial ecosystems are regulated by complex carbon and nitrogen cy-
1645 cles. As a result, terrestrial biosphere models, which are beginning to include
1646 coupled carbon and nitrogen cycles (Shi et al. 2016; Davies-Barnard et al. 2020;
1647 Braghieri et al. 2022), must accurately represent these cycles under different
1648 environmental scenarios to reliably simulate carbon and nitrogen atmosphere-
1649 biosphere fluxes (Hungate et al. 2003; Prentice et al. 2015). While the inclusion
1650 of coupled carbon and nitrogen cycles tends to reduce model uncertainty (Arora
1651 et al. 2020), large uncertainty in role of soil nitrogen availability and nitrogen ac-
1652 quisition strategy on leaf and whole plant acclimation responses to CO₂ remains
1653 (Smith and Dukes 2013; Terrer et al. 2018; Smith and Keenan 2020). This source
1654 of uncertainty likely contributes to the widespread divergence in future carbon
1655 and nitrogen flux simulations across terrestrial biosphere models (Friedlingstein
1656 et al. 2014; Zaehle et al. 2014; Meyerholt et al. 2020).

1657 Plants grown under elevated CO₂ generally have less leaf nitrogen content
1658 than those grown under ambient CO₂, a response that often corresponds with
1659 reductions in photosynthetic capacity and stomatal conductance at the leaf-level
1660 and biomass stimulation over time at the whole plant level (Curtis 1996; Drake
1661 et al. 1997; Ainsworth et al. 2002; Makino 2003; Morgan et al. 2004; Ainsworth
1662 and Long 2005; Ainsworth and Rogers 2007; Smith and Dukes 2013; Poorter et al.
1663 2022). As net primary productivity is generally limited by nitrogen availability

1664 (Vitousek and Howarth 1991; LeBauer and Treseder 2008; Fay et al. 2015), and
1665 soil nitrogen availability is often positively correlated with leaf nitrogen content
1666 and photosynthetic capacity (Field and Mooney 1986; Evans and Seemann 1989;
1667 Evans 1989; Walker et al. 2014; Firn et al. 2019; Liang et al. 2020), some
1668 have hypothesized that leaf and whole plant acclimation responses to CO₂ are
1669 constrained by soil nitrogen availability. The progressive nitrogen limitation hy-
1670 pothesis predicts that elevated CO₂ will increase plant nitrogen demand, which
1671 will increase plant nitrogen uptake and progressively deplete soil nitrogen if soil
1672 nitrogen supply does not exceed plant nitrogen demand (Luo et al. 2004). The
1673 hypothesis predicts that this response should result in strong acute stimulations in
1674 whole plant growth and primary productivity that diminish over time as nitrogen
1675 becomes more limiting. Assuming a positive relationship between soil nitrogen
1676 availability, leaf nitrogen content, and photosynthetic capacity, this hypothesis
1677 also implies that progressive reductions in soil nitrogen availability should be the
1678 mechanism that drives the downregulation in leaf nitrogen content and photosyn-
1679 thetic capacity under elevated CO₂. This hypothesis has received some support
1680 from free air CO₂ enrichment experiments (Reich et al. 2006; Norby et al. 2010),
1681 although is not consistently observed across experiments (Finzi et al. 2006; Moore
1682 et al. 2006; Liang et al. 2016).

1683 While possible that progressive nitrogen limitation may determine leaf and
1684 whole plant acclimation responses to CO₂, growing evidence indicates that leaf ni-
1685 trogen and photosynthetic capacity are more strongly determined through above-
1686 ground growing conditions than by soil resource availability (Dong et al. 2017;
1687 Dong et al. 2020; Dong et al. 2022; Smith et al. 2019; Smith and Keenan 2020;

1688 Paillassa et al. 2020; Peng et al. 2021; Querejeta et al. 2022; Westerband et al.
1689 2023), and satellite-derived chlorophyll fluorescence data indicate that increasing
1690 atmospheric CO₂ may decrease leaf and canopy demand for nitrogen (Dong et al.
1691 2022). Together, results from these studies suggest that the downregulation in
1692 leaf nitrogen content and photosynthetic capacity due to increasing CO₂ may not
1693 be as tightly linked to progressive nitrogen limitation as previously hypothesized.

1694 A unification of optimal coordination and photosynthetic least-cost the-
1695 ories predicts that leaves acclimate to elevated CO₂ by downregulating nitrogen
1696 allocation to Ribulose-1,5-bisphosphate (RuBP) carboxylase/oxygenase (Rubisco)
1697 to optimize resource use efficiencies at the leaf level, which allows for greater re-
1698 source allocation to whole plant growth (Drake et al. 1997; Wright et al. 2003;
1699 Prentice et al. 2014; Smith et al. 2019). The theory predicts that the downregu-
1700 lation in nitrogen allocation to Rubisco results in a stronger downregulation in the
1701 maximum rate of Rubisco carboxylation (V_{cmax}) than the maximum rate of RuBP
1702 regeneration (J_{max}), which maximizes photosynthetic efficiency by allowing net
1703 photosynthesis rates to be equally co-limited by Rubisco carboxylation and RuBP
1704 regeneration (Chen et al. 1993; Maire et al. 2012). This acclimation response
1705 allows plants to make more efficient use of available light while avoiding overin-
1706 vestment in Rubisco, which has high nitrogen and energetic costs of building and
1707 maintaining (Evans 1989; Evans and Clarke 2019). Instead, additional acquired
1708 resources not needed to optimize leaf photosynthesis are allocated to the mainte-
1709 nance of structures that support whole plant growth (e.g., total leaf area, whole
1710 plant biomass, etc.) or to allocation processes not related to leaf photosynthesis
1711 or growth, such as plant defense mechanisms or leaf structural tissue. Regardless,

1712 optimized resource allocation at the leaf level should allow for greater resource
1713 allocation to whole plant growth. The theory indicates that leaf acclimation re-
1714 sponses to CO₂ should be independent of changes in soil nitrogen availability.
1715 While this leaf acclimation response maximizes nitrogen allocation to structures
1716 that support whole plant growth, the theory suggests that the positive effect of
1717 elevated CO₂ on whole plant growth may be further stimulated by soil nitrogen
1718 availability through a reduction in the cost of acquiring nitrogen (Bae et al. 2015;
1719 Perkowski et al. 2021; Lu et al. 2022).

1720 Plants acquire nitrogen by allocating photosynthetically derived carbon be-
1721 lowground in exchange for nitrogen through different nitrogen acquisition strate-
1722 gies. These nitrogen acquisition strategies can include direct uptake pathways
1723 such as mass flow or diffusion (Barber 1962), symbioses with mycorrhizal fungi or
1724 symbiotic nitrogen-fixing bacteria (Vance and Heichel 1991; Marschner and Dell
1725 1994; Smith and Read 2008; Udvardi and Poole 2013), or through the release
1726 of root exudates that prime free-living soil microbial communities (Phillips et al.
1727 2011; Wen et al. 2022). Plants cannot acquire nitrogen without first allocating
1728 carbon belowground, which implies an inherent carbon cost to the plant for acquir-
1729 ing nitrogen regardless of nitrogen acquisition strategy. Carbon costs to acquire
1730 nitrogen often vary in species with different nitrogen acquisition strategies and
1731 are dependent on external environmental factors such as atmospheric CO₂, light
1732 availability, and soil nitrogen availability (Brzostek et al. 2014; Terrer et al. 2016;
1733 Terrer et al. 2018; Allen et al. 2020; Perkowski et al. 2021; Lu et al. 2022), which
1734 suggests that acquisition strategy may be an important factor in determining ef-
1735 fects of soil nitrogen availability on leaf and whole plant acclimation responses to

1736 elevated CO₂.

1737 A recent meta-analysis using data across 20 grassland and forest CO₂ en-
1738 richment experiments suggested that species which acquire nitrogen from sym-
1739 biotic nitrogen-fixing bacteria had reduced costs of nitrogen acquisition under
1740 elevated CO₂ (Terrer et al. 2018). Findings from this meta-analysis indicated
1741 that reductions in costs of nitrogen acquisition in species that form associations
1742 with symbiotic nitrogen-fixing bacteria under elevated CO₂ may drive stronger
1743 stimulations in whole plant growth and downregulations in V_{cmax} than species that
1744 associate with arbuscular mycorrhizal fungi (Smith and Keenan 2020), which gen-
1745 erally have higher costs of nitrogen acquisition under elevated CO₂ (Terrer et al.
1746 2018). However, plant investments in symbiotic nitrogen fixation generally de-
1747 cline with increasing nitrogen availability (Dovrat et al. 2018; Perkowski et al.
1748 2021), a response that has been previously inferred to be the result of a shift in
1749 the dominant mode of nitrogen acquisition to direct uptake pathways as costs of
1750 direct uptake decrease with increasing soil nitrogen availability (Rastetter et al.
1751 2001; Perkowski et al. 2021). Thus, effects of symbiotic nitrogen fixation on plant
1752 acclimation responses to CO₂ should decline with increasing soil nitrogen avail-
1753 ability, although manipulative experiments that directly test these patterns are
1754 rare.

1755 Here, I conducted a 7-week growth chamber experiment using *Glycine max*
1756 L. (Merr.) to examine the effects of soil nitrogen fertilization and inoculation with
1757 symbiotic nitrogen-fixing bacteria on leaf and whole plant acclimation responses
1758 to elevated CO₂. Following patterns expected from theory, I hypothesized that in-
1759 dividual leaves should acclimate to elevated CO₂ by more strongly downregulating

1760 V_{cmax} relative to J_{max} , allowing leaf photosynthesis to approach optimal coordi-
1761 nation. I expected this response to correspond with a stronger downregulation in
1762 leaf nitrogen content than V_{cmax} and J_{max} , which would increase the fraction of
1763 leaf nitrogen content allocated to photosynthesis and photosynthetic nitrogen use
1764 efficiency. At the whole-plant level, I hypothesized that plants would acclimate
1765 to elevated CO₂ by stimulating whole plant growth and productivity, a response
1766 that would be driven by a strong positive response of total leaf area and above-
1767 ground biomass to elevated CO₂. I predicted that leaf acclimation responses to
1768 elevated CO₂ would be independent of soil nitrogen fertilization and inoculation
1769 with symbiotic nitrogen-fixing bacteria; however, I expected that increasing soil
1770 nitrogen fertilization would increase the positive effect of elevated CO₂ on mea-
1771 sures of whole plant growth due to a stronger reduction in the cost of acquiring
1772 nitrogen under elevated CO₂ with increasing fertilization. I also expected stronger
1773 stimulations in whole plant growth due to inoculation, but that this effect would
1774 only be apparent under low fertilization due to a reduction in root nodulation
1775 with increasing fertilization.

1776 5.2 Methods

1777 5.2.1 *Seed treatments and experimental design*

1778 *Glycine max* L. (Merr) seeds were planted in 144 6-liter surface sterilized
1779 pots (NS-600, Nursery Supplies, Orange, CA, USA) containing a steam-sterilized
1780 70:30 v:v mix of Sphagnum peat moss (Premier Horticulture, Quakertown, PA,
1781 USA) to sand (Pavestone, subsidiary of Quikrete Companies, Atlanta, GA, USA).
1782 Before planting, all *G. max* seeds were surface sterilized in 2% sodium hypochlorite

1783 for 3 minutes, followed by three separate 3-minute washes with ultrapure water
1784 (MilliQ 7000; MilliporeSigma, Burlington, MA USA). A subset of surface steril-
1785 ized seeds were inoculated with *Bradyrhizobium japonicum* (Verdesian N-Dure™
1786 Soybean, Cary, NC, USA) in a slurry following manufacturer recommendations
1787 (3.12 g inoculant and 241 g deionized water per 1 kg seed).

1788 Seventy-two pots were randomly planted with surface-sterilized seeds inoc-
1789 ulated with *B. japonicum*, while the remaining 72 pots were planted with surface-
1790 sterilized uninoculated seeds. Thirty-six pots within each inoculation treatment
1791 were randomly placed in one of two atmospheric CO₂ treatments (ambient and
1792 1000 μmol mol⁻¹ CO₂). Pots within each unique inoculation-by-CO₂ treatment
1793 combination randomly received one of nine soil nitrogen fertilization treatments
1794 equivalent to 0, 35, 70, 105, 140, 210, 280, 350, or 630 ppm N. Nitrogen fertil-
1795 ization treatments were created using a modified Hoagland solution (Hoagland
1796 and Arnon 1950) designed to keep concentrations of other macronutrients and
1797 micronutrients equivalent across treatments (Table S1). Pots received the same
1798 fertilization treatment throughout the entire duration experiment, which were ap-
1799 plied twice per week in 150 mL doses as topical agents to the soil surface through-
1800 out the duration of the experiment. This experimental design yielded a fully
1801 factorial experiment with four replicates per unique fertilization-by-inoculation-
1802 by-CO₂ combination.

1803 5.2.2 *Growth chamber conditions*

1804 Upon experiment initiation, pots were randomly placed in one of six Per-
1805 cival LED-41L2 growth chambers (Percival Scientific Inc., Perry, IA, USA) over

1806 two experimental iterations due to chamber space limitation. Two iterations were
1807 conducted such that one iteration included all elevated CO₂ pots and the second
1808 iteration included all ambient CO₂ pots. Average (\pm SD) CO₂ concentrations
1809 across chambers throughout the experiment were $439 \pm 5 \mu\text{mol mol}^{-1}$ for the
1810 ambient CO₂ treatment and $989 \pm 4 \mu\text{mol mol}^{-1}$ for the elevated CO₂ treatment.

1811 Daytime growing conditions were simulated using a 16-hour photoperiod,
1812 with incoming light radiation set to chamber maximum (mean \pm SD: 1240 ± 32
1813 $\mu\text{mol m}^{-2} \text{s}^{-1}$ across chambers), air temperature set to 25°C, and relative humid-
1814 ity set to 50%. The remaining 8 hours simulated nighttime growing conditions,
1815 with incoming light radiation set to $0 \mu\text{mol m}^{-2} \text{s}^{-1}$, chamber temperature set
1816 to 17°C, and relative humidity set to 50%. Transitions between daytime and
1817 nighttime growing conditions were simulated by ramping incoming light radiation
1818 in 45-minute increments and temperature in 90-minute increments over a 3-hour
1819 period (Table S2).

1820 Including the two, 3-hour ramping periods, pots grew under average (\pm
1821 SD) daytime light intensity of $1049 \pm 27 \mu\text{mol m}^{-2} \text{s}^{-1}$. In the elevated CO₂
1822 iteration, pots grew under $24.0 \pm 0.2^\circ\text{C}$ during the day, $16.4 \pm 0.8^\circ\text{C}$ during the
1823 night, and $51.6 \pm 0.4\%$ relative humidity. In the ambient CO₂ iteration, pots grew
1824 under $23.9 \pm 0.2^\circ\text{C}$ during the day, $16.0 \pm 1.4^\circ\text{C}$ during the night, and $50.3 \pm 0.2\%$
1825 relative humidity. We accounted for climatic differences across the six chambers
1826 by shuffling the same group of pots daily throughout the growth chambers. This
1827 process was done by iteratively moving the group of pots on the top rack of a
1828 chamber to the bottom rack of the same chamber, while simultaneously moving
1829 the group of pots on the bottom rack of a chamber to the top rack of the adjacent

1830 chamber. I moved pots within and across chambers every day throughout the
1831 course of each experiment iteration.

1832 5.2.3 *Leaf gas exchange measurements*

1833 Gas exchange measurements were collected for all individuals on the sev-
1834 enth week of development. All gas exchange measurements were collected on
1835 the center leaf of the most recent fully expanded trifoliate leaf set. Specifi-
1836 cally, I measured net photosynthesis (A_{net} ; $\mu\text{mol m}^{-2} \text{s}^{-1}$), stomatal conductance
1837 (g_{sw} ; $\text{mol m}^{-2} \text{s}^{-1}$), and intercellular CO₂ (C_i ; $\mu\text{mol mol}^{-1}$) concentrations across
1838 a range of atmospheric CO₂ concentrations (i.e., an A_{net}/C_i curve) using the
1839 Dynamic Assimilation Technique™. The Dynamic Assimilation Technique™ has
1840 been shown to correspond well with traditional steady-state CO₂ response curves
1841 in *G. max* (Saathoff and Welles 2021). A_{net}/C_i curves were generated along a
1842 reference CO₂ ramp down from 420 $\mu\text{mol mol}^{-1}$ CO₂ to 20 $\mu\text{mol mol}^{-1}$ CO₂, fol-
1843 lowed by a ramp up from 420 $\mu\text{mol mol}^{-1}$ CO₂ to 1620 $\mu\text{mol mol}^{-1}$ CO₂ after
1844 a 90-second wait period at 420 $\mu\text{mol mol}^{-1}$ CO₂. The ramp rate for each curve
1845 was set to 200 $\mu\text{mol mol}^{-1} \text{min}^{-1}$, logging every five seconds, which generated 96
1846 data points per response curve. All A_{net}/C_i curves were generated after A_{net} and
1847 g_{sw} stabilized in a LI-6800 cuvette set to a 500 mol s^{-1} , 10,000 rpm mixing fan
1848 speed, 1.5 kPa vapor pressure deficit, 25°C leaf temperature, 2000 $\mu\text{mol m}^{-2} \text{s}^{-1}$
1849 incoming light radiation, and initial reference CO₂ set to 420 $\mu\text{mol mol}^{-1}$.

1850 With the same focal leaf used to generate A_{net}/C_i curves, I measured dark
1851 respiration (R_{d25} ; $\mu\text{mol m}^{-2} \text{s}^{-1}$) following at least a 30-minute period of darkness.
1852 Measurements were collected on a 5-second log interval for 60 seconds after stabi-

1853 lizing in a LI-6800 cuvette set to a 500 mol s^{-1} , 10,000 rpm mixing fan speed, 1.5
1854 kPa vapor pressure deficit, 25°C leaf temperature, and $420 \mu\text{mol mol}^{-1}$ reference
1855 CO₂ concentration (for both CO² concentrations), with incoming light radiation
1856 set to $0 \mu\text{mol m}^{-2} \text{ s}^{-1}$. A single dark respiration value was determined for each
1857 focal leaf by calculating the mean dark respiration value (i.e. the absolute value
1858 of A_{net} during the logging period) across the logging interval.

1859 5.2.4 *Leaf trait measurements*

1860 The focal leaf used to generate A_{net}/C_i curves and dark respiration was
1861 harvested immediately following gas exchange measurements. Images of each focal
1862 leaf were curated using a flat-bed scanner to determine wet leaf area using the
1863 'LeafArea' R package (Katabuchi 2015), which automates leaf area calculations
1864 using ImageJ software (Schneider et al. 2012). Each leaf was dried at 65°C for
1865 at least 48 hours, and subsequently weighed and ground until homogenized. Leaf
1866 mass per area (M_{area} ; g m⁻²) was calculated as the ratio of dry leaf biomass
1867 to fresh leaf area. Using subsamples of ground and homogenized leaf tissue, I
1868 measured leaf nitrogen content (N_{mass} ; gN g⁻¹) through elemental combustion
1869 analysis (Costech-4010, Costech, Inc., Valencia, CA, USA). Leaf nitrogen content
1870 per unit leaf area (N_{area} ; gN m⁻²) was calculated by multiplying N_{mass} and M_{area} .

1871 I extracted chlorophyll content from a second leaf in the same trifoliate
1872 leaf set as the focal leaf used to generate A_{net}/C_i curves. Prior to chlorophyll
1873 extraction, I used a cork borer to punch between 3 and 5 0.6 cm² disks from the
1874 leaf. Separate images of each punched leaf and set of leaf disks were curated using
1875 a flat-bed scanner to determine wet leaf area, again quantified using the 'LeafArea'

1876 R package (Katabuchi 2015). The punched leaf was dried and weighed after at
1877 least 65°C in the drying oven to determine M_{area} of the chlorophyll leaf.

1878 Leaf disks were shuttled into a test tube containing 10mL dimethyl sul-
1879 foxide, vortexed, and incubated at 65degreeC for 120 minutes (Barnes et al.
1880 1992). Incubated test tubes were vortexed again before loaded in 150 μL trip-
1881 licate aliquots to a 96-well plate. Dimethyl sulfoxide was also loaded in a 150
1882 μL triplicate aliquot as a blank. Absorbance measurements at 649.1 nm ($A_{649.1}$)
1883 and 665.1 nm ($A_{665.1}$) were read in each well using a plate reader (Biotek Synergy
1884 H1; Biotek Instruments, Winooski, VT USA) (Wellburn 1994), with triplicates
1885 subsequently averaged and corrected by the mean of the blank absorbance value.
1886 Blank-corrected absorbance values were used to estimate Chl_a ($\mu\text{g mL}^{-1}$) and
1887 Chl_b ($\mu\text{g mL}^{-1}$) following equations from Wellburn (1994):

$$Chl_a = 12.47A_{665.1} - 3.62A_{649.1} \quad (5.1)$$

1888 and

$$Chl_b = 25.06A_{665.1} - 6.50A_{649.1} \quad (5.2)$$

1889 Chl_a and Chl_b were converted to mmol mL^{-1} using the molar mass of chlorophyll a
1890 (893.51 g mol^{-1}) and the molar mass of chlorophyll b (907.47 g mol^{-1}), then added
1891 together to calculate total chlorophyll content in the dimethyl sulfoxide extractant
1892 (mmol mL^{-1}). Total chlorophyll content was multiplied by the volume of the
1893 dimethyl sulfoxide extractant (10 mL) and converted to area-based chlorophyll
1894 content by dividing by the total area of the leaf disks (Chl_{area} ; mmol m^{-2}). Mass-
1895 based chlorophyll content (Chl_{mass} ; mmol g^{-1}) was calculated by dividing Chl_{area}

1896 by the leaf mass per area of the punched leaf.

1897 5.2.5 *A/C_i curve fitting and parameter estimation*

1898 I fit A_{net}/C_i curves of each individual using the ‘fitaci’ function in the
1899 ‘plantecophys’ R package (Duursma 2015). This function estimates the maxi-
1900 mum rate of Rubisco carboxylation (V_{cmax} ; $\mu\text{mol m}^{-2} \text{s}^{-1}$) and maximum rate
1901 of electron transport for RuBP regeneration (J_{max} ; $\mu\text{mol m}^{-2} \text{s}^{-1}$) based on the
1902 Farquhar biochemical model of C₃ photosynthesis (Farquhar et al. 1980). Triose
1903 phosphate utilization (TPU) limitation was included in all curve fits, and all curve
1904 fits included measured dark respiration values. As A_{net}/C_i curves were generated
1905 using a common leaf temperature, curves were fit using Michaelis-Menten coeffi-
1906 cients for Rubisco affinity to CO₂ (K_c ; $\mu\text{mol mol}^{-1}$) and O₂ (K_o ; $\mu\text{mol mol}^{-1}$), and
1907 the CO₂ compensation point (Γ^* ; $\mu\text{mol mol}^{-1}$) reported in Bernacchi et al. (2001).
1908 Specifically, K_c was set to 404.9 $\mu\text{mol mol}^{-1}$, K_o was set to 278.4 $\mu\text{mol mol}^{-1}$, and
1909 Γ^* was set to 42.75 $\mu\text{mol mol}^{-1}$. The use of a common leaf temperature across
1910 curves and dark respiration measurements also eliminated the need to manually
1911 temperature standardize rate estimates. For clarity, I reference V_{cmax} , J_{max} , and
1912 R_d estimates throughout the rest of the paper as $V_{\text{cmax}25}$, $J_{\text{max}25}$, and R_{d25} .

1913 5.2.6 Stomatal limitation

1914 I quantified the extent by which stomatal conductance limited photosynthe-
1915 sis (l; unitless) following equations originally described in Farquhar and Sharkey
1916 (1982). Stomatal limitation was calculated as:

$$l = 1 - \frac{A_{net}}{A_{mod}} \quad (5.3)$$

1917 where A_{mod} represents the photosynthetic rate where $C_i = C_a$. A_{mod} was calcu-

1918 lated as:

$$A_{mod} = V_{cmax25} - \frac{420 - \Gamma^*}{420 + K_m} - R_{d25} \quad (5.4)$$

1919 K_m is the Michaelis-Menten coefficient for Rubisco-limited photosynthesis, calcu-

1920 lated as:

$$K_m = K_c \cdot \left(1 + \frac{O_i}{K_o}\right) \quad (5.5)$$

1921 where O_i refers to leaf intercellular O_2 concentrations, set to $210 \mu\text{mol mol}^{-1}$.

1922 5.2.7 *Proportion of leaf nitrogen allocated to photosynthesis and structure*

1923 I used equations from Niinemets and Tenhunen (1997) to estimate the

1924 proportion of leaf N content allocated to Rubisco bioenergetics, and light harvest-

1925 ing proteins. The proportion of leaf N allocated to Rubisco (ρ_{rub} ; gN gN^{-1}) was

1926 calculated as a function of V_{cmax25} and N_{area} :

$$\rho_{rubisco} = \frac{V_{cmax25} N_r}{V_{cr} N_{area}} \quad (5.6)$$

1927 where N_r is the amount of nitrogen in Rubisco, set to $0.16 \text{ gN (gN in Rubisco)}^{-1}$

1928 and V_{cr} is the maximum rate of RuBP carboxylation per unit Rubisco protein,

1929 set to $20.5 \mu\text{mol CO}_2 (\text{g Rubisco})^{-1}$. The proportion of leaf nitrogen allocated to

1930 bioenergetics (ρ_{bioe} ; gN gN^{-1}) was similarly calculated as a function of J_{max25} and

1931 N_{area} :

$$\rho_{\text{bioe}} = \frac{J_{\text{max}25} N_b}{J_{\text{mc}} N_{\text{area}}} \quad (5.7)$$

1932 where N_b is the amount of nitrogen in cytochrome f, set to 0.12407 gN (μmol cytochrome f) $^{-1}$ assuming a constant 1: 1: 1.2 cytochrome f: ferredoxin NADP reductase: coupling factor molar ratio (Evans and Seemann 1989; Niinemets and Tenhunen 1997), and J_{mc} is the capacity of electron transport per cytochrome f, set to 156 μmol electron (μmol cytochrome f) $^{-1}\text{s}^{-1}$.

1937 The proportion of leaf nitrogen allocated to light harvesting proteins was calculated as a function of Chl_{mass} and N_{mass} :

$$\rho_{\text{light}} = \frac{Chl_{\text{mass}}}{N_{\text{mass}} c_b} \quad (5.8)$$

1939 where c_b is the stoichiometry of the light-harvesting chlorophyll complexes of photosystem II, set to 2.75 mmol chlorophyll (gN in chlorophyll) $^{-1}$. We used the N_{mass} value of the focal leaf used to generate A_{net}/C_i curves instead of the leaf used to extract chlorophyll content, as the two leaves are from the same trifoliolate leaf set and are highly correlated with each other (Figure SX).

1944 The proportion of leaf nitrogen content allocated to photosynthetic tissue (ρ_{photo} ; gN gN $^{-1}$) was estimated as the sum of ρ_{rubisco} , ρ_{bioe} , and ρ_{light} .

1946 Finally, the proportion of leaf N content allocated to structural tissue (ρ_{str} ; gN gN $^{-1}$) was estimated as:

$$\rho_{\text{structure}} = \frac{N_{\text{cw}}}{N_{\text{area}}} \quad (5.9)$$

1948 where N_{cw} is the leaf N content allocated to cell walls (gN m^{-2}), calculated as a
1949 function of M_{area} using an empirical equation from Onoda et al. (2017):

$$N_{cw} = 0.000355 * M_{area}^{1.39} \quad (5.10)$$

1950 5.2.8 *Whole plant traits*

1951 Seven weeks after experiment initiation and immediately following gas ex-
1952 change measurements, I harvested all experimental individuals and separated
1953 biomass of each experimental individual into major organ types (leaves, stems,
1954 roots, and nodules when present). Fresh leaf area of all harvested leaves was mea-
1955 sured using an LI-3100C (Li-COR Biosciences, Lincoln, Nebraska, USA). Total
1956 fresh leaf area (cm^2) was calculated as the sum of all leaf areas, including the focal
1957 leaf used to collect gas exchange data and the focal leaf used to extract chlorophyll
1958 content. All harvested material was dried in an oven set to 65°C for at least 48
1959 hours, weighed, and ground to homogeneity. Leaves and nodules were manually
1960 ground either with a mortar and pestle, while stems and roots were ground using
1961 a Wiley mill (E3300 Mini Mill; Eberbach Corp., MI, USA). Total dry biomass (g)
1962 was calculated as the sum of dry leaf (including focal leaf for both the A_{net}/C_i
1963 curve and leaf used to extract chlorophyll content), stem, root, and root nodule
1964 biomass. I quantified carbon and nitrogen content of each respective organ type
1965 through elemental combustion (Costech-4010, Costech, Inc., Valencia, CA, USA)
1966 using subsamples of ground and homogenized organ tissue.

1967 Following the approach explained in the first experimental chapter, I calcu-
1968 lated structural carbon costs to acquire nitrogen as the ratio of total belowground

1969 carbon biomass to whole plant nitrogen biomass (N_{cost} ; gC gN⁻¹). Belowground
1970 carbon biomass (C_{bg} ; gC) was calculated as the sum of root carbon biomass
1971 and root nodule carbon biomass. Root carbon biomass and root nodule carbon
1972 biomass was calculated as the product of the organ biomass and the respective
1973 organ carbon content. Whole plant nitrogen biomass (N_{wp} ; gN) was similarly
1974 calculated as the sum of total leaf, stem, root, and root nodule nitrogen biomass,
1975 including the focal leaf used for A_{net}/C_i curve and chlorophyll extractions. Leaf,
1976 stem, root, and root nodule nitrogen biomass was calculated as the product of
1977 the organ biomass and the respective organ nitrogen content. This calculation
1978 only quantifies plant structural carbon costs to acquire nitrogen and does not
1979 include any additional costs of nitrogen acquisition associated with respiration,
1980 root exudation, or root turnover. An explicit explanation of the limitations for
1981 interpreting this calculation can be found in Perkowski et al. (2021) and Terrer
1982 et al. (2018).

1983 Finally, plant investments in nitrogen fixation were calculated as the ra-
1984 tio of root nodule biomass to root biomass, where increasing values indicate an
1985 increase in plant investments to nitrogen fixation (Dovrat et al. 2018; Dovrat
1986 et al. 2020; Perkowski et al. 2021). I also calculated the percent of leaf nitrogen
1987 acquired from the atmosphere (% N_{dfa}) using leaf $\delta^{15}\text{N}$ and the following equation
1988 from Andrews et al. (2011):

$$\%N_{\text{dfa}} = \frac{\delta^{15}N_{\text{reference}} - \delta^{15}N_{\text{sample}}}{\delta^{15}N_{\text{reference}} - B} \quad (5.11)$$

1989 where $\delta^{15}\text{N}_{\text{reference}}$ refers to a reference plant that exclusively acquires nitrogen via

1990 direct uptake, $\delta^{15}\text{N}_{\text{sample}}$ refers to an individual's leaf $\delta^{15}\text{N}$, and B refers to individuals that are entirely reliant on nitrogen fixation. Within each unique nitrogen fertilization treatment-by-CO₂ treatment combination, I calculated the mean leaf $\delta^{15}\text{N}$ for individuals growing in the non-inoculated treatment for $\delta^{15}\text{N}_{\text{reference}}$. Any individuals with visual confirmation of root nodule formation or nodule initiation were omitted from the calculation of $\delta^{15}\text{N}_{\text{reference}}$. Following recommendations from Andrews et al. (2011) I calculated B within each CO₂ treatment using the mean leaf $\delta^{15}\text{N}$ of inoculated individuals that received 0 ppm N. I did not calculate B within each unique soil nitrogen-by-CO₂ treatment combination, as previous studies suggest decreased reliance on nitrogen fixation with increasing soil nitrogen availability (Perkowski et al. 2021). This approach for estimating nitrogen fixation standardizes values such that approaching 1 indicates increasing reliance on nitrogen fixation.

2003 5.2.9 *Statistical analyses*

2004 Any uninoculated pots that had substantial root nodule formation (nodule biomass: root biomass values greater than 0.05 g g⁻¹) were removed from analyses. This was because they were assumed to have been colonized by symbiotic nitrogen-fixing bacteria from outside sources. This decision resulted in the removal of sixteen pots from our analysis: two pots in the elevated CO₂ treatment that received 35 ppm N, three pots in the elevated CO₂ treatment that received 70 ppm N, one pot in the elevated CO₂ treatment that received 210 ppm N, two pots in the elevated CO₂ treatment that received 280 ppm N, two pots in the ambient CO₂ treatment that received 0 ppm N, three pots in the ambient CO₂ treatment

2013 that received 70 ppm N, two pots in the ambient CO₂ treatment that received
2014 105 ppm N, and one pot in the ambient CO₂ treatment that received 280 ppm N.

2015 I built a series of linear mixed effects models to investigate the impacts of
2016 CO₂ concentration, soil nitrogen fertilization, and inoculation with *B. japonicum*
2017 on *G. max* gas exchange, tradeoffs between nitrogen and water use, whole plant
2018 growth, and investment in nitrogen fixation. All models included CO₂ treatment
2019 as a categorical fixed effect, inoculation treatment as a categorical fixed effect,
2020 soil nitrogen fertilization as a continuous fixed effect, with interaction terms be-
2021 tween all three fixed effects. All models also accounted for climatic difference
2022 between chambers across experiment iterations by including a random intercept
2023 term that nested starting chamber rack by CO₂ treatment. Models with this
2024 independent variable structure were created for each of the following dependent
2025 variables: N_{area} , M_{area} , N_{mass} , Chl_{area} , V_{cmax25} , J_{max25} , $J_{\text{max25}}:V_{\text{cmax25}}$, R_{d25} , g_{sw} ,
2026 stomatal limitation, ρ_{rubisco} , ρ_{bioe} , ρ_{light} , ρ_{photo} , $\rho_{\text{structure}}$, N_{cost} , C_{bg} , N_{wp} , total
2027 biomass, total leaf area, nodule biomass, and the ratio of nodule biomass to root
2028 biomass.

2029 I used Shapiro-Wilk tests of normality to determine whether linear mixed
2030 effects models satisfied residual normality assumptions. If residual normality as-
2031 sumptions were not met (Shapiro-Wilk: $p < 0.05$), then models were fit using
2032 dependent variables that were natural log transformed. All residual normality
2033 assumptions that did not originally satisfy residual normality assumptions were
2034 met with either a natural log or square root data transformation (Shapiro-Wilk:
2035 $p > 0.05$ in all cases). Specifically, models for N_{area} , N_{mass} , Chl_{area} , V_{cmax25} ,
2036 J_{max25} , $J_{\text{max25}}:V_{\text{cmax25}}$, g_{sw} , stomatal limitation, ρ_{rubisco} , ρ_{bioe} , ρ_{light} , ρ_{photo} , and to-

2037 tal leaf area satisfied residual normality assumptions without data transformation.
2038 Models for M_{area} , $\rho_{\text{structure}}$, N_{cost} , C_{bg} , N_{wp} , and total biomass satisfied residual
2039 normality assumptions with a natural log data transformation, while models for
2040 nodule biomass and nodule biomass: root biomass satisfied residual normality
2041 assumptions with a square root data transformation.

2042 In all statistical models, I used the 'lmer' function in the 'lme4' R package
2043 (Bates et al. 2015) to fit each model and the 'Anova' function in the 'car' R
2044 package (Fox and Weisberg 2019) to calculate Type II Wald's χ^2 and determine
2045 the significance ($\alpha = 0.05$) of each fixed effect coefficient. I used the 'emmeans'
2046 R package (Lenth 2019) to conduct post-hoc comparisons using Tukey's tests,
2047 where degrees of freedom were approximated using the Kenward-Roger approach
2048 (Kenward and Roger 1997). All analyses and plots were conducted in R version
2049 4.2.0 (R Core Team 2021).

2050 5.3 Results

2051 5.3.1 Leaf nitrogen content, chlorophyll content, and mass per area

2052 Elevated CO₂ reduced N_{area} , N_{mass} , and Chl_{area} by 29%, 50%, and 31%,
2053 respectively, and stimulated M_{area} by 44% ($p < 0.001$ in all cases; Table 1). An in-
2054 teraction between fertilization and CO₂ (CO₂-by-fertilization interaction: $p_{N_{\text{area}}} =$
2055 0.017, $p_{N_{\text{mass}}} < 0.001$, $p_{M_{\text{area}}} = 0.006$, $p_{Chl_{\text{area}}} = 0.083$; Table 1) indicated that the
2056 general positive effect of increasing fertilization on N_{area} , N_{mass} , and Chl_{area} ($p <$
2057 0.001 in all cases; Table 1) was generally stronger under ambient CO₂ (Tukey _{N_{area}} :
2058 $p = 0.026$; Tukey _{N_{mass}} : $p < 0.001$; Tukey _{M_{area}} : $p = 0.009$; Tukey _{Chl_{area}} : $p = 0.065$;
2059 Table 1; Figs. 1a-d). This pattern resulted in a stronger reduction in N_{area} , N_{mass} ,

2060 and Chl_{area} as well as a stronger stimulation in M_{area} under elevated CO₂ with
2061 increasing fertilization. An additional interaction between inoculation and CO₂
2062 on N_{area} (CO₂-by-inoculation interaction: $p = 0.030$; Table 1) indicated that the
2063 general positive effect of inoculation on N_{area} ($p < 0.001$; Table 1) was stronger
2064 under elevated CO₂ (45% increase; Tukey: $p < 0.001$) than under ambient CO₂
2065 (18% increase; Tukey: $p < 0.001$), a result that increased the reduction in N_{area}
2066 in inoculated pots under elevated CO₂. Inoculation treatment did not modify the
2067 downregulation in N_{mass} (CO₂-by-inoculation interaction: $p = 0.148$; Table 1) and
2068 Chl_{area} ($p = 0.147$; Table 1) or the stimulation in M_{area} ($p = 0.866$; Table 1) un-
2069 der elevated CO₂. However, interactions between fertilization and inoculation on
2070 N_{area} (fertilization-by-inoculation interaction: $p < 0.001$; Table 1; Fig. 1a), N_{mass}
2071 ($p = 0.001$; Table 1; Fig. 1b), M_{area} ($p = 0.025$; Table 1; Fig. 1c), and Chl_{area} (p
2072 < 0.001 ; Table 1; Fig. 1d) indicated that the general positive effect of increasing
2073 fertilization on each trait was stronger in uninoculated pots (Tukey _{N_{area}} : $p <$
2074 0.001; Tukey _{N_{mass}} : $p = 0.001$; Tukey _{M_{area}} : $p = 0.031$; Tukey _{Chl_{area}} : $p < 0.001$).

Table 5.1. Effects of soil nitrogen fertilization, inoculation, and CO₂ treatments on N_{area} , N_{mass} , M_{area} , and Chl_{area}

	N_{area}			N_{mass}			M_{area}^a			
	df	Coefficient	χ^2	p	Coefficient	χ^2	p	Coefficient	χ^2	p
(Intercept)	-	1.10E+00	-	-	3.05E-02	-	-	3.64E+00	-	-
CO ₂	1	-5.67E-01	155.908	<0.001	-1.80E-02	272.362	<0.001	3.04E-01	151.319	<0.001
Inoculation (I)	1	6.21E-01	86.029	<0.001	7.54E-03	15.576	<0.001	1.81E-01	19.158	<0.001
Fertilization (N)	1	3.06E-03	316.408	<0.001	5.78E-05	106.659	<0.001	3.10E-04	21.440	<0.001
CO ₂ *I	1	2.63E-01	4.729	0.030	3.96E-03	2.025	0.155	-3.37E-02	0.029	0.866
CO ₂ *N	1	-3.68E-04	5.723	0.017	-2.85E-05	22.542	<0.001	2.80E-04	7.619	0.006
I*N	1	-1.36E-03	43.381	<0.001	-2.00E-05	11.137	0.001	-3.36E-04	5.022	0.025
CO ₂ *I*N	1	-3.23E-04	0.489	0.484	-2.59E-06	0.041	0.839	1.15E-04	0.208	0.649
<hr/>										
Chl_{area}										
	df	Coefficient	χ^2	p						
(Intercept)	-	2.13E-02	-	-						
CO ₂	1	-1.33E-02	69.233	<0.001						
Inoculation (I)	1	1.24E-01	136.341	<0.001						
Fertilization (N)	1	3.35E-04	163.111	<0.001						
CO ₂ *I	1	-3.18E-02	2.102	0.147						
CO ₂ *N	1	-8.79E-05	2.999	<i>0.083</i>						
I*N	1	-2.65E-04	75.769	<0.001						
CO ₂ *I*N	1	7.68E-05	2.144	0.147						

123

2075 *Significance determined using Type II Wald χ^2 tests ($\alpha = 0.05$). P -values < 0.05 are in bold, while p -values between
 2076 0.05 and 0.1 are italicized. A superscript “a” is included after trait labels to indicate if models were fit with natural
 2077 log transformed response variables. Key: df = degrees of freedom, N_{area} = leaf nitrogen content per unit leaf area,
 2078 N_{mass} = leaf nitrogen content, M_{area} = leaf mass per unit leaf area.

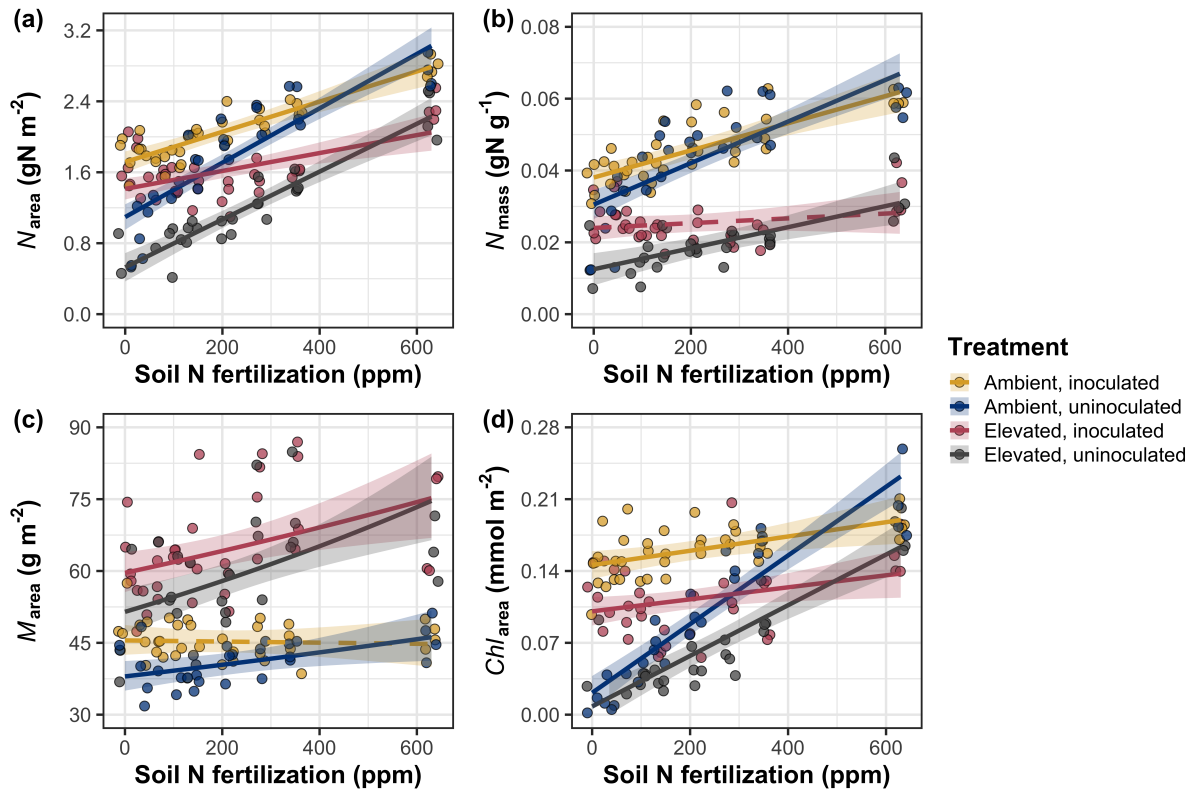


Figure 5.1. Effects of CO_2 , fertilization, and inoculation on leaf nitrogen per unit leaf area (a), leaf nitrogen content (b), leaf mass per unit leaf area (c), and chlorophyll content per unit leaf area (d). Soil nitrogen fertilization is represented on the x-axis in all panels. Yellow points and trendlines indicate inoculated individuals grown under ambient CO_2 , blue points and trendlines indicate uninoculated individuals grown under ambient CO_2 , red points and trendlines indicate inoculated individuals grown under elevated CO_2 , and grey points indicate uninoculated individuals grown under elevated CO_2 . Solid trendlines indicate regression slopes that are different from zero ($p < 0.05$), while dashed trendlines indicate slopes that are not distinguishable from zero ($p > 0.05$).

2079 5.3.2 *Leaf biochemistry and stomatal conductance*

2080 Elevated CO₂ resulted in plants with 16% lower V_{cmax25} ($p < 0.001$; Table
2081 2) and 10% lower J_{max25} ($p = 0.014$; Table 2) as compared to those grown un-
2082 der ambient CO₂, but did not influence R_{d25} ($p = 0.613$; Table 2). A relatively
2083 stronger downregulation in V_{cmax25} than J_{max25} resulted in an 8% stimulation in
2084 $J_{max25}:V_{cmax25}$ under elevated CO₂ ($p < 0.001$; Table 2; Fig. 2E). The downregu-
2085 latory effect of CO₂ on V_{cmax25} and J_{max25} was not modified across the fertilization
2086 gradient (CO₂-by-fertilization interaction: $p = 0.185$, $p = 0.389$ for V_{cmax25} and
2087 J_{max25} , respectively; Table 2; Fig. 2A, 2C) or between inoculation treatments
2088 (CO₂-by-inoculation interaction: $p = 0.799$ and $p = 0.714$ for V_{cmax25} and J_{max25} ,
2089 respectively; Table 2). However, a strong interaction between fertilization and
2090 inoculation (fertilization-by-inoculation interaction: $p \leq 0.001$ in all cases; Table
2091 2) indicated that the general positive effect of increasing fertilization on V_{cmax25} (p
2092 < 0.001 ; Table 2), J_{max25} ($p < 0.001$; Table 2), and R_{d25} ($p = 0.015$; Table 2) was
2093 only observed in uninoculated pots (Tukey: $p \leq 0.001$ in all cases), as there was
2094 no apparent effect of fertilization on V_{cmax25} (Tukey: $p = 0.456$), J_{max25} (Tukey: p
2095 = 0.180), or R_{d25} (Tukey: $p = 0.443$) in inoculated pots (Figs. 2B, 2D, 2F, 2H). A
2096 relatively stronger positive effect of increasing fertilization on V_{cmax25} than J_{max25}
2097 resulted in a general reduction in $J_{max25}:V_{cmax25}$ with increasing fertilization ($p <$
2098 0.001), though this pattern was only seen in uninoculated pots (Tukey: $p = 0.003$)
2099 and not inoculated plants (Tukey: $p > 0.05$).

2100 Elevated CO₂ reduced stomatal conductance by 20% ($p < 0.001$; Table 2)
2101 compared to ambient CO₂, but this downregulation did not influence stomatal
2102 limitation of photosynthesis ($p = 0.355$; Table 2). As with V_{cmax25} and J_{max25} , the

2103 downregulation of stomatal conductance due to elevated CO₂ was not modified
2104 across the fertilization gradient (CO₂-by-fertilization interaction: $p = 0.141$; Table
2105 2) or between inoculation treatments (CO₂-by-inoculation interaction: $p = 0.179$;
2106 Table 2). Fertilization also did not modify the general null effect of CO₂ on stom-
2107 atal limitation (CO₂-by-fertilization interaction: $p = 0.554$; Table 2), although
2108 an interaction between CO₂ and inoculation (CO₂-by-inoculation interaction: p
2109 = 0.043; Table 2) indicated that inoculation increased stomatal limitation un-
2110 der ambient CO₂ (Tukey: $p = 0.021$), but not under elevated CO₂ (Tukey: p
2111 > 0.999). An interaction between inoculation and fertilization on stomatal con-
2112 ductance (fertilization-by-inoculation interaction: $p < 0.001$; Table 2) indicated
2113 that increasing fertilization increased stomatal conductance in uninoculated pots
2114 (Tukey: $p = 0.003$) but decreased stomatal conductance in inoculated pots (Tukey:
2115 $p = 0.021$). The similar in magnitude, but opposite direction, trend in the effect of
2116 increasing fertilization on stomatal conductance between inoculation treatments
2117 likely drove a null general response of stomatal conductance to increasing fertil-
2118 ization ($p = 0.642$; Table 2).

Table 5.2. Effects of soil nitrogen fertilization, inoculation, and CO₂ on leaf biochemistry

	<i>V_{cmax25}</i>			<i>J_{max25}</i>			<i>R_{d25}</i>			
	df	Coefficient	χ^2	p	Coefficient	χ^2	p	Coefficient	χ^2	p
(Intercept)	-	4.36E+01	-	-	8.30E+01	-	-	1.69E+00	-	-
CO ₂	1	-7.05E+00	18.039	<0.001	-9.11E+00	6.042	0.014	4.53E-01	0.256	0.613
Inoculation (I)	1	5.87E+01	98.579	<0.001	9.62E+01	85.064	<0.001	1.04E+00	3.094	0.079
Fertilization (N)	1	1.32E-01	37.053	<0.001	2.09E-01	25.356	<0.001	2.86E-03	5.965	0.015
CO ₂ *I	1	-4.65E+00	0.065	0.799	7.84E-01	0.667	0.414	-5.71E-01	2.563	0.109
CO ₂ *N	1	-3.58E-02	1.758	0.185	-4.33E-02	0.742	0.389	-1.55E-03	2.675	0.102
I*N	1	-1.35E-01	60.394	<0.001	-2.30E-01	57.410	<0.001	-2.84E-03	12.083	0.001
CO ₂ *I*N	1	2.73E-02	0.748	0.387	3.46E-02	0.377	0.539	7.21E-04	0.244	0.622

	<i>J_{max25}:V_{cmax25}</i>			<i>g_{sw}</i>			Stomatal limitation			
	df	Coefficient	χ^2	p	Coefficient	χ^2	p	Coefficient	χ^2	p
(Intercept)	-	1.92E+00	-	-	1.95E-01	-	-	2.12E-01	-	-
CO ₂	1	5.71E-02	92.010	<0.001	-6.23E-02	9.718	0.002	3.91E-02	0.856	0.355
Inoculation (I)	1	-1.79E-01	27.768	<0.001	1.30E-01	22.351	<0.001	7.87E-02	4.582	0.032
Fertilization (N)	1	-4.61E-04	28.147	<0.001	2.50E-04	0.066	0.797	2.60E-04	32.218	<0.001
CO ₂ *I	1	8.94E-02	2.916	0.088	6.69E-02	1.810	0.179	-7.84E-02	4.093	0.043
CO ₂ *N	1	2.35E-04	3.210	0.073	-8.50E-05	2.165	0.141	-1.24E-04	0.350	0.554
I*N	1	3.27E-04	9.607	0.002	-3.09E-04	14.696	<0.001	-1.67E-04	2.547	0.110
CO ₂ *I*N	1	-1.66E-04	1.102	0.294	-8.89E-05	0.234	0.629	1.67E-04	2.231	0.135

127

2119 *Significance determined using Type II Wald χ^2 tests ($\alpha = 0.05$). *P*-values < 0.05 are in bold, while *p*-values between
 2120 0.05 and 0.1 are italicized. Key: *V_{cmax25}* – maximum rate of Rubisco carboxylation at 25°C; *J_{max25}* – maximum rate
 2121 of electron transport for RuBP regeneration at 25°C, *R_{d25}* - dark respiration at 25°C; *J_{max25}:V_{cmax25}* – the ratio of
 2122 *J_{max25}* to *V_{cmax25}*; *g_{sw}* - stomatal conductance.

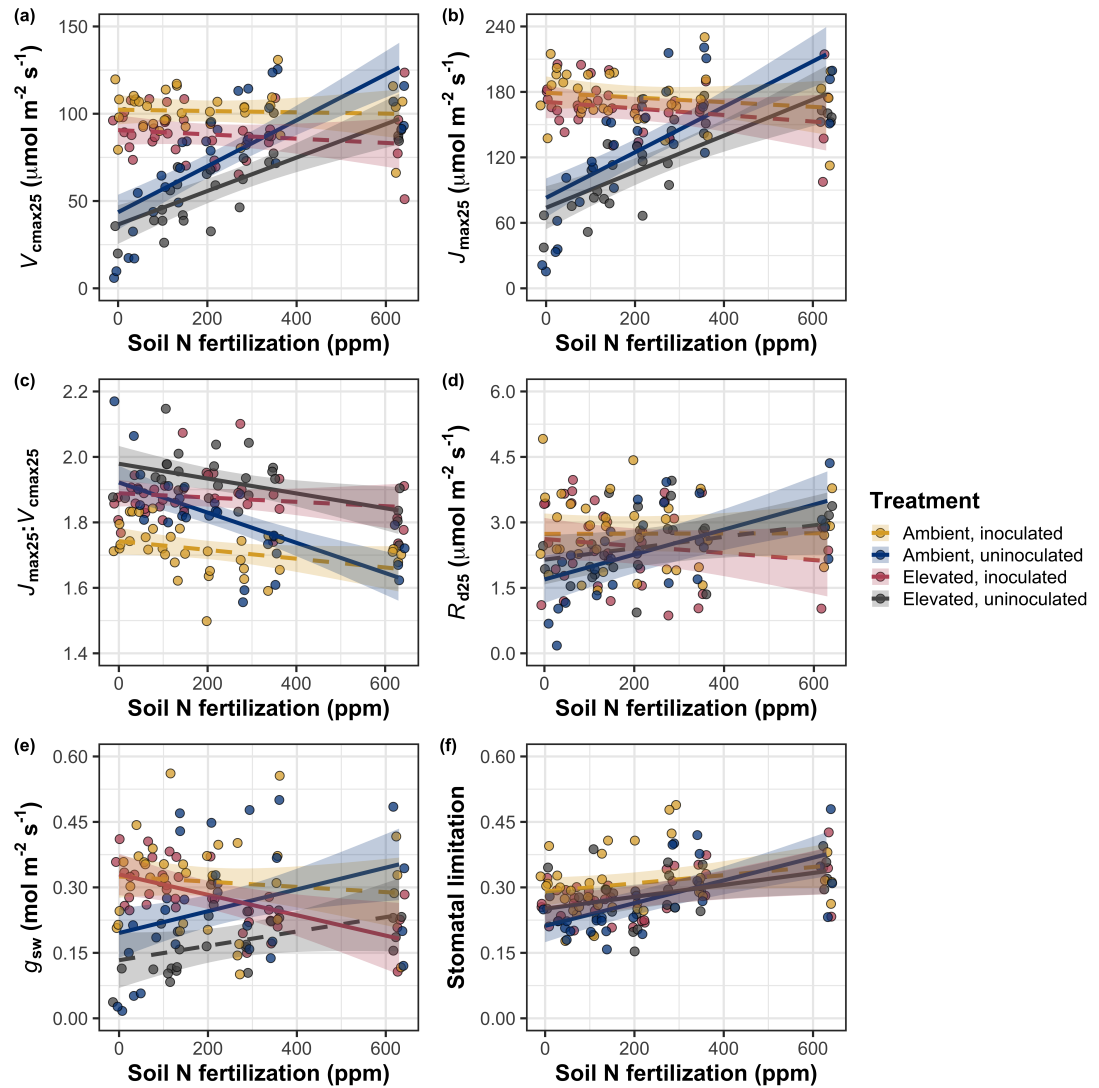


Figure 5.2. Effects of CO₂, fertilization, and inoculation on maximum rate of Rubisco carboxylation (a), the maximum rate of RuBP regeneration (b), and the ratio of the maximum rate of RuBP regeneration to the maximum rate of Rubisco carboxylation leaf mass per unit leaf area (c), dark respiration (d), stomatal conductance (e), and stomatal limitation (f). Soil nitrogen fertilization is represented on the x-axis in all panels. Colored points and trendlines are as explained in Figure 1.

2123 5.3.3 *Leaf nitrogen allocation*

2124 A relatively stronger downregulation in N_{area} than $V_{\text{cmax}25}$ or $J_{\text{max}25}$ resulted
2125 in an 20% and 29% respective stimulation in ρ_{rubisco} and ρ_{bioe} under elevated CO₂
2126 ($p < 0.001$ in both cases; Table 3). There was no apparent CO₂ effect on ρ_{light}
2127 ($p = 0.700$; Table 3), but the strong stimulation in ρ_{rubisco} and ρ_{bioe} resulted
2128 in a 21% stimulation of ρ_{photo} under elevated CO₂ ($p < 0.001$; Table 3; Fig.
2129 3A). The stimulation of ρ_{rubisco} , ρ_{bioe} , and ρ_{photo} due to elevated CO₂ was not
2130 modified across the fertilization gradient (CO₂-by-fertilization interaction: p_{rubisco}
2131 = 0.269, $p_{\text{bioe}} = 0.298$, $p_{\text{photo}} = 0.281$; Table 3). A marginal interaction between
2132 inoculation and CO₂ on ρ_{rubisco} and ρ_{photo} (CO₂-by-inoculation interaction: p_{rubisco}
2133 = 0.057, $p_{\text{photo}} = 0.057$; Table 3) indicated that the general positive effect of
2134 inoculation on ρ_{rubisco} and ρ_{photo} ($p < 0.001$ in both cases; Table 3) was only
2135 apparent under ambient CO₂ (Tukey: $p < 0.001$ in both cases), with no apparent
2136 effect of inoculation under elevated CO₂ (Tukey_{rubisco}: $p = 0.200$; Tukey_{photo}: p
2137 = 0.147). Inoculation did not modify the stimulation of ρ_{bioe} under elevated CO₂
2138 (CO₂-by-inoculation interaction: $p = 0.122$; Table 3) or the null effect of CO₂ on
2139 ρ_{bioe} (CO₂-by-inoculation interaction: $p = 0.298$; Table 3). Strong interactions
2140 between fertilization and inoculation on ρ_{rubisco} , ρ_{bioe} , and ρ_{photo} (fertilization-
2141 by-inoculation interaction: $p < 0.001$ in all cases; Table 3) indicated that the
2142 general negative effect of increasing fertilization ($p < 0.001$ in all cases; Table
2143 3) was only observed in inoculated pots (Tukey: $p < 0.001$ in all cases), with
2144 no apparent effect of fertilization on ρ_{rubisco} (Tukey: $p = 0.612$), ρ_{bioe} (Tukey:
2145 $p = 0.544$), or ρ_{photo} (Tukey: $p = 0.521$; Fig 3B) in uninoculated pots. An
2146 additional interaction between fertilization and inoculation on ρ_{light} (fertilization-

2147 by-inoculation interaction: $p < 0.001$; Table 3) indicated a negative effect of
2148 increasing fertilization on ρ_{light} in inoculated pots (Tukey: $p = 0.041$), but a
2149 positive effect of increasing fertilization in uninoculated pots (Tukey: $p < 0.001$).

2150 The stimulation in M_{area} resulted in an 133% stimulation of $\rho_{\text{structure}}$ under
2151 elevated CO₂ ($p < 0.001$; Table 3; Fig 3C). An interaction between fertilization
2152 and CO₂ (CO₂-by-fertilization interaction: $p = 0.039$; Table 3) indicated that the
2153 general negative effect of increasing fertilization ($p < 0.001$; Table 3) on $\rho_{\text{structure}}$
2154 was marginally stronger under ambient CO₂ (Tukey: $p = 0.055$), resulting in a
2155 stronger stimulation in $\rho_{\text{structure}}$ under elevated CO₂ with increasing fertilization.
2156 A marginal interaction between inoculation and CO₂ (CO₂-by-inoculation inter-
2157 action: $p = 0.057$; Table 3) indicated that the general positive effect of inoculation
2158 on $\rho_{\text{structure}}$ ($p < 0.001$; Table 3) was only observed under elevated CO₂ (Tukey:
2159 $p < 0.001$), with no apparent inoculation effect observed under ambient CO₂
2160 (Tukey: $p = 0.513$). Finally, an interaction between fertilization and inoculation
2161 (fertilization-by-inoculation interaction: $p < 0.001$; Table 3; Fig. 3D) indicated
2162 that, while increasing fertilization generally increased $\rho_{\text{structure}}$ ($p < 0.001$; Table
2163 3), this response was generally stronger in uninoculated pots (Tukey: $p = 0.001$).

Table 5.3. Effects of soil N availability, soil pH, species, and N_{area} on leaf nitrogen allocation

		ρ_{rubisco}		ρ_{bioe}		ρ_{light}				
	df	Coefficient	χ^2	p	Coefficient	χ^2	p	Coefficient	χ^2	p
(Intercept)	-	2.70E-01	-	-	5.26E-02	-	-	8.48E-03	-	-
CO ₂	1	1.42E-01	23.510	<0.001	3.00E-02	53.899	<0.001	2.03E-03	0.149	0.700
Inoculation (I)	1	1.83E-01	23.475	<0.001	2.80E-02	13.860	<0.001	2.04E-02	147.234	<0.001
Fertilization (N)	1	1.35E-04	16.609	<0.001	1.22E-05	26.827	<0.001	3.22E-05	19.378	<0.001
CO ₂ *I	1	-1.07E-01	3.629	0.057	-1.67E-02	2.390	0.122	-5.33E-03	0.684	0.408
CO ₂ *N	1	-2.16E-04	1.223	0.269	-3.59E-05	1.085	0.298	-7.01E-06	0.351	0.553
I*N	1	-4.26E-04	20.045	<0.001	-6.87E-05	15.458	<0.001	-4.37E-05	64.042	<0.001
CO ₂ *I*N	1	2.50E-04	3.327	0.068	4.08E-05	2.651	0.103	1.74E-05	3.735	0.053

		ρ_{photo}		$\rho_{\text{structure}}^a$				
	df	Coefficient	χ^2	p	Coefficient	χ^2	p	
(Intercept)	-	3.32E-01	-	-	-2.93E+00	-	-	
CO ₂	1	1.81E-01	27.651	<0.001	8.77E-01	229.571	<0.001	
Inoculation (I)	1	2.31E-01	26.238	<0.001	-2.55E-01	13.872	<0.001	
Fertilization (N)	1	1.76E-04	15.899	<0.001	-1.51E-03	38.128	<0.001	
CO ₂ *I	1	-1.36E-01	3.671	0.055	-2.99E-01	3.622	0.057	
CO ₂ *N	1	-2.72E-04	1.163	0.281	3.14E-04	4.266	0.039	
I*N	1	-5.37E-04	21.355	<0.001	7.00E-04	11.025	0.001	
CO ₂ *I*N	1	3.29E-04	4.009	0.045	4.52E-04	0.669	0.413	

131

2164 *Significance determined using Type II Wald χ^2 tests ($\alpha = 0.05$). P-values < 0.05 are in bold, while p-values
 2165 between 0.05 and 0.1 are italicized. A superscript “a” is included after trait labels to indicate if models were fit with
 2166 natural log transformed response variables. Key: df=degrees of freedom, ρ_{rubisco} = proportion of leaf N allocated to
 2167 photosynthesis, ρ_{bioe} = proportion of leaf N allocated to bioenergetics, ρ_{light} =proportion of leaf N allocated to light
 2168 harvesting proteins, ρ_{photo} =proportion of leaf N allocated to photosynthesis, $\rho_{\text{structure}}$ =proportion of leaf N allocated
 2169 to cell wall structural tissue

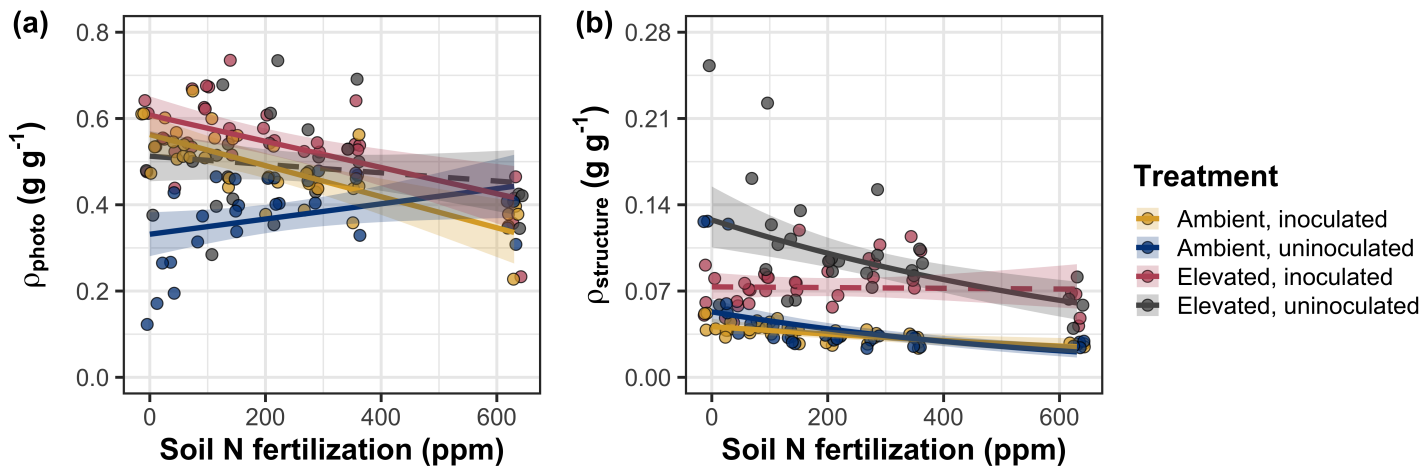


Figure 5.3. Effects of CO_2 , fertilization, and inoculation on the relative fraction of leaf nitrogen allocated to photosynthesis (a) and the fraction of leaf nitrogen allocated to structure (b). Soil nitrogen fertilization is represented on the x-axis in both panels. Colored points and trendlines are as explained in Figure 1.

2170 5.3.4 *Whole plant growth and total leaf area*

2171 Total leaf area was 51% greater and total biomass was 102% greater un-
2172 der elevated CO₂ ($p < 0.001$ in both cases; Table 4), a pattern that was en-
2173 hanced by fertilization (CO₂-by-fertilization interaction: $p < 0.001$ in both cases;
2174 Table 4; Fig. 4a-b) but was not modified across inoculation treatments (CO₂-
2175 by-inoculation interaction: $p_{total_leaf_area} = 0.151$, $p_{total_biomass} = 0.472$; Table 4).
2176 Specifically, the general positive effect of increasing fertilization on total leaf area
2177 and whole plant biomass ($p < 0.001$ in both cases; Table 4) was stronger under
2178 elevated CO₂ (Tukey: $p < 0.001$ in both cases). The general positive effect of
2179 increasing fertilization on total leaf area was modified by inoculation treatment
2180 (fertilization-by-inoculation interaction: $p < 0.001$ in both cases; Table 4), in-
2181 dicating a stronger positive effect of increasing fertilization in uninoculated pots
2182 (Tukey: $p_{total_leaf_area} = 0.002$, $p_{total_biomass} = 0.001$).

2183 5.3.5 *Carbon costs to acquire nitrogen*

2184 A general 62% stimulation in N_{cost} under elevated CO₂ was modified thr-
2185 ough a strong three-way interaction between CO₂, fertilization, and inoculation
2186 (CO₂-by-inoculation-by-fertilization interaction: $p < 0.001$; Table 4). This in-
2187 teraction revealed a general negative effect of increasing fertilization on N_{cost} (p
2188 < 0.001 ; Table 4) that was observed in all treatment combinations (Tukey: $p <$
2189 0.001 in all cases) except for inoculated pots grown under elevated CO₂ (Tukey:
2190 $p = 0.779$; Fig. 5c). This response also resulted in generally stronger negative ef-
2191 ffects of increasing fertilization on N_{cost} in uninoculated pots grown under elevated
2192 CO₂ than uninoculated pots grown under ambient CO₂ (Tukey: $p = 0.001$) and

2193 inoculated pots grown under either ambient CO₂ (Tukey: $p < 0.001$) or elevated
2194 CO₂ (Tukey: $p < 0.001$), while uninoculated pots grown under ambient CO₂ had
2195 generally stronger negative effects of increasing fertilization on N_{cost} than inocu-
2196 lated pots grown under elevated CO₂ (Tukey: $p = 0.002$), but not inoculated pots
2197 grown under ambient CO₂ (Tukey: $p = 0.216$). The general reduction in N_{cost}
2198 with increasing fertilization and in uninoculated pots were driven by a stronger
2199 positive effect of increasing fertilization on N_{wp} (denominator of N_{cost}) than C_{bg}
2200 (numerator of N_{cost}), while the general stimulation in N_{cost} under elevated CO₂
2201 was driven by a stronger positive effect of elevated CO₂ on C_{bg} than N_{wp} (Table
2202 4).

Table 5.4. Effects of soil N availability, soil pH, species, and N_{area} on total leaf area, whole plant biomass, and costs of nitrogen acquisition

	Total leaf area			Total biomass			N_{cost}			
	df	Coefficient	χ^2	p	Coefficient	χ^2	p	Coefficient	χ^2	p
(Intercept)	-	8.78E+01	-	-	9.96E-01	-	-	8.67E+00	-	-
CO_2	1	3.36E+01	69.291	<0.001	5.07E-01	131.477	<0.001	8.75E+00	88.189	<0.001
Inoculation (I)	1	1.88E+02	35.715	<0.001	7.96E-01	34.264	<0.001	-1.68E+00	136.343	<0.001
Fertilization (N)	1	9.35E-01	274.199	<0.001	3.14E-03	269.046	<0.001	-8.50E-03	80.501	<0.001
$\text{CO}_2 * \text{I}$	1	6.44E+01	2.064	0.151	-7.69E-02	0.518	0.472	-8.38E+00	85.237	<0.001
$\text{CO}_2 * \text{N}$	1	5.05E-01	18.655	<0.001	1.61E-03	16.877	<0.001	-9.17E-03	1.050	0.306
$\text{I} * \text{N}$	1	-3.84E-01	10.804	0.001	-1.45E-03	15.779	<0.001	4.20E-03	46.489	<0.001
$\text{CO}_2 * \text{I} * \text{N}$	1	-2.97E-03	<0.001	0.990	-1.14E-04	0.023	0.880	1.32E-02	18.125	<0.001

	C_{bg}			N_{wp}			
	df	Coefficient	χ^2	p	Coefficient	χ^2	p
(Intercept)	-	-1.70E+00	-	-	1.24E-01	-	-
CO_2	1	9.21E-01	84.134	<0.001	-3.41E-03	23.890	<0.001
Inoculation (I)	1	1.18E+00	41.030	<0.001	1.68E-01	134.460	<0.001
N fertilization (N)	1	3.38E-03	152.248	<0.001	6.69E-04	529.021	<0.001
$\text{CO}_2 * \text{I}$	1	-6.18E-01	8.965	0.003	3.68E-02	1.190	0.275
$\text{CO}_2 * \text{N}$	1	-3.66E-05	1.188	0.276	1.58E-04	5.915	0.015
$\text{I} * \text{N}$	1	-2.22E-03	22.648	<0.001	-3.20E-04	55.562	<0.001
$\text{CO}_2 * \text{I} * \text{N}$	1	8.09E-04	1.109	0.292	-7.54E-05	0.620	0.431

135

- 2203 *Significance determined using Type II Wald χ^2 tests ($\alpha = 0.05$). P-values < 0.05 are in bold, while p -values
 2204 between 0.05 and 0.1 are italicized. A superscript “a” after trait labels indicates if models were fit using natural log
 2205 transformed response variables, while a superscript “b” indicates if models were fit using square root transformed
 2206 variables. Key: df=degrees of freedom

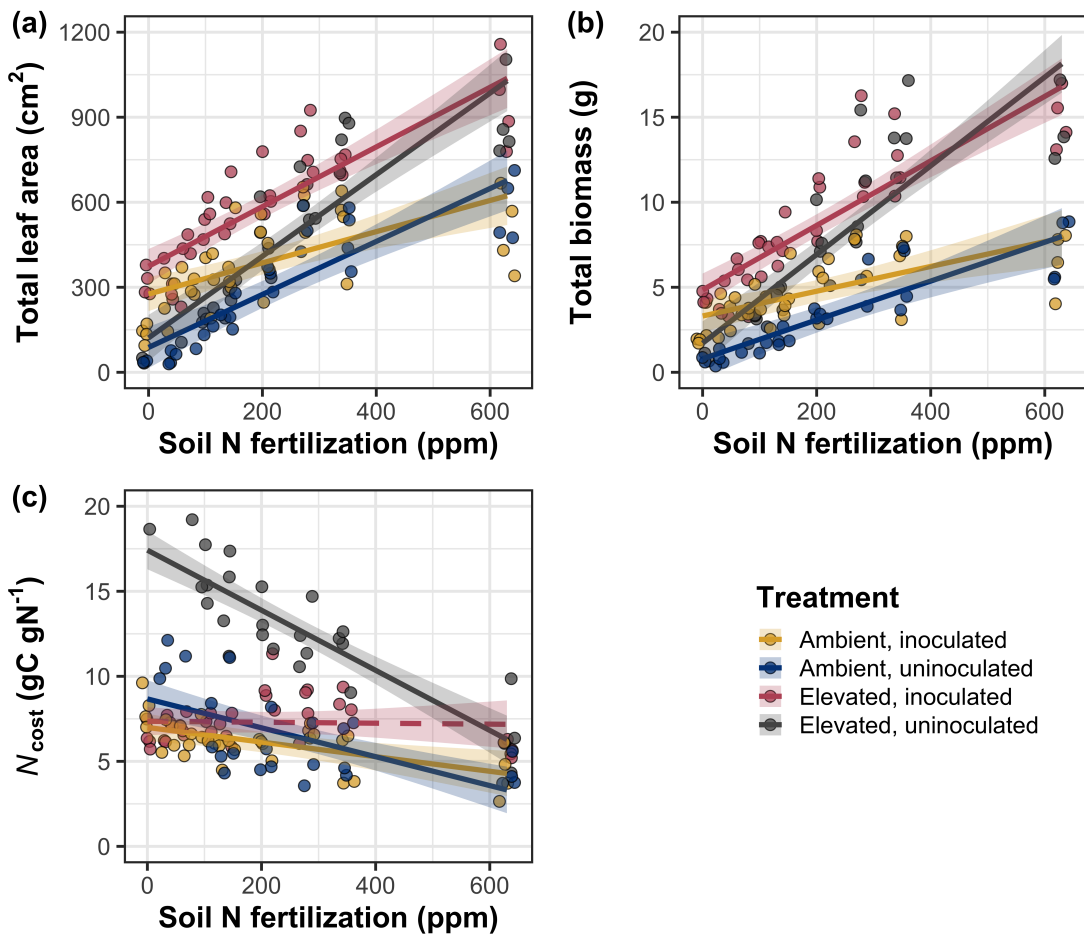


Figure 5.4. Effects of CO_2 , fertilization, and inoculation on total leaf area (a), total biomass (b), and structural carbon costs to acquire nitrogen (c). Soil nitrogen fertilization is represented continuously on the x-axis in all panels. Colored points and trendlines are as explained in Figure 1.

2207 5.3.6 *Nitrogen fixation*

2208 Nodule biomass was stimulated by 30% under elevated CO₂ ($p < 0.001$;
2209 Table 5), a pattern that was modified across the fertilization gradient (CO₂-by-
2210 fertilization interaction: $p = 0.479$; Table 5), but not between inoculation treat-
2211 ments (CO₂-by-inoculation interaction: $p = 0.404$; Table 5). Specifically, the
2212 general negative effect of increasing fertilization on nodule biomass ($p < 0.001$;
2213 Table 5) was stronger under elevated CO₂ than ambient CO₂ (Tukey: $p < 0.001$;
2214 Fig. 5a), which reduced the stimulation in nodule biomass under elevated CO₂
2215 with increasing fertilization. A strong interaction between fertilization and inocu-
2216 lation (fertilization-by-inoculation interaction: $p < 0.001$; Table 5) was driven by
2217 a stronger negative effect of increasing fertilization in inoculated pots (Tukey: p
2218 < 0.001 ; Fig. 5a).

2219 There was no effect of CO₂ on nodule: root biomass ($p = 0.767$; Table 5),
2220 although an interaction between CO₂ and inoculation (CO₂-by-inoculation inter-
2221 action: $p < 0.001$; Table 5) indicated that the general positive effect of inoculation
2222 on nodule: root biomass ($p < 0.001$; Table 5) was stronger under ambient CO₂
2223 (3129% increase; Tukey: $p < 0.001$) than elevated CO₂ (379% increase; Tukey:
2224 $p < 0.001$; Fig. 5b). The null effect of CO₂ on nodule: root biomass was con-
2225 sistently observed across the fertilization gradient ($p = 0.183$; Table 5; Fig. 5b).
2226 An interaction between fertilization and inoculation (fertilization-by-inoculation
2227 interaction: $p < 0.001$; Table 5) indicated that the general negative effect of in-
2228 creasing fertilization on nodule: root biomass ($p < 0.001$; Table 5) was stronger
2229 in inoculated pots (Tukey: $p < 0.001$; Fig. 5b).

2230 There was no effect of CO₂ on %N_{dfa} ($p = 0.472$; Table 5), a pattern

2231 that was not modified by inoculation (CO_2 -by-inoculation interaction: $p = 0.156$;
2232 Table 5) or fertilization (CO_2 -by-fertilization interaction: $p = 0.099$; Table 5).
2233 An interaction between fertilization and inoculation (fertilization-by-inoculation
2234 interaction: $p < 0.001$; Table 5) indicated that the general negative effect of
2235 increasing fertilization on $\%N_{\text{dfa}}$ ($p < 0.001$; Table 5) was only observed in inoc-
2236 ulated pots (Tukey: $p < 0.001$), with no apparent effect of fertilization on $\%N_{\text{dfa}}$
2237 in uninoculated pots (Tukey: $p = 0.651$; Table 5; Fig. 5c).

Table 5.5. Effects of soil N availability, soil pH, species, and N_{area} on root nodule biomass and plant investments in symbiotic nitrogen fixation

	Root nodule biomass ^b			Root nodule: root biomass ^b			% N_{dfa}^b			
	df	Coefficient	χ^2	p	Coefficient	χ^2	p	Coefficient	χ^2	p
(Intercept)	-	9.41E-03	-	-	1.33E-02	-	-	7.48E-01	-	-
CO ₂	1	1.20E-01	19.258	<0.001	9.94E-02	0.087	0.768	-1.00E-01	0.518	0.472
Inoculation (I)	1	5.74E-01	755.020	<0.001	5.40E-01	903.691	<0.001	9.01E+00	955.570	<0.001
Fertilization (N)	1	7.71E-06	84.376	<0.001	-5.99E-06	258.099	<0.001	3.64E-04	292.938	<0.001
CO ₂ *I	1	-4.68E-02	0.950	0.330	-1.38E-01	20.614	<0.001	-1.44E-01	2.010	0.156
CO ₂ *N	1	-1.59E-04	2.106	0.147	-1.73E-04	1.773	0.183	-6.21E-05	2.716	0.099
I*N	1	-5.82E-04	44.622	<0.001	-7.45E-04	133.918	<0.001	-1.58E-02	231.290	<0.001
CO ₂ *I*N	1	7.26E-05	0.196	0.658	1.76E-04	2.359	0.125	2.77E-03	2.119	0.145

2238 *Significance determined using Type II Wald χ^2 tests ($\alpha = 0.05$). P-values < 0.05 are in bold, while p-values between
 2239 0.05 and 0.1 are italicized. Superscript letters indicate model coefficients fit to square-root (^b) transformed data.
 2240 Key: % N_{dfa} =percent nitrogen fixed from the atmosphere.

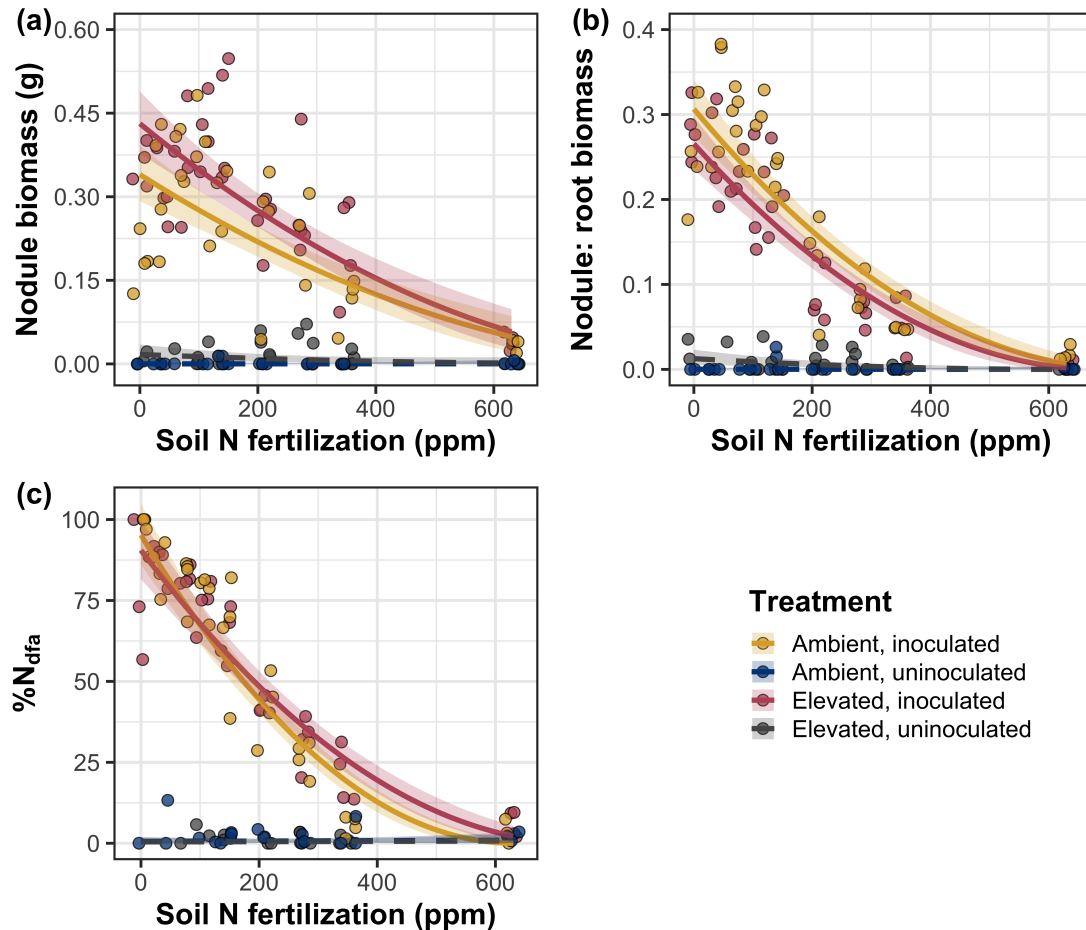


Figure 5.5. Effects of CO_2 , fertilization, and inoculation on nodule biomass (a), nodule: root biomass (b), and percent nitrogen fixed from the atmosphere (c). Soil nitrogen fertilization is represented on the x-axis. Yellow points and trendlines indicate inoculated individuals grown under ambient CO_2 , blue points and trendlines indicate uninoculated individuals grown under ambient CO_2 , red points and trendlines indicate inoculated individuals grown under elevated CO_2 , and grey points indicate uninoculated individuals grown under elevated CO_2 . Solid trendlines indicate slopes that are different from zero ($p < 0.05$), while dashed trendlines indicate slopes that are not different from zero ($p > 0.05$). Curvilinear trendlines occur as a result of back-transforming models where response variables received either a natural log or square root transformation prior to fitting.

2241 5.4 Discussion

2242 In this study, I determined leaf and whole plant acclimation responses of
2243 7-week *G. max* seedlings grown under two CO₂ concentrations, two inoculation
2244 treatments, and nine soil nitrogen fertilization treatments in a full-factorial growth
2245 chamber experiment. In support of my hypotheses and patterns expected from
2246 theory, elevated CO₂ reduced N_{area} , V_{cmax25} , and J_{max25} . The relatively stronger
2247 downregulation in V_{cmax25} than J_{max25} under elevated CO₂ resulted in a stimulation
2248 in $J_{\text{max25}}:V_{\text{cmax25}}$ under elevated CO₂. The downregulation of V_{cmax25} and J_{max25}
2249 under elevated CO₂ was similar across fertilization and inoculation treatments,
2250 indicating that the CO₂ responses were not due to nitrogen limitation. Interest-
2251 ingly, results indicate that elevated CO₂ increased the fraction of leaf nitrogen
2252 allocated to photosynthesis and structure, leading to a stimulation in nitrogen
2253 use efficiency under elevated CO₂ despite the apparent downregulation in N_{area} ,
2254 V_{cmax25} , and J_{max25} . The downregulation in leaf photosynthetic processes under
2255 elevated CO₂ also corresponded with a strong stimulation in total leaf area and to-
2256 tal biomass. Strong stimulations in whole plant growth due to elevated CO₂ were
2257 generally enhanced with increasing fertilization and were negatively related to
2258 structural carbon costs to acquire nitrogen. Inoculation generally did not modify
2259 whole plant responses to elevated CO₂ across the fertilization gradient, likely due
2260 to a strong reduction in root nodulation with increasing fertilization. However,
2261 strong positive effects of inoculation on whole plant growth were observed under
2262 low fertilization, consistent with our hypothesis. Overall, observed leaf and whole
2263 plant acclimation responses to CO₂ support hypotheses and patterns expected
2264 from photosynthetic least-cost theory, showing that leaf acclimation responses to

2265 CO₂ were decoupled from soil nitrogen availability and ability to acquire nitro-
2266 gen via symbiotic nitrogen fixation. Instead, leaf and whole plant acclimation
2267 responses to CO₂ were driven by optimal resource investment to photosynthetic
2268 capacity, where optimal resource investment at the leaf level maximized nitrogen
2269 allocation to structures that support whole plant growth.

2270 5.4.1 *Soil nitrogen fertilization has divergent effects on leaf and whole plant
2271 acclimation responses to CO₂*

2272 Elevated CO₂ reduced N_{area} , V_{cmax25} , J_{max25} , and stomatal conductance by
2273 29%, 16%, 10%, and 20%, respectively (Table 5.2). The larger downregulation in
2274 V_{cmax25} than J_{max25} led to an 8% stimulation in $J_{\text{max25}}:V_{\text{cmax25}}$ (Table 5.2), while
2275 the larger downregulation in N_{area} than V_{cmax25} resulted in a 21% stimulation
2276 in the fraction of leaf nitrogen allocated to photosynthesis under elevated CO₂.
2277 These acclimation responses are directionally consistent with previous studies that
2278 have investigated or reviewed leaf acclimation responses to CO₂ (Drake et al.
2279 1997; Makino et al. 1997; Ainsworth et al. 2002; Ainsworth and Long 2005;
2280 Ainsworth and Rogers 2007; Smith and Dukes 2013; Smith and Keenan 2020;
2281 Poorter et al. 2022), and follow patterns expected from photosynthetic least-cost
2282 theory (Wright et al. 2003; Prentice et al. 2014; Smith et al. 2019; Smith and
2283 Keenan 2020). Together, the stimulation in $J_{\text{max25}}:V_{\text{cmax25}}$ and the fraction of leaf
2284 nitrogen allocated to photosynthesis, and nitrogen use efficiency under elevated
2285 CO₂ provide strong support for the idea that leaves were downregulating V_{cmax25}
2286 in response to elevated CO₂ in order to optimally coordinate photosynthesis such
2287 that net photosynthesis rates approached becoming equally co-limited by Rubisco

2288 carboxylation and RuBP regeneration (Chen et al. 1993; Maire et al. 2012).

2289 Increasing fertilization and inoculation induced strong positive effects on
2290 N_{area} (Fig. 1a), $V_{\text{cmax}25}$ (Fig. 5.2a), $J_{\text{max}25}$ (Fig. 5.2b). The general positive
2291 response of N_{area} to increasing fertilization and in inoculated pots was enhanced
2292 under ambient CO₂, which, paired with the general downregulation in N_{area} un-
2293 der elevated CO₂, resulted in a stronger downregulation of N_{area} under elevated
2294 CO₂ with increasing fertilization and in inoculated pots (Fig. 5.1a). These pat-
2295 terns suggest that N_{area} responses to CO₂ were at least partially dependent on
2296 soil nitrogen fertilization and nitrogen acquisition strategy. However, the general
2297 stimulation in the fraction of leaf nitrogen allocated to Rubisco, bioenergetics,
2298 or photosynthesis under elevated CO₂ was not modified across the fertilization
2299 gradient and was only marginally enhanced in inoculated pots. These patterns
2300 suggest that the increased downregulation of Narea under elevated CO₂ with in-
2301 creasing fertilization was not associated with a change in relative investment to
2302 photosynthetic tissue. Instead, a stronger downregulation in the fraction of leaf
2303 nitrogen allocated to structure under ambient CO₂ resulted in a stronger stim-
2304 ulation in $\rho_{\text{structure}}$ under elevated CO₂ with increasing fertilization (Fig. 5.3b),
2305 indicating that fertilization shifted relative investment in leaf structural tissue un-
2306 der elevated CO₂. These results, combined with a stimulation in PNUE (Fig. SX)
2307 and iWUE (Fig. SX) under elevated CO₂ that was independent of fertilization
2308 or inoculation treatment, provide additional support for the hypothesis that leaf
2309 acclimation photosynthetic responses to CO₂ were independent of fertilization;
2310 though fertilization may contribute to changes in leaf morphology under elevated
2311 CO₂ through shifts in M_{area} (Onoda et al. 2017; Wang et al. 2017; Dong et al.

2312 2022).

2313 The downregulation in N_{area} , V_{cmax25} , and J_{max25} under elevated CO₂ cor-
2314 responded with a respective 62% and 100% stimulation in total leaf area (Fig.
2315 5.4a) and total biomass (Fig. 5.4b). The stimulation in total leaf area and total
2316 biomass under elevated CO₂ also corresponded with generally higher structural
2317 carbon costs to acquire nitrogen (Fig. 5.4c), a pattern driven by a stimulation
2318 in belowground carbon biomass and reduction in whole plant nitrogen biomass.
2319 Alone, this result suggests that elevated CO₂ reduces plant nitrogen uptake effi-
2320 ciency, which does not explain why plants grown under elevated CO₂ generally had
2321 higher biomass and total leaf area. However, a strong negative effect of increasing
2322 fertilization on structural carbon costs to acquire nitrogen, which were generally
2323 similar between CO₂ concentrations, was driven by a stronger increase in whole
2324 plant nitrogen biomass than belowground carbon biomass. Thus, increases in the
2325 positive response of whole plant growth and total leaf area under elevated CO₂
2326 with increasing fertilization were likely driven by an increase in nitrogen uptake
2327 efficiency, allowing plants to satisfy any increase in whole plant nitrogen demand
2328 associated with increased CO₂.

2329 Interestingly, these results indicate that the general stimulation in total
2330 leaf area and whole plant growth under elevated CO₂ was not modified by inoc-
2331 ulation despite an apparent general negative effect of inoculation on N_{cost} . This
2332 response could have been due to strong negative effect of increasing fertilization on
2333 nodulation (Fig. 5.5), which may have caused the strong increase in the positive
2334 effect of elevated CO₂ on whole plant growth with increasing fertilization to mask
2335 any increase in the positive effect of elevated CO₂ on whole plant growth due to

2336 inoculation. Reductions in nodulation with increasing fertilization are commonly
2337 observed patterns that have been inferred to be a response that allows species
2338 optimize nitrogen uptake efficiency as costs to acquire nitrogen via direct uptake
2339 become more similar (Fig. 5.4c) (Gibson and Harper 1985; Rastetter et al. 2001).
2340 In this study, pairwise comparisons indicated strong positive effects of inocula-
2341 tion on total leaf area and total biomass (158% increase in total leaf area, 119%
2342 increase in total biomass) under elevated CO₂ at 0 ppm N, but no observable
2343 inoculation effect on total leaf area or total biomass under elevated CO₂ at 350
2344 ppm N or 630 ppm N. While these responses did not generally differ from those
2345 observed under ambient CO₂, they do confirm the hypothesis that positive effects
2346 of inoculation on whole plant growth responses to elevated CO₂ would decrease
2347 with increasing fertilization.

2348 Combined, results reported here suggest that soil nitrogen availability has
2349 a divergent role in modifying leaf and whole plant acclimation responses to CO₂.
2350 Leaf acclimation responses were generally decoupled from fertilization, while whole
2351 plant acclimation responses relied heavily on an increase in nitrogen uptake ef-
2352 ficiency and consequent reduction in costs of acquiring nitrogen associated with
2353 increasing fertilization. However, whole plant responses to CO₂ indicated that
2354 fertilization may play a more important role in determining whole plant acclima-
2355 tion responses to CO₂ than nitrogen acquisition strategy, although these patterns
2356 were likely driven by reductions in nodulation with increasing fertilization. These
2357 results suggest that plants acclimate to CO₂ in nitrogen-limited systems by mini-
2358 mizing the number of optimally coordinated leaves, and that the downregulation
2359 in leaf nitrogen content under elevated CO₂ is not a direct response to changes in

2360 soil nitrogen availability as previously implied.

2361 5.4.2 *Implications for future model development*

2362 Many terrestrial biosphere models predict photosynthetic capacity through
2363 plant functional group-specific linear regressions between N_{area} and V_{cmax} (Rogers
2364 2014; Rogers et al. 2017), which assumes that leaf nitrogen-photosynthesis rela-
2365 tionships are constant across growing environments. Our results build on previ-
2366 ous work suggesting that leaf nitrogen-photosynthesis relationships dynamically
2367 change across growing environments (Luo et al. 2021; Dong et al. 2022). Specif-
2368 ically, results from this experiment indicate that CO_2 concentration increased
2369 the fraction of leaf nitrogen content allocated to photosynthesis, while a general
2370 negative effect of increasing fertilization on the fraction of leaf nitrogen content
2371 allocated to photosynthesis was dependent on inoculation treatment. Similar in-
2372 creases in N_{area} , $V_{\text{cmax}25}$, and $J_{\text{max}25}$ with increasing fertilization resulted in no
2373 change in the fraction of leaf nitrogen allocated to photosynthesis in uninoculated
2374 pots, while larger increases in N_{area} than $V_{\text{cmax}25}$ and $J_{\text{max}25}$ with increasing fertil-
2375 ization decreased the fraction of leaf nitrogen allocated to photosynthesis in inoc-
2376 ulated pots (Fig. 5.3a). As inoculated pots were able to access less finite supply of
2377 nitrogen across the fertilization gradient, these patterns suggest that constant leaf
2378 nitrogen-photosynthesis relationships may only apply in environments where ni-
2379 trogen is limiting and will likely change with increasing CO_2 concentrations. Thus,
2380 terrestrial biosphere models that parameterize photosynthetic capacity through
2381 linear relationships between N_{area} and V_{cmax} (Rogers 2014; Rogers et al. 2017)
2382 may be overestimating photosynthetic capacity in systems where nitrogen is not

2383 as limiting and may contribute to erroneous model simulations under future CO₂
2384 concentrations.

2385 These results also demonstrate that optimal resource investment to photo-
2386 synthetic capacity defines leaf acclimation responses to elevated CO₂, and that
2387 these responses were independent of fertilization or inoculation treatment. Cur-
2388 rent approaches for simulating photosynthetic responses to CO₂ generally invoke
2389 patterns expected from progressive nitrogen limitation, where the downregulation
2390 in N_{area} , and therefore photosynthetic capacity, due to elevated CO₂ are com-
2391 monly a function of progressive reductions in soil nitrogen availability. Results
2392 reported here contradict this formulation, suggesting that the leaf acclimation re-
2393 sponse is driven by optimal resource investment to photosynthetic capacity and
2394 is independent of soil resource supply. Optimality models that leverage prin-
2395 ciples from optimal coordination and photosynthetic least-cost theories (Wang
2396 et al. 2017; Stocker et al. 2020; Scott and Smith 2022) are capable of capturing
2397 such acclimation responses to CO₂ (Smith and Keenan 2020), suggesting that the
2398 implementation of these models may improve the simulation of photosynthetic
2399 processes in terrestrial biosphere models under increasing CO₂ concentrations.

2400 5.4.3 *Study limitations and future directions*

2401 There are two study limitations that must be addressed to contextualize
2402 patterns observed in this study. First, restricting the volume of belowground
2403 substrate via a potted experiment does not adequately replicate belowground en-
2404 vironments of natural systems, and therefore may modify effects of soil resource
2405 availability and inoculation on plant nitrogen uptake, particularly if pot size limits

2406 whole plant growth (Poorter et al. 2012). I attempted to minimize the extent of
2407 pot size limitation experienced in the first experimental chapters while account-
2408 ing for the expected stimulation in whole plant growth under elevated CO₂ by
2409 using 6-liter pots. Despite attempts to minimize growth limitation imposed by
2410 pot volume, fertilization and CO₂ treatments increased the biomass: pot volume
2411 ratio such that all treatment combinations to exceed 1 g L⁻¹ biomass: pot volume
2412 under high fertilization. The 1 g L⁻¹ biomass: pot volume recommendation from
2413 Poorter et al. (2012) was designated to avoid growth limitation imposed by pot
2414 volume. However, if pot size limitation indeed limited whole plant growth, then
2415 structural carbon costs to acquire nitrogen, belowground carbon biomass, whole
2416 plant nitrogen biomass, and whole plant biomass should each exhibit strong sat-
2417 uration points with increasing fertilization, which was not observed here. Addi-
2418 tionally, a second set of photosynthetic measurements from one week prior to the
2419 harvest (6 weeks post-germination) revealed ... As pot limitation is expected
2420 to decrease net photosynthesis, and focal leaves were of similar ages between the
2421 sixth and seventh week, one might expect growth limitation induced by constricted
2422 pot volume to result in a dampened effect of inoculation and fertilization on net
2423 photosynthesis, V_{cmax} , and J_{max25} . Analyses from the sixth week of development
2424 revealed ... Additionally, analyses revealed a stronger/weaker downregulation in
2425 V_{cmax25} and J_{max25} on week 7, though disentangling the causality of this response
2426 (i.e. whether due to pot size limitation or simply a stronger acclimation response)
2427 would be difficult.

2428 Second, this study evaluated leaf and whole plant responses to CO₂ in 7-
2429 week seedlings. Given the long-term scale of the progressive nitrogen limitation

2430 hypothesis, patterns observed here should be validated in longer-term nitrogen
2431 manipulation experiments. Previous work in free air CO₂ enrichment experiments
2432 show some support for patterns expected from the progressive nitrogen limitation
2433 hypothesis (Reich et al. 2006; Norby et al. 2010), although results are not consis-
2434 tent across experimental sites (Finzi et al. 2006; Moore et al. 2006; Liang et al.
2435 2016). We found some support for patterns expected by the progressive nitrogen
2436 limitation hypothesis, namely an increase in plant nitrogen uptake under elevated
2437 CO₂ (Luo et al. 2004), though leaf acclimation responses to CO₂ were strongly
2438 indicative of optimal resource investment to photosynthetic capacity as expected
2439 from photosynthetic least-cost theory (Prentice et al. 2014; Smith et al. 2019;
2440 Smith and Keenan 2020).

2441 5.4.4 *Conclusions*

2442 This study provides strong evidence suggesting that leaf acclimation re-
2443 sponds to elevated CO₂ did not vary with soil nitrogen fertilization or ability
2444 to acquire nitrogen through symbiotic nitrogen fixation. However, whole plant
2445 acclimation responses to CO₂ were dependent on fertilization, where increasing
2446 fertilization increased the positive effect of whole plant growth under elevated
2447 CO₂. Results also indicate that fertilization played a relatively more important
2448 role in modifying whole plant responses to CO₂, perhaps due to a reduction in
2449 nodulation across the fertilization gradient. These patterns strongly support the
2450 hypothesis that leaf and whole plant acclimation responses are driven by opti-
2451 mal resource investment to photosynthetic capacity, and that leaf acclimation
2452 responses to CO₂ were not modified by changes in soil nitrogen availability. Ad-

2453 ditionally, strong interactions between fertilization and inoculation on leaf and
2454 whole plant traits indicated positive effects of fertilization on leaf and whole plant
2455 traits in uninoculated pots, but null effects of fertilization on leaf and whole plant
2456 traits in inoculated pots. These results build on previous work suggesting that
2457 constant leaf nitrogen-photosynthesis relationships are dynamic and change across
2458 growing environments, calling the use of constant relationships by terrestrial bio-
2459 sphere models into question.

2460

Chapter 6

2461

Conclusions

2462 Experiments included in this dissertation leverage patterns expected from
2463 photosynthetic least-cost theory to investigate effects of soil resource availability
2464 and aboveground climate on costs of nitrogen acquisition, leaf nitrogen-water use
2465 tradeoffs, and plant acclimation responses to elevated CO₂. Photosynthetic least-
2466 cost theory provides a contemporary framework for understanding impacts of
2467 climatic and edaphic characteristics on plant ecophysiological processes, namely
2468 leaf nitrogen allocation and photosynthetic capacity. When I began planning
2469 experiments for this dissertation in August 2018,, empirical tests of the theory
2470 were sparse and model development was just beginning with a goal of eventually
2471 implementing the theory in terrestrial biosphere models. At the time, it was
2472 critical that experimentation be done to test underlying assumptions of the theory
2473 and validate its suitability for implementing in terrestrial biosphere models.

2474 Early iterations of model development held the unit cost of acquiring ni-
2475 trogen relative to water constant (Wang et al. 2017), in part because limited data
2476 existed to evaluate how this parameter changes across spatiotemporal scales and
2477 different environmental gradients. However, the Fixation and Uptake of Nitrogen
2478 model (Fisher et al. 2010; Brzostek et al. 2014) indicates that costs of nitro-
2479 gen acquisition decreased with increasing soil nitrogen availability and varies in
2480 species with different nitrogen acquisition strategies, suggesting that the unit cost
2481 of acquiring nitrogen relative to water should change across nitrogen availability
2482 gradients. Additionally,

2483 All experimental chapters in this dissertation provide strong and consist-
2484 tent support for patterns expected from the theory across different experimental
2485 approaches, spatiotemporal scales, and different plant functional groups. In this
2486 chapter, I first summarize experimental approaches and primary findings of each
2487 experimental chapter. Then, I use findings from the four experimental chapters
2488 to synthesize recommendations for future photosynthetic least-cost theory model
2489 development, and propose experiments that will allow for further understanding
2490 of mechanisms that drive patterns expected from photosynthetic least-cost theory
2491 across environmental gradients.

2492

References

- 2493** Abrams, M. D. and S. A. Mostoller (1995). Gas exchange, leaf structure and
2494 nitrogen in contrasting successional tree species growing in open and under-
2495 story sites during a drought. *Tree Physiology* 15(6), 361–370.
- 2496** Adams, M. A., T. L. Turnbull, J. I. Sprent, and N. Buchmann (2016). Legumes
2497 are different: Leaf nitrogen, photosynthesis, and water use efficiency. *Pro-
2498 ceedings of the National Academy of Sciences of the United States of Amer-
2499 ica* 113(15), 4098–4103.
- 2500** Ainsworth, E. A., P. A. Davey, C. J. Bernacchi, O. C. Dermody, E. A. Heaton,
2501 D. J. Moore, P. B. Morgan, S. L. Naidu, H. S. Y. Ra, X. G. Zhu, P. S. Curtis,
2502 and S. P. Long (2002). A meta-analysis of elevated [CO₂] effects on soybean
2503 (*Glycine max*) physiology, growth and yield. *Global Change Biology* 8(8),
2504 695–709.
- 2505** Ainsworth, E. A. and S. P. Long (2005). What have we learned from 15 years of
2506 free-air CO₂ enrichment (FACE)? A meta-analytic review of the responses
2507 of photosynthesis, canopy properties and plant production to rising CO₂.
2508 *New Phytologist* 165(2), 351–372.
- 2509** Ainsworth, E. A. and A. Rogers (2007). The response of photosynthesis and
2510 stomatal conductance to rising [CO₂]: mechanisms and environmental in-
2511 teractions. *Plant, Cell and Environment* 30(3), 258–270.
- 2512** Allen, K., J. B. Fisher, R. P. Phillips, J. S. Powers, and E. R. Brzostek (2020).
2513 Modeling the carbon cost of plant nitrogen and phosphorus uptake across
2514 temperate and tropical forests. *Frontiers in Forests and Global Change* 3,

- 2515 1–12.
- 2516 Allison, S. D., C. I. Czimczik, and K. K. Treseder (2008). Microbial activity
2517 and soil respiration under nitrogen addition in Alaskan boreal forest. *Global
2518 Change Biology* 14(5), 1156–1168.
- 2519 Andersen, M. K., H. Hauggaard-Nielsen, P. Ambus, and E. S. Jensen (2005).
2520 Biomass production, symbiotic nitrogen fixation and inorganic N use in dual
2521 and tri-component annual intercrops. *Plant and Soil* 266(1-2), 273–287.
- 2522 Andrews, M., E. K. James, J. I. Sprent, R. M. Boddey, E. Gross, and F. B. dos
2523 Reis (2011). Nitrogen fixation in legumes and actinorhizal plants in natural
2524 ecosystems: Values obtained using ^{15}N natural abundance. *Plant Ecology
2525 and Diversity* 4(2-3), 117–130.
- 2526 Arndal, M. F., A. Tolver, K. S. Larsen, C. Beier, and I. K. Schmidt (2018). Fine
2527 root growth and vertical distribution in response to elevated CO₂, warming
2528 and drought in a mixed heathland–grassland. *Ecosystems* 21(1), 15–30.
- 2529 Arnone, J. A. (1997). Indices of plant N availability in an alpine grassland under
2530 elevated atmospheric CO₂. *Plant and Soil* 190(1), 61–66.
- 2531 Arora, V. K., A. Katavouta, R. G. Williams, C. D. Jones, V. Brovkin,
2532 P. Friedlingstein, J. Schwinger, L. Bopp, O. Boucher, P. Cadule, M. A.
2533 Chamberlain, J. R. Christian, C. Delire, R. A. Fisher, T. Hajima, T. Ilyina,
2534 E. Joetzjer, M. Kawamiya, C. D. Koven, J. P. Krasting, R. M. Law, D. M.
2535 Lawrence, A. Lenton, K. Lindsay, J. Pongratz, T. Raddatz, R. Séférian,
2536 K. Tachiiri, J. F. Tjiputra, A. Wiltshire, T. Wu, and T. Ziehn (2020).
2537 Carbon-concentration and carbon-climate feedbacks in CMIP6 models and
2538 their comparison to CMIP5 models. *Biogeosciences* 17(16), 4173–4222.

- 2539 Bae, K., T. J. Fahey, R. D. Yanai, and M. Fisk (2015). Soil nitrogen availabil-
2540 ity affects belowground carbon allocation and soil respiration in northern
2541 hardwood forests of New Hampshire. *Ecosystems* 18(7), 1179–1191.
- 2542 Barber, S. A. (1962). A diffusion and mass-flow concept of soil nutrient avail-
2543 ability. *Soil Science* 93(1), 39–49.
- 2544 Barnes, J. D., L. Balaguer, E. Manrique, S. Elvira, and A. W. Davison (1992).
2545 A reappraisal of the use of DMSO for the extraction and determination
2546 of chlorophylls a and b in lichens and higher plants. *Environmental and*
2547 *Experimental Botany* 32(2), 85–100.
- 2548 Bates, D., M. Mächler, B. Bolker, and S. Walker (2015). Fitting linear mixed-
2549 effects models using lme4. *Journal of Statistical Software* 67(1), 1–48.
- 2550 Beaudette, D., J. Skovlin, S. Roeker, and A. Brown (2022). soilDB: Soil
2551 Database Interface.
- 2552 Bengtson, P., J. Barker, and S. J. Grayston (2012). Evidence of a strong cou-
2553 pling between root exudation, C and N availability, and stimulated SOM
2554 decomposition caused by rhizosphere priming effects. *Ecology and Evolu-*
2555 *tion* 93(8), 1843–1852.
- 2556 Bernacchi, C. J., E. L. Singsaas, C. Pimentel, A. R. Portis, and S. P. Long
2557 (2001). Improved temperature response functions for models of Rubisco-
2558 limited photosynthesis. *Plant, Cell and Environment* 24(2), 253–259.
- 2559 Bialic-Murphy, L., N. G. Smith, P. Voothuluru, R. M. McElderry, M. D.
2560 Roche, S. T. Cassidy, S. N. Kivlin, and S. Kalisz (2021). Invasion-induced
2561 root–fungal disruptions alter plant water and nitrogen economies. *Ecology*

- 2562** *Letters* 24(6), 1145–1156.
- 2563** Bloom, A. J., F. S. Chapin, and H. A. Mooney (1985). Resource limitation
2564 in plants - an economic analogy. *Annual Review of Ecology and Systemat-*
2565 *ics* 16(1), 363–392.
- 2566** Bloomfield, K. J., B. D. Stocker, T. F. Keenan, and I. C. Prentice (2023).
2567 Environmental controls on the light use efficiency of terrestrial gross primary
2568 production. *Global Change Biology* 29(4), 0–2.
- 2569** Bonan, G. B., M. D. Hartman, W. J. Parton, and W. R. Wieder (2013). Eval-
2570 uating litter decomposition in earth system models with long-term litter
2571 bag experiments: an example using the Community Land Model version 4
2572 (CLM4). *Global Change Biology* 19(3), 957–974.
- 2573** Bonan, G. B., P. J. Lawrence, K. W. Oleson, S. Levis, M. Jung, M. Reich-
2574 stein, D. M. Lawrence, and S. C. Swenson (2011). Improving canopy pro-
2575 cesses in the Community Land Model version 4 (CLM4) using global flux
2576 fields empirically inferred from FLUXNET data. *Journal of Geophysical Re-*
2577 *search* 116(G2), G02014.
- 2578** Booth, B. B. B., C. D. Jones, M. Collins, I. J. Totterdell, P. M. Cox, S. Sitch,
2579 C. Huntingford, R. A. Betts, G. R. Harris, and J. Lloyd (2012). High sen-
2580 sitivity of future global warming to land carbon cycle processes. *Environ-*
2581 *mental Research Letters* 7(2), 024002.
- 2582** Borer, E. T., W. S. Harpole, P. B. Adler, E. M. Lind, J. L. Orrock, E. W.
2583 Seabloom, and M. D. Smith (2014). Finding generality in ecology: A model
2584 for globally distributed experiments. *Methods in Ecology and Evolution* 5(1),
2585 65–73.

- 2586 Braghieri, R. K., J. B. Fisher, K. Allen, E. Brzostek, M. Shi, X. Yang, D. M.
2587 Ricciuto, R. A. Fisher, Q. Zhu, and R. P. Phillips (2022). Modeling global
2588 carbon costs of plant nitrogen and phosphorus acquisition. *Journal of Ad-*
2589 *vances in Modeling Earth Systems* 14(8), 1–23.
- 2590 Brix, H. (1971). Effects of nitrogen fertilization on photosynthesis and respi-
2591 ration in Douglas-fir. *Forest Science* 17(4), 407–414.
- 2592 Brzostek, E. R., J. B. Fisher, and R. P. Phillips (2014). Modeling the carbon
2593 cost of plant nitrogen acquisition: Mycorrhizal trade-offs and multipath
2594 resistance uptake improve predictions of retranslocation. *Journal of Geo-*
2595 *physical Research: Biogeosciences* 119, 1684–1697.
- 2596 Bubier, J. L., R. Smith, S. Juutinen, T. R. Moore, R. Minocha, S. Long, and
2597 S. Minocha (2011). Effects of nutrient addition on leaf chemistry, morphol-
2598 ogy, and photosynthetic capacity of three bog shrubs. *Oecologia* 167(2),
2599 355–368.
- 2600 Cernusak, L. A., N. Ubierna, K. Winter, J. A. M. Holtum, J. D. Marshall, and
2601 G. D. Farquhar (2013). Environmental and physiological determinants of
2602 carbon isotope discrimination in terrestrial plants. *New Phytologist* 200(4),
2603 950–965.
- 2604 Chen, J.-L., J. F. Reynolds, P. C. Harley, and J. D. Tenhunen (1993). Coor-
2605 dination theory of leaf nitrogen distribution in a canopy. *Oecologia* 93(1),
2606 63–69.
- 2607 Clark, D. B., L. M. Mercado, S. Sitch, C. D. Jones, N. Gedney, M. J. Best,
2608 M. Pryor, G. G. Rooney, R. L. H. Essery, E. Blyth, O. Boucher, R. J.
2609 Harding, C. Huntingford, and P. M. Cox (2011). The Joint UK Land Envi-

- 2610 ronment Simulator (JULES), model description. Part 2: Carbon fluxes and
2611 vegetation dynamics. *Geoscientific Model Development* 4(3), 701–722.
- 2612 Cornwell, W. K., J. H. C. Cornelissen, K. Amatangelo, E. Dorrepaal, V. T.
2613 Eviner, O. Godoy, S. E. Hobbie, B. Hoorens, H. Kurokawa, N. Pérez-
2614 Harguindeguy, H. M. Quested, L. S. Santiago, D. A. Wardle, I. J. Wright,
2615 R. Aerts, S. D. Allison, P. van Bodegom, V. Brovkin, A. Chatain, T. V.
2616 Callaghan, S. Díaz, E. Garnier, D. E. Gurvich, E. Kazakou, J. A. Klein,
2617 J. Read, P. B. Reich, N. A. Soudzilovskaia, M. V. Vaieretti, and M. Westoby
2618 (2008). Plant species traits are the predominant control on litter decompo-
2619 sition rates within biomes worldwide. *Ecology Letters* 11(10), 1065–1071.
- 2620 Cornwell, W. K., I. J. Wright, J. Turner, V. Maire, M. M. Barbour, L. A.
2621 Cernusak, T. E. Dawson, D. S. Ellsworth, G. D. Farquhar, H. Griffiths,
2622 C. Keitel, A. Knohl, P. B. Reich, D. G. Williams, R. Bhaskar, J. H. C. Cor-
2623 nelissen, A. Richards, S. Schmidt, F. Valladares, C. Körner, E.-D. Schulze,
2624 N. Buchmann, and L. S. Santiago (2018). Climate and soils together regulate
2625 photosynthetic carbon isotope discrimination within C₃ plants worldwide.
2626 *Global Ecology and Biogeography* 27(9), 1056–1067.
- 2627 Cramer, W. and I. C. Prentice (1988). Simulation of regional soil moisture
2628 deficits on a European scale. *Norsk Geografisk Tidsskrift - Norwegian Jour-*
2629 *nal of Geography* 42(2-3), 149–151.
- 2630 Curtis, P. S. (1996). A meta-analysis of leaf gas exchange and nitrogen in trees
2631 grown under elevated carbon dioxide. *Plant, Cell and Environment* 19(2),
2632 127–137.
- 2633 Daly, C., M. Halbleib, J. I. Smith, W. P. Gibson, M. K. Doggett, G. H. Taylor,

- 2634** J. Curtis, and P. P. Pasteris (2008). Physiographically sensitive mapping
2635 of climatological temperature and precipitation across the conterminous
2636 United States. *International Journal of Climatology* 28(15), 2031–2064.
- 2637** Davies-Barnard, T., J. Meyerholt, S. Zaehle, P. Friedlingstein, V. Brovkin,
2638 Y. Fan, R. A. Fisher, C. D. Jones, H. Lee, D. Peano, B. Smith, D. Wårlind,
2639 and A. J. Wiltshire (2020). Nitrogen cycling in CMIP6 land surface models:
2640 progress and limitations. *Biogeosciences* 17(20), 5129–5148.
- 2641** Davis, T. W., I. C. Prentice, B. D. Stocker, R. T. Thomas, R. J. Whitley,
2642 H. Wang, B. J. Evans, A. V. Gallego-Sala, M. T. Sykes, and W. Cramer
2643 (2017). Simple process-led algorithms for simulating habitats (SPLASH
2644 v.1.0): robust indices of radiation, evapotranspiration and plant-available
2645 moisture. *Geoscientific Model Development* 10, 689–708.
- 2646** Delaire, M., E. Frak, M. Sigogne, B. Adam, F. Beaujard, and X. Le Roux
2647 (2005). Sudden increase in atmospheric CO₂ concentration reveals strong
2648 coupling between shoot carbon uptake and root nutrient uptake in young
2649 walnut trees. *Tree Physiology* 25(2), 229–235.
- 2650** Doane, T. A. and W. R. Horwáth (2003). Spectrophotometric determination of
2651 nitrate with a single reagent. *Analytical Letters* 36(12), 2713–2722.
- 2652** Dong, N., I. C. Prentice, B. J. Evans, S. Caddy-Retalic, A. J. Lowe, and I. J.
2653 Wright (2017). Leaf nitrogen from first principles: field evidence for adaptive
2654 variation with climate. *Biogeosciences* 14(2), 481–495.
- 2655** Dong, N., I. C. Prentice, I. J. Wright, B. J. Evans, H. F. Togashi, S. Caddy-
2656 Retalic, F. A. McInerney, B. Sparrow, E. Leitch, and A. J. Lowe (2020).
2657 Components of leaf-trait variation along environmental gradients. *New Phy-*

- 2658** *tologist* 228(1), 82–94.
- 2659** Dong, N., I. C. Prentice, I. J. Wright, H. Wang, O. K. Atkin, K. J. Bloomfield,
- 2660** T. F. Domingues, S. M. Gleason, V. Maire, Y. Onoda, H. Poorter, and N. G.
- 2661** Smith (2022). Leaf nitrogen from the perspective of optimal plant function.
- 2662** *Journal of Ecology* 110(11), 2585–2602.
- 2663** Dong, N., I. J. Wright, J. M. Chen, X. Luo, H. Wang, T. F. Keenan, N. G.
- 2664** Smith, and I. C. Prentice (2022). Rising CO₂ and warming reduce global
- 2665** canopy demand for nitrogen. *New Phytologist* 235(5), 1692–1700.
- 2666** Dovrat, G., H. Bakhshian, T. Masci, and E. Sheffer (2020). The nitrogen eco-
- 2667** nomic spectrum of legume stoichiometry and fixation strategy. *New Phytol-*
- 2668** *ogist* 227(2), 365–375.
- 2669** Dovrat, G., T. Masci, H. Bakhshian, E. Mayzlish Gati, S. Golan, and E. Shef-
- 2670** fer (2018). Drought-adapted plants dramatically downregulate dinitrogen
- 2671** fixation: Evidences from Mediterranean legume shrubs. *Journal of Ecol-*
- 2672** *ogy* 106(4), 1534–1544.
- 2673** Drake, B. G., M. A. Gonzàlez-Meler, and S. P. Long (1997). More efficient
- 2674** plants: a consequence of rising atmospheric CO₂? *Annual Review of Plant*
- 2675** *Biology* 48, 609–639.
- 2676** Duursma, R. A. (2015). Plantecophys - An R Package for Analyzing and Mod-
- 2677** elling Leaf Gas Exchange Data. *PLOS ONE* 10(11), e0143346.
- 2678** Eastman, B. A., M. B. Adams, E. R. Brzostek, M. B. Burnham, J. E. Carrara,
- 2679** C. Kelly, B. E. McNeil, C. A. Walter, and W. T. Peterjohn (2021). Altered
- 2680** plant carbon partitioning enhanced forest ecosystem carbon storage after 25

- 2681 years of nitrogen additions. *New Phytologist* 230(4), 1435–1448.
- 2682 Ellsworth, D. S. and P. B. Reich (1996). Photosynthesis and leaf nitrogen in five
2683 Amazonian tree species during early secondary succession. *Ecology* 77(2),
2684 581–594.
- 2685 Espelta, J. M., P. Cortés, M. Mangirón, and J. Retana (2005). Differences in
2686 biomass partitioning, leaf nitrogen content, and water use efficiency d13C
2687 result in similar performance of seedlings of two Mediterranean oaks with
2688 contrasting leaf habit. *Ecoscience* 12(4), 447–454.
- 2689 Evans, J. R. (1989). Photosynthesis and nitrogen relationships in leaves of C₃
2690 plants. *Oecologia* 78(1), 9–19.
- 2691 Evans, J. R. and V. C. Clarke (2019). The nitrogen cost of photosynthesis.
2692 *Journal of Experimental Botany* 70(1), 7–15.
- 2693 Evans, J. R. and H. Poorter (2001). Photosynthetic acclimation of plants to
2694 growth irradiance: the relative importance of specific leaf area and nitrogen
2695 partitioning in maximizing carbon gain. *Plant, Cell and Environment* 24(8),
2696 755–767.
- 2697 Evans, J. R. and J. R. Seemann (1989). The allocation of protein nitrogen in
2698 the photosynthetic apparatus: costs, consequences, and control. *Photosyn-*
2699 *thesis* 8, 183–205.
- 2700 Exbrayat, J.-F., A. A. Bloom, P. Falloon, A. Ito, T. L. Smallman, and
2701 M. Williams (2018). Reliability ensemble averaging of 21st century projec-
2702 tions of terrestrial net primary productivity reduces global and regional
2703 uncertainties. *Earth System Dynamics* 9(1), 153–165.

- 2704** Farquhar, G. D., J. R. Ehleringer, and K. T. Hubick (1989). Carbon Isotope
2705 Discrimination and Photosynthesis. *Annual Review of Plant Physiology and*
2706 *Plant Molecular Biology* 40(1), 503–537.
- 2707** Farquhar, G. D. and T. D. Sharkey (1982). Stomatal conductance and photo-
2708 synthesis. *Annual Review of Plant Physiology* 33(1), 317–345.
- 2709** Farquhar, G. D., S. von Caemmerer, and J. A. Berry (1980). A biochemical
2710 model of photosynthetic CO₂ assimilation in leaves of C₃ species.
2711 *Planta* 149(1), 78–90.
- 2712** Fay, P. A., S. M. Prober, W. S. Harpole, J. M. H. Knops, J. D. Bakker, E. T.
2713 Borer, E. M. Lind, A. S. MacDougall, E. W. Seabloom, P. D. Wragg, P. B.
2714 Adler, D. M. Blumenthal, Y. M. Buckley, C. Chu, E. E. Cleland, S. L.
2715 Collins, K. F. Davies, G. Du, X. Feng, J. Firn, D. S. Gruner, N. Hagenah,
2716 Y. Hautier, R. W. Heckman, V. L. Jin, K. P. Kirkman, J. A. Klein, L. M.
2717 Ladwig, Q. Li, R. L. McCulley, B. A. Melbourne, C. E. Mitchell, J. L. Moore,
2718 J. W. Morgan, A. C. Risch, M. Schütz, C. J. Stevens, D. A. Wedin, and
2719 L. H. Yang (2015). Grassland productivity limited by multiple nutrients.
2720 *Nature Plants* 1(7), 15080.
- 2721** Feng, X. (1999). Trends in intrinsic water-use efficiency of natural trees for the
2722 past 100-200 years: A response to atmospheric CO₂ concentration. *Geochim-
ica et Cosmochimica Acta* 63(13-14), 1891–1903.
- 2724** Field, C. B. and H. A. Mooney (1986). The photosynthesis-nitrogen relationship
2725 in wild plants. In T. J. Givnish (Ed.), *On the Economy of Plant Form and
Function*, pp. 25–55. Cambridge: Cambridge University Press.
- 2727** Finzi, A. C., D. J. P. Moore, E. H. DeLucia, J. Lichter, K. S. Hofmockel, R. B.

- 2728 Jackson, H. S. Kim, R. Matamala, H. R. McCarthy, R. Oren, J. S. Pippen,
2729 and W. H. Schlesinger (2006). Progressive nitrogen limitation of ecosystem
2730 processes under elevated CO₂ in a warm-temperate forest. *Ecology* 87(1),
2731 15–25.
- 2732 Firn, J., J. M. McGree, E. Harvey, H. Flores Moreno, M. Schutz, Y. M. Buckley,
2733 E. T. Borer, E. W. Seabloom, K. J. La Pierre, A. M. MacDougall, S. M.
2734 Prober, C. J. Stevens, L. L. Sullivan, E. Porter, E. Ladouceur, C. Allen,
2735 K. H. Moromizato, J. W. Morgan, W. S. Harpole, Y. Hautier, N. Eisen-
2736 hauer, J. P. Wright, P. B. Adler, C. A. Arnillas, J. D. Bakker, L. Biederman,
2737 A. A. D. Broadbent, C. S. Brown, M. N. Bugalho, M. C. Caldeira, E. E. Cle-
2738 land, A. Ebeling, P. A. Fay, N. Hagenah, A. R. Kleinhesselink, R. Mitchell,
2739 J. L. Moore, C. Nogueira, P. L. Peri, C. Roscher, M. D. Smith, P. D. Wragg,
2740 and A. C. Risch (2019). Leaf nutrients, not specific leaf area, are consistent
2741 indicators of elevated nutrient inputs. *Nature Ecology and Evolution* 3(3),
2742 400–406.
- 2743 Fisher, J. B., S. Sitch, Y. Malhi, R. A. Fisher, C. Huntingford, and S.-Y. Tan
2744 (2010). Carbon cost of plant nitrogen acquisition: A mechanistic, globally
2745 applicable model of plant nitrogen uptake, retranslocation, and fixation.
2746 *Global Biogeochemical Cycles* 24(1), 1–17.
- 2747 Fox, J. and S. Weisberg (2019). *An R companion to applied regression* (Third
2748 edit ed.). Thousand Oaks, California: Sage.
- 2749 Franklin, O., R. E. McMurtrie, C. M. Iversen, K. Y. Crous, A. C. Finzi, D. Tis-
2750 sue, D. S. Ellsworth, R. Oren, and R. J. Norby (2009). Forest fine-root
2751 production and nitrogen use under elevated CO₂: contrasting responses

- 2752** in evergreen and deciduous trees explained by a common principle. *Global
2753 Change Biology* 15(1), 132–144.
- 2754** Friedlingstein, P., M. Meinshausen, V. K. Arora, C. D. Jones, A. Anav, S. K.
2755 Liddicoat, and R. Knutti (2014). Uncertainties in CMIP5 climate projections
2756 due to carbon cycle feedbacks. *Journal of Climate* 27(2), 511–526.
- 2757** Friel, C. A. and M. L. Friesen (2019). Legumes modulate allocation to rhizobial
2758 nitrogen fixation in response to factorial light and nitrogen manipulation.
2759 *Frontiers in Plant Science* 10, 1316.
- 2760** Fujikake, H., A. Yamazaki, N. Ohtake, K. Sueoshi, S. Matsuhashi, T. Ito,
2761 C. Mizuniwa, T. Kume, S. Hoshimoto, N.-S. Ishioka, S. Watanabe, A. Osa,
2762 T. Sekine, H. Uchida, A. Tsuji, and T. Ohyama (2003). Quick and reversible
2763 inhibition of soybean root nodule growth by nitrate involves a decrease in
2764 sucrose supply to nodules. *Journal of Experimental Botany* 54(386), 1379–
2765 1388.
- 2766** Ghimire, B., W. J. Riley, C. D. Koven, J. Kattge, A. Rogers, P. B. Reich, and
2767 I. J. Wright (2017). A global trait-based approach to estimate leaf nitro-
2768 gen functional allocation from observations:. *Ecological Applications* 27(5),
2769 1421–1434.
- 2770** Giardina, C. P., M. D. Coleman, J. E. Hancock, J. S. King, E. A. Lilleskov,
2771 W. M. Loya, K. S. Pregitzer, M. G. Ryan, and C. C. Trettin (2005). The
2772 response of belowground carbon allocation in forests to global change. In
2773 D. Binkley and O. Manyailo (Eds.), *Tree Species Effects on Soils: Implica-
2774 tions for Global Change* (Volume 55 ed.), Chapter Chapter 7, pp. 119–154.
2775 Berlin/Heidelberg: Springer-Verlag.

- 2776** Gibson, A. H. and J. E. Harper (1985). Nitrate effect on nodulation of soybean
2777 by *Bradyrhizobium japonicum*. *Crop Science* 25(3), 497–501.
- 2778** Gill, A. L. and A. C. Finzi (2016). Belowground carbon flux links biogeochemical
2779 cycles and resource-use efficiency at the global scale. *Ecology Letters* 19(12),
2780 1419–1428.
- 2781** Goll, D. S., V. Brovkin, B. R. Parida, C. H. Reick, J. Kattge, P. B. Reich, P. M.
2782 van Bodegom, and Ü. Niinemets (2012). Nutrient limitation reduces land
2783 carbon uptake in simulations with a model of combined carbon, nitrogen
2784 and phosphorus cycling. *Biogeosciences Discussions* 9(3), 3173–3232.
- 2785** Gregory, L. M., A. M. McClain, D. M. Kramer, J. D. Pardo, K. E. Smith, O. L.
2786 Tessmer, B. J. Walker, L. G. Ziccardi, and T. D. Sharkey (2021, oct). The
2787 triose phosphate utilization limitation of photosynthetic rate: Out of global
2788 models but important for leaf models. *Plant, Cell and Environment* 44(10),
2789 3223–3226.
- 2790** Grossiord, C., T. N. Buckley, L. A. Cernusak, K. A. Novick, B. Poulter, R. T. W.
2791 Siegwolf, J. S. Sperry, and N. G. McDowell (2020). Plant responses to rising
2792 vapor pressure deficit. *New Phytologist* 226(6), 1550–1566.
- 2793** Guerrieri, R., M. Mencuccini, L. J. Sheppard, M. Saurer, M. P. Perks, P. Levy,
2794 M. A. Sutton, M. Borghetti, and J. Grace (2011). The legacy of enhanced
2795 N and S deposition as revealed by the combined analysis of $\delta^{13}\text{C}$, $\delta^{18}\text{O}$ and
2796 $\delta^{15}\text{N}$ in tree rings. *Global Change Biology* 17(5), 1946–1962.
- 2797** Gulmon, S. L. and C. C. Chu (1981). The effects of light and nitrogen on pho-
2798 tosynthesis, leaf characteristics, and dry matter allocation in the chaparral
2799 shrub, <i>Diplacus aurantiacus</i>. *Oecologia* 49(2), 207–212.

- 2800 Gutschick, V. P. (1981). Evolved strategies in nitrogen acquisition by plants.
- 2801 *The American Naturalist* 118(5), 607–637.
- 2802 Hallik, L., Ü. Niinemets, and I. J. Wright (2009). Are species shade and drought
- 2803 tolerance reflected in leaf-level structural and functional differentiation in
- 2804 Northern Hemisphere temperate woody flora? *New Phytologist* 184(1), 257–
- 2805 274.
- 2806 Harrison, M. T., E. J. Edwards, G. D. Farquhar, A. B. Nicotra, and J. R.
- 2807 Evans (2009). Nitrogen in cell walls of sclerophyllous leaves accounts for
- 2808 little of the variation in photosynthetic nitrogen-use efficiency. *Plant, Cell*
- 2809 and *Environment* 32(3), 259–270.
- 2810 Harrison, S. P., W. Cramer, O. Franklin, I. C. Prentice, H. Wang,
- 2811 Å. Bränström, H. de Boer, U. Dieckmann, J. Joshi, T. F. Keenan,
- 2812 A. Lavergne, S. Manzoni, G. Mengoli, C. Morfopoulos, J. Peñuelas,
- 2813 S. Pietsch, K. T. Rebel, Y. Ryu, N. G. Smith, B. D. Stocker, and I. J.
- 2814 Wright (2021). Eco-evolutionary optimality as a means to improve vegeta-
- 2815 tion and land-surface models. *New Phytologist* 231(6), 2125–2141.
- 2816 Henneron, L., P. Kardol, D. A. Wardle, C. Cros, and S. Fontaine (2020). Rhizo-
- 2817 sphere control of soil nitrogen cycling: a key component of plant economic
- 2818 strategies. *New Phytologist* 228(4), 1269–1282.
- 2819 Hijmans, R. J. (2022). terra: Spatial Data Analysis.
- 2820 Hikosaka, K. and A. Shigeno (2009). The role of Rubisco and cell walls in the
- 2821 interspecific variation in photosynthetic capacity. *Oecologia* 160(3), 443–
- 2822 451.

- 2823 Hoagland, D. R. and D. I. Arnon (1950). The water culture method for growing
2824 plants without soil. *California Agricultural Experiment Station: 347* 347(2),
2825 1–32.
- 2826 Hobbie, E. A. (2006). Carbon allocation to ectomycorrhizal fungi correlates
2827 with belowground allocation in culture studies. *Ecology* 87(3), 563–569.
- 2828 Hobbie, E. A. and J. E. Hobbie (2008). Natural abundance of ^{15}N in nitrogen-
2829 limited forests and tundra can estimate nitrogen cycling through mycorrhizal
2830 fungi: a review. *Ecosystems* 11(5), 815–830.
- 2831 Hoek, T. A., K. Axelrod, T. Biancalani, E. A. Yurtsev, J. Liu, and J. Gore
2832 (2016). Resource availability modulates the cooperative and competitive na-
2833 ture of a microbial cross-feeding mutualism. *PLOS Biology* 14(8), e1002540.
- 2834 Höglberg, M. N., M. J. I. Briones, S. G. Keel, D. B. Metcalfe, C. Campbell, A. J.
2835 Midwood, B. Thornton, V. Hurry, S. Linder, T. Näsholm, and P. Höglberg
2836 (2010). Quantification of effects of season and nitrogen supply on tree below-
2837 ground carbon transfer to ectomycorrhizal fungi and other soil organisms in
2838 a boreal pine forest. *New Phytologist* 187(2), 485–493.
- 2839 Höglberg, P., M. N. Höglberg, S. G. Göttlicher, N. R. Betson, S. G. Keel, D. B.
2840 Metcalfe, C. Campbell, A. Schindlbacher, V. Hurry, T. Lundmark, S. Linder,
2841 and T. Näsholm (2008). High temporal resolution tracing of photosynthate
2842 carbon from the tree canopy to forest soil microorganisms. *New Phytolo-*
2843 *gist* 177(1), 220–228.
- 2844 Houlton, B. Z., Y.-P. Wang, P. M. Vitousek, and C. B. Field (2008). A uni-
2845 fying framework for dinitrogen fixation in the terrestrial biosphere. *Na-*
2846 *ture* 454(7202), 327–330.

- 2847 Huber, M. L., R. A. Perkins, A. Laesecke, D. G. Friend, J. V. Sengers, M. J.
2848 Assael, I. N. Metaxa, E. Vogel, R. Mareš, and K. Miyagawa (2009). New
2849 international formulation for the viscosity of H₂O. *Journal of Physical and*
2850 *Chemical Reference Data* 38(2), 101–125.
- 2851 Hungate, B. A., J. S. Dukes, M. R. Shaw, Y. Luo, and C. B. Field (2003).
2852 Nitrogen and climate change. *Science* 302(5650), 1512–1513.
- 2853 IPCC (2021). *Climate Change 2021: The Physical Science Basis. Contribution*
2854 *of Working Group I to the Sixth Assessment Report of the Intergovernmental*
2855 *Panel on Climate Change*, Volume In Press. Cambridge, United Kingdom
2856 and New York, NY, USA: Cambridge University Press.
- 2857 Johnson, N. C., J. H. Graham, and F. A. Smith (1997). Functioning of mycor-
2858 rhizal associations along the mutualism-parasitism continuum. *New Phytol-*
2859 *ogist* 135(4), 575–585.
- 2860 Kachurina, O. M., H. Zhang, W. R. Raun, and E. G. Krenzer (2000). Simul-
2861 taneous determination of soil aluminum, ammonium- and nitrate- nitrogen
2862 using 1 M potassium chloride. *Communications in Soil Science and Plant*
2863 *Analysis* 31(7-8), 893–903.
- 2864 Kaiser, C., M. R. Kilburn, P. L. Clode, L. Fuchslueger, M. Koranda, J. B. Cliff,
2865 Z. M. Solaiman, and D. V. Murphy (2015). Exploring the transfer of recent
2866 plant photosynthates to soil microbes: mycorrhizal pathway vs direct root
2867 exudation. *New Phytologist* 205(4), 1537–1551.
- 2868 Katabuchi, M. (2015). LeafArea: An R package for rapid digital analysis of leaf
2869 area. *Ecological Research* 30(6), 1073–1077.

- 2870 Kattge, J. and W. Knorr (2007). Temperature acclimation in a biochemical
2871 model of photosynthesis: a reanalysis of data from 36 species. *Plant, Cell*
2872 and *Environment* 30(9), 1176–1190.
- 2873 Kattge, J., W. Knorr, T. Raddatz, and C. Wirth (2009). Quantifying photosyn-
2874 thetic capacity and its relationship to leaf nitrogen content for global-scale
2875 terrestrial biosphere models. *Global Change Biology* 15(4), 976–991.
- 2876 Kayler, Z., A. Gessler, and N. Buchmann (2010). What is the speed of link
2877 between aboveground and belowground processes? *New Phytologist* 187(4),
2878 885–888.
- 2879 Kayler, Z., C. Keitel, K. Jansen, and A. Gessler (2017). Experimental evi-
2880 dence of two mechanisms coupling leaf-level C assimilation to rhizosphere
2881 CO₂ release. *Environmental and Experimental Botany* 135,
2882 21–26.
- 2883 Keeling, C. D., W. G. Mook, and P. P. Tans (1979, jan). Recent trends in the
2884 ¹³C/¹²C ratio of atmospheric carbon dioxide.
2885 *Nature* 277(5692), 121–123.
- 2886 Kenward, M. G. and J. H. Roger (1997). Small sample inference for fixed effects
2887 from restricted maximum likelihood. *Biometrics* 53(3), 983.
- 2888 Knapp, A. K., M. L. Avolio, C. Beier, C. J. W. Carroll, S. L. Collins, J. S.
2889 Dukes, L. H. Fraser, R. J. Griffin-Nolan, D. L. Hoover, A. Jentsch, M. E.
2890 Loik, R. P. Phillips, A. K. Post, O. E. Sala, I. J. Slette, L. Yahdjian, and
2891 M. D. Smith (2017). Pushing precipitation to the extremes in distributed
2892 experiments: recommendations for simulating wet and dry years. *Global*
2893 *Change Biology* 23(5), 1774–1782.

- 2894 Knorr, W. (2000). Annual and interannual CO₂ exchanges of the
2895 terrestrial biosphere: process-based simulations and uncertainties. *Global*
2896 *Ecology and Biogeography* 9(3), 225–252.
- 2897 Knorr, W. and M. Heimann (2001). Uncertainties in global terrestrial biosphere
2898 modeling: 1. A comprehensive sensitivity analysis with a new photosynthesis
2899 and energy balance scheme. *Global Biogeochemical Cycles* 15(1), 207–225.
- 2900 Kulmatiski, A., P. B. Adler, J. M. Stark, and A. T. Tredennick (2017). Water
2901 and nitrogen uptake are better associated with resource availability than
2902 root biomass. *Ecosphere* 8(3), e01738.
- 2903 Lavergne, A., D. Sandoval, V. J. Hare, H. Graven, and I. C. Prentice (2020).
2904 Impacts of soil water stress on the acclimated stomatal limitation of pho-
2905 tosynthesis: Insights from stable carbon isotope data. *Global Change Biol-*
2906 *ogy* 26(12), 7158–7172.
- 2907 Lawrence, D. M., R. A. Fisher, C. D. Koven, K. W. Oleson, S. C. Swen-
2908 son, G. B. Bonan, N. Collier, B. Ghimire, L. Kampenhout, D. Kennedy,
2909 E. Kluzek, P. J. Lawrence, F. Li, H. Li, D. L. Lombardozzi, W. J. Riley,
2910 W. J. Sacks, M. Shi, M. Vertenstein, W. R. Wieder, C. Xu, A. A. Ali,
2911 A. M. Badger, G. Bisht, M. Broeke, M. A. Brunke, S. P. Burns, J. Buzan,
2912 M. Clark, A. Craig, K. M. Dahlin, B. Drewniak, J. B. Fisher, M. Flanner,
2913 A. M. Fox, P. Gentine, F. M. Hoffman, G. Keppel-Aleks, R. Knox, S. Ku-
2914 mar, J. Lenaerts, L. R. Leung, W. H. Lipscomb, Y. Lu, A. Pandey, J. D.
2915 Pelletier, J. Perket, J. T. Randerson, D. M. Ricciuto, B. M. Sanderson,
2916 A. Slater, Z. M. Subin, J. Tang, R. Q. Thomas, M. Val Martin, and X. Zeng
2917 (2019). The Community Land Model Version 5: description of new features,

- 2918 benchmarking, and impact of forcing uncertainty. *Journal of Advances in*
2919 *Modeling Earth Systems* 11(12), 4245–4287.
- 2920 LeBauer, D. S. and K. K. Treseder (2008). Nitrogen limitation of net primary
2921 productivity. *Ecology* 89(2), 371–379.
- 2922 Lefcheck, J. S. (2016). piecewiseSEM: Piecewise structural equation modelling
2923 in r for ecology, evolution, and systematics. *Methods in Ecology and Evolu-*
2924 *tion* 7(5), 573–579.
- 2925 Lenth, R. (2019). emmeans: estimated marginal means, aka least-squares
2926 means.
- 2927 Li, W., H. Zhang, G. Huang, R. Liu, H. Wu, C. Zhao, and N. G. McDowell
2928 (2020). Effects of nitrogen enrichment on tree carbon allocation: A global
2929 synthesis. *Global Ecology and Biogeography* 29(3), 573–589.
- 2930 Liang, J., X. Qi, L. Souza, and Y. Luo (2016). Processes regulating progressive
2931 nitrogen limitation under elevated carbon dioxide: a meta-analysis. *Biogeo-*
2932 *sciences* 13(9), 2689–2699.
- 2933 Liang, X., T. Zhang, X. Lu, D. S. Ellsworth, H. BassiriRad, C. You, D. Wang,
2934 P. He, Q. Deng, H. Liu, J. Mo, and Q. Ye (2020). Global response patterns of
2935 plant photosynthesis to nitrogen addition: A meta-analysis. *Global Change*
2936 *Biology* 26(6), 3585–3600.
- 2937 Lu, J., J. Yang, C. Keitel, L. Yin, P. Wang, W. Cheng, and F. A. Dijkstra
2938 (2022). Belowground Carbon Efficiency for Nitrogen and Phosphorus Ac-
2939 quisition Varies Between *Lolium perenne* and *Trifolium repens* and Depends
2940 on Phosphorus Fertilization. *Frontiers in Plant Science* 13, 1–9.

- 2941** Luo, X., T. F. Keenan, J. M. Chen, H. Croft, I. C. Prentice, N. G. Smith,
2942 A. P. Walker, H. Wang, R. Wang, C. Xu, and Y. Zhang (2021). Global
2943 variation in the fraction of leaf nitrogen allocated to photosynthesis. *Nature
2944 Communications* 12(1), 4866.
- 2945** Luo, Y., W. S. Currie, J. S. Dukes, A. C. Finzi, U. A. Hartwig, B. A. Hungate,
2946 R. E. McMurtrie, R. Oren, W. J. Parton, D. E. Pataki, R. M. Shaw, D. R.
2947 Zak, and C. B. Field (2004). Progressive nitrogen limitation of ecosystem
2948 responses to rising atmospheric carbon dioxide. *BioScience* 54(8), 731–739.
- 2949** Maire, V., P. Martre, J. Kattge, F. Gastal, G. Esser, S. Fontaine, and J.-F.
2950 Soussana (2012). The coordination of leaf photosynthesis links C and N
2951 fluxes in C₃ plant species. *PLoS ONE* 7(6), e38345.
- 2952** Makino, A. (2003). Rubisco and nitrogen relationships in rice: leaf photosyn-
2953 thesis and plant growth. *Soil Science and Plant Nutrition* 49(3), 319–327.
- 2954** Makino, A., M. Harada, T. Sato, H. Nakano, and T. Mae (1997). Growth and N
2955 Allocation in Rice Plants under CO₂ Enrichment. *Plant Physiology* 115(1),
2956 199–203.
- 2957** Markham, J. H. and C. Zekveld (2007). Nitrogen fixation makes biomass al-
2958 location to roots independent of soil nitrogen supply. *Canadian Journal of
2959 Botany* (9), 787–793.
- 2960** Marschner, H. and B. Dell (1994). Nutrient uptake in mycorrhizal symbiosis.
2961 *Plant and Soil* 159(1), 89–102.
- 2962** Matamala, R. and W. H. Schlesinger (2000). Effects of elevated atmospheric
2963 CO₂ on fine root production and activity in an intact tem-

- 2964** perate forest ecosystem. *Global Change Biology* 6(8), 967–979.
- 2965** Medlyn, B. E., E. Dreyer, D. S. Ellsworth, M. Forstreuter, P. C. Harley,
- 2966** M. U. F. Kirschbaum, X. Le Roux, P. Montpied, J. Strassmeyer, A. Wal-
- 2967** croft, K. Wang, and D. Loustau (2002). Temperature response of parameters
- 2968** of a biochemically based model of photosynthesis. II. A review of experimen-
- 2969** tal data. *Plant, Cell and Environment* 25(9), 1167–1179.
- 2970** Menge, D. N. L., S. A. Levin, and L. O. Hedin (2008). Evolutionary tradeoffs can
- 2971** select against nitrogen fixation and thereby maintain nitrogen limitation.
- 2972** *Proceedings of the National Academy of Sciences* 105(5), 1573–1578.
- 2973** Menne, M. J., I. Durre, R. S. Vose, B. E. Gleason, and T. G. Houston (2012).
- 2974** An overview of the global historical climatology network-daily database.
- 2975** *Journal of Atmospheric and Oceanic Technology* 29(7), 897–910.
- 2976** Meyerholt, J., K. Sickel, and S. Zaehle (2020). Ensemble projections elucidate
- 2977** effects of uncertainty in terrestrial nitrogen limitation on future carbon up-
- 2978** take. *Global Change Biology* 26(7), 3978–3996.
- 2979** Meyerholt, J., S. Zaehle, and M. J. Smith (2016). Variability of pro-
- 2980** jected terrestrial biosphere responses to elevated levels of atmospheric
- 2981** CO₂ due to uncertainty in biological nitrogen fixation. *Bio-*
- 2982** *geosciences* 13(5), 1491–1518.
- 2983** Minochka, R., S. Long, A. H. Magill, J. D. Aber, and W. H. McDowell (2000).
- 2984** Foliar free polyamine and inorganic ion content in relation to soil and soil
- 2985** solution chemistry in two fertilized forest stands at the Harvard Forest,
- 2986** Massachusetts. *Plant and Soil* 222(1-2), 119–137.

- 2987** Moore, D. J., S. Aref, R. M. Ho, J. S. Pippen, J. G. Hamilton, and E. H. De
2988 Lucia (2006). Annual basal area increment and growth duration of *Pinus*
2989 *taeda* in response to eight years of free-air carbon dioxide enrichment. *Global*
2990 *Change Biology* 12(8), 1367–1377.
- 2991** Morgan, J. A., D. E. Pataki, C. Körner, H. Clark, S. J. Del Grosso, J. M.
2992 Grünzweig, A. K. Knapp, A. R. Mosier, P. C. D. Newton, P. A. Niklaus,
2993 J. B. Nippert, R. S. Nowak, W. J. Parton, H. W. Polley, and M. R. Shaw
2994 (2004). Water relations in grassland and desert ecosystems exposed to ele-
2995 vated atmospheric CO₂. *Oecologia* 140(1), 11–25.
- 2996** Muñoz, N., X. Qi, M. W. Li, M. Xie, Y. Gao, M. Y. Cheung, F. L. Wong, and
2997 H.-M. Lam (2016). Improvement in nitrogen fixation capacity could be part
2998 of the domestication process in soybean. *Heredity* 117(2), 84–93.
- 2999** Nadelhoffer, K. J. and J. W. Raich (1992). Fine root production estimates and
3000 belowground carbon allocation in forest ecosystems. *Ecology* 73(4), 1139–
3001 1147.
- 3002** Niinemets, Ü. and J. D. Tenhunen (1997). A model separating leaf struc-
3003 tural and physiological effects on carbon gain along light gradients for the
3004 shade-tolerant species <i>Acer saccharum</i>. *Plant, Cell and Environ-*
3005 *ment* 20(7), 845–866.
- 3006** Norby, R. J., J. Ledford, C. D. Reilly, N. E. Miller, and E. G. O'Neill
3007 (2004). Fine-root production dominates response of a deciduous forest to
3008 atmospheric CO₂ enrichment. *Proceedings of the National Academy of Sci-*
3009 *ences* 101(26), 9689–9693.
- 3010** Norby, R. J., J. M. Warren, C. M. Iversen, B. E. Medlyn, and R. E. Mc-

- 3011** Murtrie (2010). CO₂ enhancement of forest productivity constrained by
3012 limited nitrogen availability. *Proceedings of the National Academy of Sci-
ences* 107(45), 19368–19373.
- 3014** Novick, K. A., D. L. Ficklin, P. C. Stoy, C. A. Williams, G. Bohrer, A. C.
3015 Oishi, S. A. Papuga, P. D. Blanken, A. Noormets, B. N. Sulman, R. L.
3016 Scott, L. Wang, and R. P. Phillips (2016). The increasing importance of
3017 atmospheric demand for ecosystem water and carbon fluxes. *Nature Climate
Change* 6(11), 1023–1027.
- 3019** Noyce, G. L., M. L. Kirwan, R. L. Rich, and J. P. Megonigal (2019). Asyn-
3020 chronous nitrogen supply and demand produce nonlinear plant allocation
3021 responses to warming and elevated CO₂. *Proceedings of the
National Academy of Sciences* 116(43), 21623–21628.
- 3023** Onoda, Y., K. Hikosaka, and T. Hirose (2004). Allocation of nitrogen to
3024 cell walls decreases photosynthetic nitrogen-use efficiency. *Functional Ecol-
ogy* 18(3), 419–425.
- 3026** Onoda, Y., I. J. Wright, J. R. Evans, K. Hikosaka, K. Kitajima, Ü. Niinemets,
3027 H. Poorter, T. Tosens, and M. Westoby (2017). Physiological and structural
3028 trade-offs underlying the leaf economics spectrum. *New Phytologist* 214(4),
3029 1447–1463.
- 3030** Oreskes, N., K. Shrader-Frechette, and K. Belitz (1994). Verification, vali-
3031 dation, and confirmation of numerical models in the Earth sciences. *Sci-
ence* 263(5147), 641–646.
- 3033** Paillassa, J., I. J. Wright, I. C. Prentice, S. Pepin, N. G. Smith, G. Ethier,
3034 A. C. Westerband, L. J. Lamarque, H. Wang, W. K. Cornwell, and V. Maire

- 3035 (2020). When and where soil is important to modify the carbon and water
3036 economy of leaves. *New Phytologist* 228(1), 121–135.
- 3037 Parvin, S., S. Uddin, S. Tausz Posch, R. Armstrong, and M. Tausz (2020). Car-
3038 bon sink strength of nodules but not other organs modulates photosynthesis
3039 of faba bean (*i>Vicia faba</i>)) grown under elevated [CO₂] and different
3040 water supply. *New Phytologist* 227(1), 132–145.*
- 3041 Peng, Y., K. J. Bloomfield, L. A. Cernusak, T. F. Domingues, and I. C. Pren-
3042 tice (2021). Global climate and nutrient controls of photosynthetic capacity.
3043 *Communications Biology* 4(1), 462.
- 3044 Perkowski, E. A., E. F. Waring, and N. G. Smith (2021). Root mass carbon
3045 costs to acquire nitrogen are determined by nitrogen and light availabil-
3046 ity in two species with different nitrogen acquisition strategies. *Journal of*
3047 *Experimental Botany* 72(15), 5766–5776.
- 3048 Phillips, R. P., E. R. Brzostek, and M. G. Midgley (2013). The mycorrhizal-
3049 associated nutrient economy: a new framework for predicting carbon-
3050 nutrient couplings in temperate forests. *New Phytologist* 199(1), 41–51.
- 3051 Phillips, R. P., A. C. Finzi, and E. S. Bernhardt (2011). Enhanced root ex-
3052 udation induces microbial feedbacks to N cycling in a pine forest under
3053 long-term CO₂ fumigation. *Ecology Letters* 14(2), 187–194.
- 3054 Pinheiro, J. and D. Bates (2022). nlme: linear and nonlinear mixed effects
3055 models.
- 3056 Poggio, L., L. M. De Sousa, N. H. Batjes, G. B. M. Heuvelink, B. Kempen,
3057 E. Ribeiro, and D. Rossiter (2021). SoilGrids 2.0: Producing soil information

- 3058 for the globe with quantified spatial uncertainty. *Soil* 7(1), 217–240.
- 3059 Pons, T. L. and R. W. Pearcy (1994). Nitrogen reallocation and photosynthetic
3060 acclimation in response to partial shading in soybean plants. *Physiologia
3061 Plantarum* 92(4), 636–644.
- 3062 Poorter, H., J. Bühler, D. Van Dusschoten, J. Climent, and J. A. Postma (2012).
3063 Pot size matters: A meta-analysis of the effects of rooting volume on plant
3064 growth. *Functional Plant Biology* 39(11), 839–850.
- 3065 Poorter, H., O. Knopf, I. J. Wright, A. A. Temme, S. W. Hogewoning, A. Graf,
3066 L. A. Cernusak, and T. L. Pons (2022). A meta-analysis of responses of C₃
3067 plants to atmospheric CO₂: dose–response curves for 85 traits ranging from
3068 the molecular to the whole-plant level. *New Phytologist* 233(4), 1560–1596.
- 3069 Prentice, I. C., N. Dong, S. M. Gleason, V. Maire, and I. J. Wright (2014).
3070 Balancing the costs of carbon gain and water transport: testing a new theo-
3071 retical framework for plant functional ecology. *Ecology Letters* 17(1), 82–91.
- 3072 Prentice, I. C., X. Liang, B. E. Medlyn, and Y.-P. Wang (2015). Reliable, ro-
3073 bust and realistic: The three R’s of next-generation land-surface modelling.
3074 *Atmospheric Chemistry and Physics* 15, 5987–6005.
- 3075 Priestley, C. H. B. and R. J. Taylor (1972). On the Assessment of Surface
3076 Heat Flux and Evaporation Using Large-Scale Parameters. *Monthly Weather
3077 Review* 100(2), 81–92.
- 3078 Querejeta, J. I., I. Prieto, C. Armas, F. Casanoves, J. S. Diémé, M. Diouf,
3079 H. Yossi, B. Kaya, F. I. Pugnaire, and G. M. Rusch (2022). Higher leaf
3080 nitrogen content is linked to tighter stomatal regulation of transpiration

- 3081 and more efficient water use across dryland trees. *New Phytologist* 235(4),
3082 1351–1364.
- 3083 R Core Team (2021). R: A language and environment for statistical computing.
- 3084 Raich, J. W., D. A. Clark, L. Schwendenmann, and T. E. Wood (2014). Above-
3085 ground tree growth varies with belowground carbon allocation in a tropical
3086 rainforest environment. *PLoS ONE* 9(6), e100275.
- 3087 Rastetter, E. B., P. M. Vitousek, C. B. Field, G. R. Shaver, D. Herbert, and
3088 G. I. Ågren (2001). Resource optimization and symbiotic nitrogen fixation.
3089 *Ecosystems* 4(4), 369–388.
- 3090 Reich, P. B. (2014). The world-wide 'fast-slow' plant economics spectrum: a
3091 traits manifesto. *Journal of Ecology* 102(2), 275–301.
- 3092 Reich, P. B., S. E. Hobbie, T. Lee, D. S. Ellsworth, J. B. West, D. Tilman,
3093 J. M. H. Knops, S. Naeem, and J. Trost (2006). Nitrogen limitation con-
3094 strains sustainability of ecosystem response to CO₂. *Nature* 440(7086), 922–925.
- 3095 Rhine, E. D., R. L. Mulvaney, E. J. Pratt, and G. K. Sims (1998). Improving
3096 the Berthelot reaction for determining ammonium in soil extracts and water.
3097 *Soil Science Society of America Journal* 62(2), 473.
- 3098 Rogers, A. (2014). The use and misuse of $V_{c\max}$ in Earth System Models. *Photo-*
3099 *tosynthesis Research* 119(1-2), 15–29.
- 3100 Rogers, A., B. E. Medlyn, J. S. Dukes, G. B. Bonan, S. Caemmerer, M. C.
3101 Dietze, J. Kattge, A. D. B. Leakey, L. M. Mercado, Ü. Niinemets, I. C.
3102 Prentice, S. P. Serbin, S. Sitch, D. A. Way, and S. Zaehle (2017). A roadmap

- 3104 for improving the representation of photosynthesis in Earth system models.
- 3105 *New Phytologist* 213(1), 22–42.
- 3106 Saathoff, A. J. and J. Welles (2021). Gas exchange measurements in the un-
- 3107 steady state. *Plant Cell and Environment* 44(11), 3509–3523.
- 3108 Saleh, A. M., M. Abdel-Mawgoud, A. R. Hassan, T. H. Habeeb, R. S. Yehia,
- 3109 and H. AbdElgawad (2020). Global metabolic changes induced by arbuscular
- 3110 mycorrhizal fungi in oregano plants grown under ambient and elevated levels
- 3111 of atmospheric CO₂. *Plant Physiology and Biochemistry* 151, 255–263.
- 3112 Saxton, K. E. and W. J. Rawls (2006). Soil water characteristic estimates by
- 3113 texture and organic matter for hydrologic solutions. *Soil Science Society of*
- 3114 *America Journal* 70(5), 1569–1578.
- 3115 Schaefer, K., C. R. Schwalm, C. Williams, M. A. Arain, A. Barr, J. M. Chen,
- 3116 K. J. Davis, D. Dimitrov, T. W. Hilton, D. Y. Hollinger, E. Humphreys,
- 3117 B. Poulter, B. M. Racza, A. D. Richardson, A. Sahoo, P. Thornton, R. Var-
- 3118 gas, H. Verbeeck, R. Anderson, I. Baker, T. A. Black, P. Bolstad, J. Chen,
- 3119 P. S. Curtis, A. R. Desai, M. C. Dietze, D. Dragoni, C. M. Gough, R. F.
- 3120 Grant, L. Gu, A. K. Jain, C. Kucharik, B. E. Law, S. Liu, E. Lokipitiya,
- 3121 H. A. Margolis, R. Matamala, J. H. McCaughey, R. Monson, J. W. Munger,
- 3122 W. Oechel, C. Peng, D. T. Price, D. Ricciuto, W. J. Riley, N. Roulet,
- 3123 H. Tian, C. Tonitto, M. Torn, E. Weng, and X. Zhou (2012). A model-
- 3124 data comparison of gross primary productivity: Results from the North
- 3125 American Carbon Program site synthesis. *Journal of Geophysical Research:*
- 3126 *Biogeosciences* 117(G3), G03010.
- 3127 Schneider, C. A., W. S. Rasband, and K. W. Eliceiri (2012). NIH Image to

- 3128** ImageJ: 25 years of image analysis. *Nature Methods* 9(7), 671–675.
- 3129** Scott, H. G. and N. G. Smith (2022). A Model of C4 Photosynthetic Acclimation
- 3130** Based on Least-Cost Optimality Theory Suitable for Earth System Model
- 3131** Incorporation. *Journal of Advances in Modeling Earth Systems* 14(3), 1–16.
- 3132** Shi, M., J. B. Fisher, E. R. Brzostek, and R. P. Phillips (2016). Carbon cost
- 3133** of plant nitrogen acquisition: Global carbon cycle impact from an improved
- 3134** plant nitrogen cycle in the Community Land Model. *Global Change Biology*
- 3135** 22(3), 1299–1314.
- 3136** Shi, M., J. B. Fisher, R. P. Phillips, and E. R. Brzostek (2019). Neglecting
- 3137** plant–microbe symbioses leads to underestimation of modeled climate im-
- 3138** pacts. *Biogeosciences* 16(2), 457–465.
- 3139** Smith, B., D. Wärldin, A. Arneth, T. Hickler, P. Leadley, J. Siltberg, and
- 3140** S. Zaehle (2014). Implications of incorporating N cycling and N limitations
- 3141** on primary production in an individual-based dynamic vegetation model.
- 3142** *Biogeosciences* 11(7), 2027–2054.
- 3143** Smith, N. G. and J. S. Dukes (2013). Plant respiration and photosynthesis in
- 3144** global-scale models: incorporating acclimation to temperature and CO₂.
- 3145** *Global Change Biology* 19(1), 45–63.
- 3146** Smith, N. G. and T. F. Keenan (2020). Mechanisms underlying leaf photosyn-
- 3147** thetic acclimation to warming and elevated CO₂ as inferred from least-cost
- 3148** optimality theory. *Global Change Biology* 26(9), 5202–5216.
- 3149** Smith, N. G., T. F. Keenan, I. C. Prentice, H. Wang, I. J. Wright, Ü. Niinemets,
- 3150** K. Y. Crous, T. F. Domingues, R. Guerrieri, F. oko Ishida, J. Kattge, E. L.

- 3151** Kruger, V. Maire, A. Rogers, S. P. Serbin, L. Tarvainen, H. F. Togashi,
3152 P. A. Townsend, M. Wang, L. K. Weerasinghe, and S.-X. Zhou (2019).
3153 Global photosynthetic capacity is optimized to the environment. *Ecology*
3154 *Letters* 22(3), 506–517.
- 3155** Smith, N. G., D. L. Lombardozzi, A. Tawfik, G. B. Bonan, and J. S. Dukes
3156 (2017). Biophysical consequences of photosynthetic temperature acclimation
3157 for climate. *Journal of Advances in Modeling Earth Systems* 9(1), 536–547.
- 3158** Smith, N. G., S. L. Malyshev, E. Shevliakova, J. Kattge, and J. S. Dukes
3159 (2016). Foliar temperature acclimation reduces simulated carbon sensitivity
3160 to climate. *Nature Climate Change* 6(4), 407–411.
- 3161** Smith, S. E. and D. J. Read (2008). *Mycorrhizal Symbiosis*. Academic Press.
- 3162** Soil Survey Staff (2022). Web Soil Survey.
- 3163** Soudzilovskaia, N. A., J. C. Douma, A. A. Akhmetzhanova, P. M. van Bode-
3164 gom, W. K. Cornwell, E. J. Moens, K. K. Treseder, and J. H. C. Cornelissen
3165 (2015). Global patterns of plant root colonization intensity by mycorrhizal
3166 fungi explained by climate and soil chemistry. *Global Ecology and Biogeogra-*
3167 *phy* 24(3), 371–382.
- 3168** Stocker, B. D., H. Wang, N. G. Smith, S. P. Harrison, T. F. Keenan, D. San-
3169 doval, T. Davis, and I. C. Prentice (2020). P-model v1.0: An optimality-
3170 based light use efficiency model for simulating ecosystem gross primary pro-
3171 duction. *Geoscientific Model Development* 13(3), 1545–1581.
- 3172** Stocker, B. D., J. Zscheischler, T. F. Keenan, I. C. Prentice, J. Peñuelas, and
3173 S. I. Seneviratne (2018). Quantifying soil moisture impacts on light use

- 3174** efficiency across biomes. *New Phytologist* 218(4), 1430–1449.
- 3175** Sulman, B. N., D. T. Roman, K. Yi, L. Wang, R. P. Phillips, and K. A.
- 3176** Novick (2016). High atmospheric demand for water can limit forest car-
- 3177** bon uptake and transpiration as severely as dry soil. *Geophysical Research*
- 3178** *Letters* 43(18), 9686–9695.
- 3179** Sulman, B. N., E. Shevliakova, E. R. Brzostek, S. N. Kivlin, S. L. Malyshev,
- 3180** D. N. L. Menge, and X. Zhang (2019). Diverse mycorrhizal associations
- 3181** enhance terrestrial C storage in a global model. *Global Biogeochemical Cy-*
- 3182** *cles* 33(4), 501–523.
- 3183** Sweet, S. K., D. W. Wolfe, A. DeGaetano, and R. Benner (2017). Anatomy
- 3184** of the 2016 drought in the Northeastern United States: Implications for
- 3185** agriculture and water resources in humid climates. *Agricultural and Forest*
- 3186** *Meteorology* 247, 571–581.
- 3187** Taylor, B. N. and D. N. L. Menge (2018). Light regulates tropical symbiotic
- 3188** nitrogen fixation more strongly than soil nitrogen. *Nature Plants* 4(9), 655–
- 3189** 661.
- 3190** Terrer, C., S. Vicca, B. A. Hungate, R. P. Phillips, and I. C. Prentice (2016).
- 3191** Mycorrhizal association as a primary control of the CO₂ fertilization effect.
- 3192** *Science* 353(6294), 72–74.
- 3193** Terrer, C., S. Vicca, B. D. Stocker, B. A. Hungate, R. P. Phillips, P. B. Reich,
- 3194** A. C. Finzi, and I. C. Prentice (2018). Ecosystem responses to elevated CO₂
- 3195** governed by plant–soil interactions and the cost of nitrogen acquisition. *New*
- 3196** *Phytologist* 217(2), 507–522.

- 3197** Thieurmel, B. and A. Elmarhraoui (2019). suncalc: Compute sun position,
- 3198** sunlight phases, moon position, and lunar phase.
- 3199** Thomas, R. Q., E. N. J. Brookshire, and S. Gerber (2015). Nitrogen limita-
- 3200** tion on land: how can it occur in Earth system models? *Global Change*
- 3201** *Biology* 21(5), 1777–1793.
- 3202** Thomas, R. Q., S. Zaehle, P. H. Templer, and C. L. Goodale (2013). Global pat-
- 3203** terns of nitrogen limitation: confronting two global biogeochemical models
- 3204** with observations. *Global Change Biology* 19(10), 2986–2998.
- 3205** Thornton, P. E., J.-F. Lamarque, N. A. Rosenbloom, and N. M. Mahowald
- 3206** (2007). Influence of carbon-nitrogen cycle coupling on land model response
- 3207** to CO₂ fertilization and climate variability. *Global Bioge-*
- 3208** *chemical Cycles* 21(4), GB4018.
- 3209** Tingey, D. T., D. L. Phillips, and M. G. Johnson (2000). Elevated CO₂ and
- 3210** conifer roots: effects on growth, life span and turnover. *New Phytolo-*
- 3211** *gist* 147(1), 87–103.
- 3212** Udvardi, M. and P. S. Poole (2013). Transport and metabolism in legume-
- 3213** rhizobia symbioses. *Annual Review of Plant Biology* 64, 781–805.
- 3214** USDA NRCS (2022). The PLANTS Database.
- 3215** Uselman, S. M., R. G. Qualls, and R. B. Thomas (2000). Effects of increased
- 3216** atmospheric CO₂, temperature, and soil N availability on root exudation
- 3217** of dissolved organic carbon by an N-fixing tree (*Robinia pseudoacacia* L.).
- 3218** *Plant and Soil* 222, 191–202.
- 3219** van Diepen, L. T. A., E. A. Lilleskov, K. S. Pregitzer, and R. M. Miller (2007).

- 3220** Decline of arbuscular mycorrhizal fungi in northern hardwood forests exposed to chronic nitrogen additions. *New Phytologist* 176(1), 175–183.
- 3221**
- 3222** Vance, C. P. and G. H. Heichel (1991). Carbon in N₂ fixation: Limitation or
- 3223** exquisite adaptation. *Annual Review of Plant Physiology and Plant Molec-*
- 3224** *ular Biology* 42(1), 373–392.
- 3225** Viet, H. D., J.-H. Kwak, K.-S. Lee, S.-S. Lim, M. Matsushima, S. X. Chang,
- 3226** K.-H. Lee, and W.-J. Choi (2013). Foliar chemistry and tree ring δ¹³C of
- 3227** *Pinus densiflora* in relation to tree growth along a soil pH gradient. *Plant*
- 3228** *and Soil* 363(1-2), 101–112.
- 3229** Vitousek, P. M., K. Cassman, C. C. Cleveland, T. Crews, C. B. Field, N. B.
- 3230** Grimm, R. W. Howarth, R. Marino, L. Martinelli, E. B. Rastetter, and
- 3231** J. I. Sprent (2002). Towards an ecological understanding of biological nitro-
- 3232** gen fixation. In *The Nitrogen Cycle at Regional to Global Scales*, pp. 1–45.
- 3233** Springer Netherlands.
- 3234** Vitousek, P. M. and R. W. Howarth (1991). Nitrogen limitation on land and in
- 3235** the sea: How can it occur? *Biogeochemistry* 13(2), 87–115.
- 3236** Vitousek, P. M., S. Porder, B. Z. Houlton, and O. A. Chadwick (2010).
- 3237** Terrestrial phosphorus limitation: mechanisms, implications, and nitro-
- 3238** gen–phosphorus interactions. *Ecological Applications* 20(1), 5–15.
- 3239** Walker, A. P., A. P. Beckerman, L. Gu, J. Kattge, L. A. Cernusak, T. F.
- 3240** Domingues, J. C. Scales, G. Wohlfahrt, S. D. Wullschleger, and F. I. Wood-
- 3241** ward (2014). The relationship of leaf photosynthetic traits - V_{cmax} and J_{max}
- 3242** - to leaf nitrogen, leaf phosphorus, and specific leaf area: a meta-analysis
- 3243** and modeling study. *Ecology and Evolution* 4(16), 3218–3235.

- 3244** Wang, H., I. C. Prentice, T. F. Keenan, T. W. Davis, I. J. Wright, W. K. Cornwell, B. J. Evans, and C. Peng (2017). Towards a universal model for carbon dioxide uptake by plants. *Nature Plants* 3(9), 734–741.
- 3247** Wang, W., Y. Wang, G. Hoch, Z. Wang, and J. Gu (2018). Linkage of root morphology to anatomy with increasing nitrogen availability in six temperate tree species. *Plant and Soil* 425(1-2), 189–200.
- 3250** Weatherburn, M. W. (1967). Phenol-hypochlorite reaction for determination of ammonia. *Analytical Chemistry* 39(8), 971–974.
- 3252** Wellburn, A. R. (1994). The spectral determination of chlorophylls a and b, as well as total carotenoids, using various solvents with spectrophotometers of different resolution. *Journal of Plant Physiology* 144(3), 307–313.
- 3255** Wen, Z., P. J. White, J. Shen, and H. Lambers (2022). Linking root exudation to belowground economic traits for resource acquisition. *New Phytologist* 233(4), 1620–1635.
- 3258** Westerband, A. C., I. J. Wright, V. Maire, J. Paillassa, I. C. Prentice, O. K. Atkin, K. J. Bloomfield, L. A. Cernusak, N. Dong, S. M. Gleason, C. Guilherme Pereira, H. Lambers, M. R. Leishman, Y. Malhi, and R. H. Nolan (2023). Coordination of photosynthetic traits across soil and climate gradients. *Global Change Biology* 29(3), 1–29.
- 3263** Wieder, W. R., C. C. Cleveland, W. K. Smith, and K. Todd-Brown (2015). Future productivity and carbon storage limited by terrestrial nutrient availability. *Nature Geoscience* 8(6), 441–444.
- 3266** Wieder, W. R., D. M. Lawrence, R. A. Fisher, G. B. Bonan, S. J. Cheng, C. L.

- 3267** Goodale, A. S. Grandy, C. D. Koven, D. L. Lombardozzi, K. W. Oleson,
3268 and R. Q. Thomas (2019). Beyond static benchmarking: using experimental
3269 manipulations to evaluate land model assumptions. *Global Biogeochemical*
3270 *Cycles* 33(10), 1289–1309.
- 3271** Wright, I. J., P. B. Reich, and M. Westoby (2003). Least-cost input mixtures
3272 of water and nitrogen for photosynthesis. *The American Naturalist* 161(1),
3273 98–111.
- 3274** Wright, I. J., P. B. Reich, M. Westoby, D. D. Ackerly, Z. Baruch, F. Bongers,
3275 J. Cavender-Bares, T. Chapin, J. H. C. Cornelissen, M. Diemer, J. Flexas,
3276 E. Garnier, P. K. Groom, J. Gulias, K. Hikosaka, B. B. Lamont, T. Lee,
3277 W. Lee, C. Lusk, J. J. Midgley, M.-L. Navas, Ü. Niinemets, J. Oleksyn,
3278 N. Osada, H. Poorter, P. Poot, L. Prior, V. I. Pyankov, C. Roumet, S. C.
3279 Thomas, M. G. Tjoelker, E. J. Veneklaas, and R. Villar (2004). The world-
3280 wide leaf economics spectrum. *Nature* 428(6985), 821–827.
- 3281** Xu-Ri and I. C. Prentice (2017). Modelling the demand for new nitrogen fixation
3282 by terrestrial ecosystems. *Biogeosciences* 14(7), 2003–2017.
- 3283** Zaehle, S., B. E. Medlyn, M. G. De Kauwe, A. P. Walker, M. C. Dietze, T. Hick-
3284 ler, Y. Luo, Y. P. Wang, B. El-Masri, P. Thornton, A. Jain, S. Wang,
3285 D. Warlind, E. Weng, W. Parton, C. M. Iversen, A. Gallet-Budynek, H. Mc-
3286 carthy, A. C. Finzi, P. J. Hanson, I. C. Prentice, R. Oren, and R. J. Norby
3287 (2014). Evaluation of 11 terrestrial carbon-nitrogen cycle models against
3288 observations from two temperate Free-Air CO₂ Enrichment studies. *New*
3289 *Phytologist* 202(3), 803–822.
- 3290** Zaehle, S., S. Sitch, B. Smith, and F. Hatterman (2005). Effects of parame-

- 3291** ter uncertainties on the modeling of terrestrial biosphere dynamics. *Global*
3292 *Biogeochemical Cycles* 19(3), GB3020.
- 3293** Zhu, Q., W. J. Riley, J. Tang, N. Collier, F. M. Hoffman, X. Yang, and G. Bisht
3294 (2019). Representing nitrogen, phosphorus, and carbon interactions in the
3295 E3SM land model: development and global benchmarking. *Journal of Ad-*
3296 *vances in Modeling Earth Systems* 11(7), 2238–2258.
- 3297** Ziegler, C., M. E. Dusenge, B. Nyirambangutse, E. Zibera, G. Wallin, and
3298 J. Uddling (2020). Contrasting Dependencies of Photosynthetic Capacity
3299 on Leaf Nitrogen in Early- and Late-Successional Tropical Montane Tree
3300 Species. *Frontiers in Plant Science* 11, 1–12.
- 3301** Ziehn, T., J. Kattge, W. Knorr, and M. Scholze (2011). Improving the pre-
3302 dictability of global CO₂ assimilation rates under climate change. *Geophys-*
3303 *ical Research Letters* 38(10), L10404.